Copyright Warning & Restrictions

The copyright law of the United States (Title 17, United States Code) governs the making of photocopies or other reproductions of copyrighted material.

Under certain conditions specified in the law, libraries and archives are authorized to furnish a photocopy or other reproduction. One of these specified conditions is that the photocopy or reproduction is not to be "used for any purpose other than private study, scholarship, or research." If a, user makes a request for, or later uses, a photocopy or reproduction for purposes in excess of "fair use" that user may be liable for copyright infringement,

This institution reserves the right to refuse to accept a copying order if, in its judgment, fulfillment of the order would involve violation of copyright law.

Please Note: The author retains the copyright while the New Jersey Institute of Technology reserves the right to distribute this thesis or dissertation

Printing note: If you do not wish to print this page, then select "Pages from: first page # to: last page #" on the print dialog screen

NJIT New Jersey's Science & Technology University

The Van Houten library has removed some of the personal information and all signatures from the approval page and biographical sketches of theses and dissertations in order to protect the identity of NJIT graduates and faculty.

ABSTRACT

DIFFUSIVE AND WAVELIKE PHENOMENA IN THERMAL PROCESSING OF MATERIALS

by
John A. Pelesko

Contemporary materials science abounds with novel processing methods. Devices such as lasers, microwave sources, and electron beam guns, provide unprecedented control over the deposition of energy within a material. The modern materials scientist has the ability to deposit energy volumetrically, to precisely control the location of energy deposition within a material, and to deposit energy in extremely short intervals of time. While making possible numerous thermal processing methods, these devices also push the limits of our understanding of the response of materials to energy deposition. In order to optimize and control these processing methods, it becomes necessary to further our understanding of this response.

Here, we investigate several problems, motivated by the study of thermal processing methods, whose analyses further our understanding of these new parameter regimes. First, we consider two classes of problems arising in microwave processing of ceramics. These problems are characterized by volumetric energy deposition and a weak coupling between thermal diffusion and electromagnetic wave propagation. Next, we investigate a sequence of problems motivated by and arising in the study of an electron beam joining process. These problems are characterized by rapid volumetric energy deposition and a strong coupling between thermal diffusion and elastic wave propagation.

DIFFUSIVE AND WAVELIKE PHENOMENA IN THERMAL PROCESSING OF MATERIALS

by
John A. Pelesko

A Dissertation
Submitted to the Faculty of
New Jersey Institute of Technology
in Partial Fulfillment of the Requirements for the Degree of
Doctor of Philosophy

Department of Mathematics

October 1997

Copyright © 1997 by John A. Pelesko

ALL RIGHTS RESERVED

APPROVAL PAGE

DIFFUSIVE AND WAVELIKE PHENOMENA IN THERMAL PROCESSING OF MATERIALS

John A. Pelesko

Gregory A. Kriegsmann, Ph.D., Dissertation Advisor — Date
Distinguished Professor, Department of Mathematics, NJIT

Michael R. Booty, Ph.D., Committee Member — Date
Associate Professor, Department of Mathematics, NJIT

Jonathan H. C. Luke, Ph.D., Committee Member — Date
Associate Professor, Department of Mathematics, NJIT

Frederick M. Mako, Ph.D., Committee Member — Date
President, FM Technologies, Inc.

Richard Silberglitt, Ph.D., Committee Member — Date
Vice President, Materials Processing, FM Technologies, Inc.

David C. Stickler, Ph.D., Committee Member — Date
Professor, Department of Mathematics, NJIT

BIOGRAPHICAL SKETCH

Author: John A. Pelesko

Degree: Doctor of Philosophy

Date: October 1997

Undergraduate and Graduate Education:

- Doctor of Philosophy in Applied Mathematics,
  New Jersey Institute of Technology, Newark, NJ, 1997
- Bachelor of Science in Pure Mathematics (*cum laude*),
  University of Massachusetts, Boston, MA, 1992

Major: Applied Mathematics

Publications:

J.A. Pelesko, "Thermomechanical Interaction in a Simple Oscillator," Submitted for publication in the *IMA Journal of Applied Mathematics*, 1997.

J.A. Pelesko and G.A. Kriegsmann, "Microwave Heating of Ceramic Laminates," *The Journal of Engineering Mathematics*, 1997. In press.

J.A. Pelesko and G.A. Kriegsmann, "Microwave Heating of Ceramic Laminates," in *Materials Research Society Symposium Proceedings*, (Pittsburg, PA), pp. 184-189, Materials Research Society, April 1996.

B. Bukiet, J.A. Pelesko, X.L. Li and P.L. Sachdev, "A Characterisitic Based Numerical Method with Tracking for Nonlinear Wave Equations," *Computers and Mathematics with Applications*, vol. 31, no. 7, pp. 75-99, 1996.

A. Crowe, K. Gurski, J.A. Pelesko, and J. Spencer, "Improved Estimation of the Heat Transfer Characterisitics of a Power Condenser," in *Claremont Colleges Mathematics Modeling Workshop Proceedings*, (Claremont, CA), pp. 59-80, June 1994.

To Holly

ACKNOWLEDGMENT

I extend my deepest appreciation to Dr. Gregory A. Kriegsmann, who by guidance and example has taught me not only science, but what it means to be a scientist. Special thanks are due to each of my committee members, Dr. Michael R. Booty, Dr. Jonathan H.C. Luke, Dr. Frederick M. Mako, Dr. Richard Silberglitt, and Dr. David C. Stickler, all of who played an active role in this work. I would also like to thank my family for their continuing support and encouragement, especially my parents, for showing me the joy of learning and the value of knowledge.

This work is dedicated to my wife, Holly. Her strength, love, and unwavering support have made this thesis possible. For this and for many other things, I thank her. Finally, for their inspiration, I thank M.T.B. and C.G. who otherwise wish to remain nameless.

TABLE OF CONTENTS

TABLE OF CONTENTS
(Continued)

Chapter **Page**

TABLE OF CONTENTS
(Continued)

LIST OF FIGURES

LIST OF FIGURES
(Continued)

Figure **Page**

CHAPTER 1

INTRODUCTION

Contemporary materials science abounds with novel processing methods. Devices such as lasers, microwave sources, and electron beam guns provide unprecedented control over the deposition of energy within a material. The modern materials scientist has the ability to deposit energy volumetrically, to precisely control the location of energy deposition within a material, and to deposit energy in extremely short intervals of time. While making possible numerous thermal processing methods, these devices also push the limits of our understanding of the response of materials to energy deposition. In order to optimize and control these processing methods, it becomes necessary to further our understanding of this response. The work presented here is aimed at this goal.

We begin in Chapters 2 and 3 by addressing two classes of problems which arise in microwave heating of ceramics. In recent years, microwave processing of ceramic materials has become an area of intense activity, [1]. Investigators in the field hope to capitalize on the volumetric nature of microwave energy deposition to efficiently produce high-quality materials and products. However, they are beset with numerous difficulties. Some materials of commercial interest, such as alumina, are essentially transparent to microwaves, while still others, such as silicon carbide, absorb microwaves readily. Many investigators have explored 'hybrid' heating techniques in an effort to overcome the difficulties associated with processing either type of material, [2, 3, 4, 5]. Most hybrid heating schemes involve the simultaneous heating of electrically and thermally disparate materials. In Chapter 2 we explore two such situations where this simultaneous heating may be viewed as the microwave heating of a ceramic laminate. Through analysis of our model, we show that these types of hybrid heating schemes reduce power requirements, allow for stable heating, and

smooth thermal gradients. In Chapter 3, we extend our analysis of hybrid heating schemes designed to allow the processing of low-loss ceramics, to the case of ceramic composites. In particular, we consider a composite comprised of many small lossy ceramic particles embedded in a ceramic cement. We show how variations in particle properties affect the microwave heating of the composite.

As mentioned above, modern materials processing methods push the limits of our understanding of the response of materials to energy deposition. In Chapters 2 and 3, we consider problems arising from microwave heating experiments. These problems are characterized by volumetric energy deposition, and a non-linear coupling between diffusive heat flow and Maxwell's equations. In some sense, this coupling is weak. That is, there is a disparity of timescales on which heat flows and electromagnetic waves oscillate.

In Chapter 4, we turn our attention to a new parameter regime, one in which diffusive and wavelike timescales are comparable. Here, the diffusion of which we speak is still that of heat, while the wavelike nature is that of elastic waves. We begin to address the fundamental question of the inter-convertibility of mechanical and thermal energy. Our intent is not to explore deep questions arising in non-equilibrium thermodynamics, but rather to develop a simple model which yields insight into the parameters governing the coupling between coherent mechanical and incoherent internal or thermal energy. We accomplish this by constructing an idealized model which combines the canonical systems of mechanics and thermodynamics; the mass-spring oscillator and the piston-cylinder system. Through analysis of this model, we show that the rate of thermal energy transport plays a key role in determining the strength of the coupling between thermal and mechanical energy.

Finally, in Chapter 5, we apply the insight obtained from the piston-spring model to another materials processing method. This time, the problem of interest is the joining of ceramics and metals. The method we explore is the use of a single-

pulse high-energy electron beam to accomplish this joining. In this scheme, [6], a single high-energy pulse of electrons is incident upon a three layer composite. The composite consists of a ceramic, a thin metallic interlayer, and a metal workpiece. The electron beam, which is incident upon the outer face of the ceramic, deposits energy in each material. However, due to differences in heat capacity, the interlayer attains a higher temperature than the ceramic or metal workpiece. The interlayer melts, and a joint is formed. This process is characterized by controlled volumetric energy deposition on extremely short temporal and spatial scales. This method of energy deposition gives rise to thermoelastic stress waves which propagate throughout the sample. If the stresses become too large, the sample may crack or deform. In order to avoid such undesirable effects, it becomes necessary to understand how these stresses are formed, how they propagate, and finally how they decay. We analyze a sequence of models, increasing in complexity, and derive expressions for the maximum stress created by the pulse, indicate how these stresses decay, and demonstrate how variations in material properties affect the creation, propagation, and decay of stresses.

CHAPTER 2

MICROWAVE HEATING OF CERAMIC LAMINATES

In recent years, microwave processing of ceramic materials has become an area of intense activity [1]. Investigators in the field hope to efficiently produce high quality materials and products. However, they are faced with numerous difficulties. Some materials of commercial interest, such as alumina, are essentially transparent to microwaves, while others, such as silicon carbide, absorb microwaves readily. Many investigators have explored 'hybrid' heating techniques in an effort to overcome the difficulties associated with processing either type of material [2, 3, 4, 5]. Most hybrid heating schemes involve the simultaneous heating of two electrically and thermally disparate materials. When these materials are in contact, the scheme can be viewed as the heating of a ceramic laminate. In this chapter we explore two such situations.

We consider first, the microwave heating of microwave transparent, or low-loss, materials. Here, two key difficulties arise. Since the material is essentially transparent to microwaves, a large amount of power is required to heat these materials to processing temperatures. Further, the electrical conductivity of low-loss ceramics typically varies exponentially with temperature. This often leads to thermal runaway. In thermal runaway, the temperature of the material increases uncontrollably once the temperature of the material exceeds some critical temperature. Unfortunately the critical temperature is often below the desired processing temperature. One method for overcoming both of these difficulties is to surround the low-loss ceramic with a lossy susceptor. Since the susceptor absorbs microwave radiation readily, it heats the low-loss ceramic by conduction, and requires less power. Investigators have also observed that when a susceptor is used, the critical temperature at which thermal runaway occurs is increased [3]. This may allow one to heat the low-loss ceramic to the desired processing temperature while avoiding thermal runaway.

In the first part of this chapter we model the heating of a low-loss ceramic through the use of a lossy susceptor. We exploit the ratio of the two materials electrical conductivities as a small parameter in the development of an asymptotic theory. We illustrate how the use of a susceptor lowers the power requirements. Further, we show how the maximum stable temperature varies as a function of the thickness of the susceptor. We also note that thermal gradients within the low-loss ceramic are lower when a susceptor is employed than when the material is heated alone. This produces, in such processes as sintering, a more homogeneous material product [1].

In the second part of this chapter we consider the microwave heating of lossy targets. Since microwaves heat volumetrically, a microwave irradiated material is hotter inside than near the surface. A very important goal of microwave processing, as mentioned above for sintering, is the uniform heating of materials. Numerous investigators have placed low-loss insulation around lossy targets [2, 4] to reduce thermal gradients. This type of laminate is identical to the previous hybrid heating scheme with the roles of the low-loss and lossy materials reversed. Using the same asymptotic method as employed in the first part of this chapter, we develop a theory for the microwave heating of an insulated lossy target. We show how the use of insulation dramatically reduces thermal gradients within the material. We also show that the use of insulation lowers the power requirements, and we determine how the maximum stable temperature varies as a function of the insulation thickness.

2.1 Formulation of the Model

We begin by considering a ceramic laminate comprised of three thin isotropic ceramic slabs as shown in Figure 2.1. The outer two slabs are considered to be identical materials of equal thickness. Further, the composite is irradiated by identical microwaves from both sides. We choose this symmetric setup to simplify

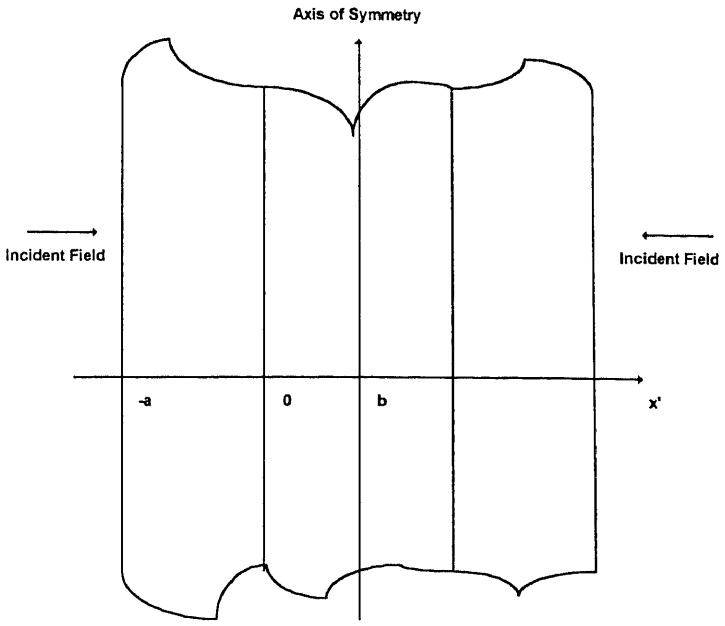

Figure 2.1 Sketch of the model geometry.

the analysis to follow; the system of governing equations is symmetric about the centerline of the laminate.

We further assume that the incident electromagnetic wave and the electric field within the materials are time harmonic, while the temperature distribution in each material is time dependent. While the governing equations do not admit such a solution it has been shown in [7] that the equations we present are the leading order equations of an asymptotic theory. This theory is based on the assumption that the time required for heat to diffuse an electromagnetic wavelength is much greater than the period of a microwave.

With these assumptions in mind, we first formulate the equations governing the temperature distributions in each material. The first material, a lossy ceramic, occupies the region $-a < x' < 0$ while the second, a low-loss ceramic, fills the region $0 < x' < b$. The axis of symmetry is taken to be at $x' = b$, hence we are modeling the microwave heating of a low-loss ceramic surrounded by lossy material. In this configuration the lossy materials are often referred to as 'susceptors' while the low-

loss material is called the 'ceramic.' We adopt this convention. The temperatures of our susceptor, T_1 and ceramic, T_2 satisfy:

$$\rho_1 c_1 \frac{\partial T_1}{\partial t'} = K_1 \frac{\partial^2 T_1}{\partial x'^2} + \frac{|E_1|^2}{2}\varsigma_1(T_1), \quad -a < x' < 0 \tag{2.1}$$

$$\rho_2 c_2 \frac{\partial T_2}{\partial t'} = K_2 \frac{\partial^2 T_2}{\partial x'^2} + \frac{|E|^2}{2}\varsigma_2(T_2), \quad 0 < x' < b. \tag{2.2}$$

Here ρ denotes density, c specific heat, K thermal conductivity, $|E|^2$ the electric field intensity, and ς_j denotes the effective electrical conductivity of the jth material which is a known function of the temperature.

The susceptor and the ceramic are assumed to be in perfect thermal contact at $x' = 0$ and hence we impose the following boundary conditions at this interface:

$$K_1 \frac{\partial T_1}{\partial x'} = K_2 \frac{\partial T_2}{\partial x'} \quad \text{at} \quad x' = 0 \tag{2.3}$$

$$T_1(0, t') = T_2(0, t'). \tag{2.4}$$

At the left hand boundary of the first material, $x' = -a$, we assume that heat is lost through both convection and radiation and hence impose:

$$K_1 \frac{\partial T_1}{\partial x'} = h(T_1 - T_A) + s\epsilon(T_1^4 - T_A^4) \quad \text{at} \quad x' = -a \tag{2.5}$$

where h is a convective heat transfer coefficient, s is the Stefan-Boltzmann constant, ϵ is the ceramic's emissivity, and T_A is the ambient temperature of the surrounding environment. At the axis of symmetry, $x' = b$, we impose the condition:

$$\frac{\partial T_2}{\partial x'} = 0 \quad \text{at} \quad x' = b. \tag{2.6}$$

Finally, we assume that both slabs are initially at the ambient temperature of the environment and impose:

$$T_1(x', 0) = T_2(x', 0) = T_A. \tag{2.7}$$

Next, we formulate the equations governing the electric field. A plane, time harmonic electromagnetic wave of frequency ω impinges upon the susceptor from

the left. A portion of this wave scatters from the interface at $x' = -a$, a portion penetrates and heats the susceptor, a portion scatters from the interface at $x' = 0$, and a portion penetrates and heats the ceramic. At $x' = b$ we will impose 'no-flux' conditions on the electric field in keeping with the symmetry assumptions outlined above. In the free space region $x' < -a$, the electric field is given by:

$$\vec{E} = E_0[\exp(ik'x' - i\omega t') + \Gamma \exp(-ik'x' - i\omega t')]\vec{k}, \qquad x' < -a \tag{2.8}$$

where E_0 is the strength of the incident field, $k' = \omega/c$, c is the speed of light in free space, and Γ is the total reflection coefficient.

Within the laminate the electric field is given by $\vec{E} = [E_j(x')\exp(-i\omega t')]\vec{k}$, $j = 1, 2$, where $j = 1$ corresponds to the susceptor and $j = 2$, the ceramic. The function E_1 satisfies:

$$\frac{d^2E_1}{dx'^2} + k_1'^2[1 + \frac{i}{\omega\epsilon_1}\varsigma_1(T_1)]E_1 = 0, \qquad -a < x' < 0 \tag{2.9}$$

in the susceptor and E_2 satisfies

$$\frac{d^2E_2}{dx'^2} + k_2'^2[1 + \frac{i}{\omega\epsilon_1}\varsigma_2(T_2)]E_2 = 0, \qquad 0 < x' < b \tag{2.10}$$

in the ceramic. Here ϵ_j is the permittivity of the jth material, $k_j' = \omega/c\sqrt{\epsilon_j/\epsilon_0}$, and ϵ_0 is the permittivity of free space. The magnetic permeabilities of both materials are assumed identical to that of free space.

At the interface $x' = -a$ the tangential electric and magnetic fields are continuous, hence E_1 and its derivative are also continuous at $x' = -a$. Combining this fact with (2.8) and eliminating Γ we find that E_1 satisfies

$$\frac{dE_1(-a)}{dx'} + ik'E_1(-a) = 2E_0ik'\exp(-ik'a). \tag{2.11}$$

The same continuity assumption applied at $x' = 0$ yields the boundary conditions

$$E_1(0) = E_2(0) \tag{2.12}$$

$$E_1'(0) = E_2'(0). \tag{2.13}$$

Finally the symmetry condition at $x' = b$ implies that

$$E_2'(b) = 0. \tag{2.14}$$

Next, we choose dimensionless temperature and length scales, scale the electric field with the amplitude of the incident wave, and rewrite the conductivities as their value at the ambient temperature multiplied by a dimensionless function of the scaled temperatures. Further, we scale time with respect to the diffusive time of the ceramic. This yields the new variables

$$v = \frac{T_1 - T_A}{T_A}, \quad u = \frac{T_2 - T_A}{T_A}, \quad e_1 = E_1/E_0, \quad e_2 = E_2/E_0,$$

$$\varsigma_1 = \sigma_1 g(v), \quad \varsigma_2 = \sigma_2 f(u), \quad t = \frac{K_2 t'}{\rho_2 c_2 b^2}, \quad x = x'/b.$$

When we introduce these into (2.1)-(2.14) the following dimensionless parameters naturally arise

$$\mu = \frac{\rho_1 c_1}{\rho_2 c_2}, \quad \gamma = \frac{K_2}{K_1}, \quad p = \frac{b\sigma_2 E_0^2}{2hT_A}, \quad \delta = \frac{\sigma_2}{\sigma_1},$$

$$B = \frac{hb}{K_2}, \quad d = a/b, \quad R = (s\epsilon T_A^3)/h, \quad k = k'b,$$

$$k_1 = k_1'b, \quad k_2 = k_2'b, \quad \nu\sigma/(\omega\epsilon_1).$$

The parameters μ and γ are dimensionless ratios of material properties. The parameter p is a dimensionless ratio of power absorbed from the electric field to power lost at the boundaries by convection. The Biot number, B, measures the relative effects of convection and conduction, R measures the relative effects of convection and radiation, and δ is a dimensionless ratio of the two ceramic's effective electrical conductivities at the ambient temperature. The parameters k, k_1, and k_2 are dimensionless wave numbers scaled with ceramic thickness, and finally ν is the ratio of the wavelength in the susceptor to the skin depth at the ambient temperature, T_A.

In terms of our dimensionless variables and parameters the governing equations for the temperatures become

$$\mu\gamma\frac{\partial v}{\partial t} = \frac{\partial^2 v}{\partial x^2} + \frac{pB\gamma}{\delta}g(v)|e_1|^2, \qquad -d < x < 0 \tag{2.15}$$

$$\frac{\partial u}{\partial t} = \frac{\partial^2 u}{\partial x^2} + pBf(u)|e_2|^2, \qquad 0 < x < 1 \tag{2.16}$$

$$\frac{\partial v}{\partial x} = \gamma\frac{\partial u}{\partial x}, \qquad x = 0 \tag{2.17}$$

$$v(0,t) = u(0,t) \tag{2.18}$$

$$\frac{\partial v}{\partial x} = B\gamma L(v), \qquad x = -d \tag{2.19}$$

$$L(v) = v + R((v+1)^4 - 1) \tag{2.20}$$

$$\frac{\partial u}{\partial x} = 0, \qquad x = 1 \tag{2.21}$$

$$v(x,0) = u(x,0) = 0. \tag{2.22}$$

Similarly, the equations governing the electric field become

$$\frac{d^2 e_1}{dx^2} + k_1^2[1 + i\nu g(v)]e_1 = 0, \qquad -d < x < 0 \tag{2.23}$$

$$\frac{d^2 e_2}{dx^2} + k_2^2[1 + i\nu\delta f(u)]e_2 = 0, \qquad 0 < x < 1 \tag{2.24}$$

$$\frac{de_1(-d)}{dx} + ike_1(-d) = 2ik\exp(-ikd) \tag{2.25}$$

$$e_1(0) = e_2(0) \tag{2.26}$$

$$e_1'(0) = e_2'(0) \tag{2.27}$$

$$e_2'(1) = 0. \tag{2.28}$$

Equations (2.15)-(2.28) are the governing equations for our microwave irradiated ceramic laminate. The appearance of the nonlinear dimensionless conductivity functions $g(v)$ and $f(u)$, and the nonlinear boundary condition (2.19) precludes an exact solution to this system of equations. In the next section we develop an asymptotic theory which gives an accurate approximation of the solutions to our model equations.

2.2 An Asymptotic Theory

We begin by recalling our assumptions regarding the electrical conductivities of the susceptor and the ceramic: the former is quite large while the later is very small. In applications, such materials might be SiC and alumina, respectively. We find for this case that $\delta \sim 10^{-5}$. We also note that for these materials, the ratio of their thermal conductivities, $\gamma \sim 10^{-2}$. We take δ to be a small parameter and order the remaining dimensionless parameters with respect to δ. In particular we assume that μ, B, R, k, k_1, k_2 and ν are all $O(1)$ and order p and γ as

$$p = P\delta, \qquad \gamma = \alpha\delta^{1/2}. \tag{2.29}$$

Here P and α are assumed to be $O(1)$. This restriction on α is true for ceramics whose conductivity ratio is as discussed above.

Next we assume an expansion in powers of $\delta^{1/2}$ for u, v, e_1 and e_2, that is

$$v \sim v_0 + \delta^{1/2}v_1 + \delta v_2 + \cdots \tag{2.30}$$

$$u \sim u_0 + \delta^{1/2}u_1 + \delta u_2 + \cdots \tag{2.31}$$

$$e_1 \sim V_0 + \delta^{1/2}V_1 + \delta V_2 + \cdots \tag{2.32}$$

$$e_2 \sim U_0 + \delta^{1/2}U_1 + \delta U_2 + \cdots. \tag{2.33}$$

Inserting (2.30)-(2.33) into (2.15)-(2.28), expanding the nonlinear terms in an asymptotic series, and equating to zero the coefficients of the powers of $\delta^{1/2}$ yields an infinite set of equations which sequentially determine the v_n, V_n, u_n and U_n. We list the first two equations for the v_n and u_n, and the only the first equation for the V_n and U_n. These are the equations needed to determine the leading order terms in the asymptotic approximation to the temperature and electric field in the laminate. They are

$$\frac{\partial^2 v_0}{\partial x^2} = 0, \qquad -d < x < 0 \tag{2.34}$$

$$\frac{\partial u_0}{\partial t} = \frac{\partial^2 u_0}{\partial x^2}, \qquad 0 < x < 1 \tag{2.35}$$

$$\frac{\partial v_0}{\partial x} = 0, \qquad x = -d, 0 \tag{2.36}$$

$$\frac{\partial u_0}{\partial x} = 0, \qquad x = 1 \tag{2.37}$$

$$v_0(0,t) = u_0(0,t) \tag{2.38}$$

$$v_0(x,0) = u_0(x,0) = 0 \tag{2.39}$$

$$\mu\alpha\frac{\partial v_0}{\partial t} = \frac{\partial^2 v_1}{\partial x^2} + BP\alpha g(v_0)|V_0|^2, \qquad -d < x < 0 \tag{2.40}$$

$$\frac{\partial u_1}{\partial t} = \frac{\partial^2 u_1}{\partial x^2}, \qquad 0 < x < 1 \tag{2.41}$$

$$\frac{\partial v_1}{\partial x} = \alpha BL(v_0), \qquad x = -d \tag{2.42}$$

$$\frac{\partial u_1}{\partial x} = 0, \qquad x = 1 \tag{2.43}$$

$$v_1(0,t) = u_1(0,t) \tag{2.44}$$

$$\frac{\partial v_1}{\partial x} = \alpha\frac{\partial u_0}{\partial x}, \qquad x = 0 \tag{2.45}$$

$$v_1(x,0) = u_1(x,0) = 0 \tag{2.46}$$

and

$$\frac{d^2 V_0}{dx^2} + k_1^2[1 + i\nu g(v_0)]V_0 = 0, \qquad -d < x < 0 \tag{2.47}$$

$$\frac{d^2 U_0}{dx^2} + k_2^2 u_0 = 0, \qquad 0 < x < 1 \tag{2.48}$$

$$\frac{dV_0(-d)}{dx} + ikV_0(-d) = 2ik\exp(-ikd) \tag{2.49}$$

$$V_0(0) = U_0(0) \tag{2.50}$$

$$V_0'(0) = U_0'(0) \tag{2.51}$$

$$V_0'(1) = 0. \tag{2.52}$$

To begin our analysis we integrate equation (2.34) twice and apply the boundary condition (2.36) to obtain $v_0 = v_0(t)$, i.e., v_0 is a function of time only. Then an examination of the electric field equations (2.47)-(2.52) reveals that

U_0 and V_0 only depend parametrically upon t through $v_0(t)$. These equations are then linear and may be solved exactly. Due to the complexity of the analytical solutions we have placed them in Appendix A. Here we regard U_0 and V_0 as known functions of temperature and position and proceed to consider the leading order equations for u_0 and v_0.

Next, we integrate equation (2.40) with respect to x over the interval $(-d, 0)$ and apply the boundary conditions (2.42) and (2.45) to obtain

$$d\mu \frac{dv_0}{dt} = \frac{\partial u_0(0,t)}{\partial x} - BL(v_0) + BPg(v_0)||V_0||^2(v_0) \tag{2.53}$$

$$||V_0||^2(v_0) = \int_{-d}^{0} |V_0|^2 \, dx \tag{2.54}$$

where the dependence of V_0 on v_0 is indicated. Since $v_0 = v_0(t)$, it follows that from (2.38) that $u_0(0,t) = v_0(t)$. Inserting this into (2.53) yields the nonlinear mixed boundary condition

$$\mu d \frac{\partial u_0}{\partial t} = \frac{\partial u_0}{\partial x} - BL(u_0) + BPg(u_0)||V_0||^2(u_0) \quad \text{at} \quad x = 0. \tag{2.55}$$

Finally, we observe that equations (2.35), (2.37), and (2.55), along with the initial condition (2.39) constitute an initial boundary value problem for the leading order temperature in the ceramic u_0. Once it is determined the temperature in the susceptor $v_0(t) = u_0(0,t)$ is determined. Thus, the leading order approximation of the temperature and electric field in the laminate is known.

2.3 Analysis of the Reduced System

For the convenience of the reader we restate the initial boundary value problem for $u_0(x,t)$. It is

$$\frac{\partial u_0}{\partial t} = \frac{\partial^2 u_0}{\partial x^2}, \qquad 0 < x < 1 \tag{2.56}$$

$$\mu d \frac{\partial u_0}{\partial t} = \frac{\partial u_0}{\partial x} - BL(u_0) + BPg(u_0)||V_0||^2(u_0), \qquad x = 0 \tag{2.57}$$

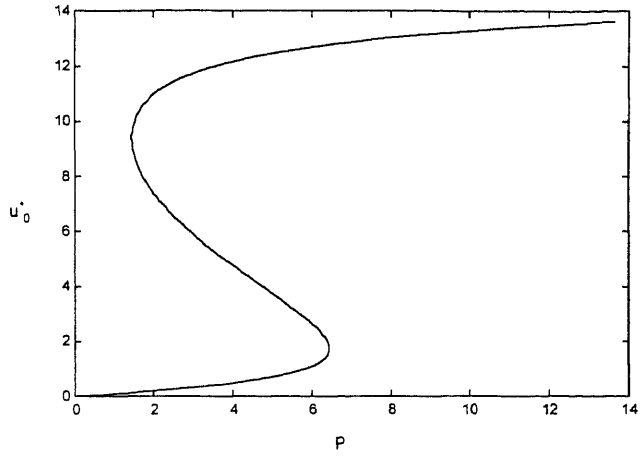

Figure 2.2 Power-response curve for susceptor-ceramic.

$$\frac{\partial u_0}{\partial x} = 0, \qquad x = 1 \tag{2.58}$$

$$u_0(x, 0) = 0. \tag{2.59}$$

The nonlinearities of the original problem now manifest themselves entirely in the boundary condition (2.57). This boundary condition also has the additional feature of possessing a time derivative. We analyze this problem in two steps. In the first step we consider the steady state solutions of (2.56) and investigate their stability. Then we use these results to help analyze and interpret the dynamical solutions of (2.56-2.59).

2.4 Steady-State Solutions

We begin by seeking steady-state solutions of (2.56). Setting the time derivatives equal to zero, integrating the resulting ordinary differential equation, and applying the boundary conditions we find that steady-state solutions, denoted u_0^*, are independent of x and must satisfy

$$P = \frac{L(u_0^*)}{g(u_0^*)||V_0||^2(u_0^*)} \tag{2.60}$$

In order to pursue the analysis further we must choose a specific form for the function g. Recall that g is the non-dimensional conductivity function for susceptor. Examination of conductivity data [8] for susceptors, such as SiC, reveals that g is an exponential function of temperature. Thus we take

$$g(u_0^*) = e^{\beta_1 u_0^*} \tag{2.61}$$

where the constant β_1 depends upon the particular material. Having chosen this exponential form for g the analysis may proceed. In general we cannot explicitly solve (2.60) for u_0^* as a function of P. However, this can be done graphically as shown in Figure 2.2 where P is plotted as a function of u_0^*, and the axis are reversed. This power-response curve has the familiar S-shape first discussed in [9]. That is, depending on the value of the parameter P, there are one, two, or three steady-state solutions. In order to sketch Figure 2.2, we set the Biot number $B = 0.01$, $k_1 = 0.1$, $k_2 = 0.15$, $\nu = 0.1$, $d = 0.1$, $\beta = 0.8$, and $k = 0.5$. These values are used to construct all remaining figures in this chapter unless otherwise noted.

We shall now analyze the linear stability of these steady-state solutions. Accordingly we seek a solution to (2.56) of the form

$$u_0(x,t) = u_0^* + w(x)e^{-\lambda^2 t} \tag{2.62}$$

where $|w(x)| << 1$. Inserting this ansatz into (2.56-2.59), expanding the nonlinear terms in Taylor series, and omitting quadratic and higher order terms in w gives the eigenvalue problem

$$\frac{d^2w}{dx^2} + \lambda^2 w = 0 \tag{2.63}$$

$$[\mu d\lambda^2 - Bg(u_0^*)||V_0||^2(u_0^*)P'(u_0^*)]w(0) + w'(0) = 0 \tag{2.64}$$

$$w'(1) = 0, \tag{2.65}$$

where $P'(u_0^*)$ is obtained by differentiating (2.60) with respect to u_0^*. This linear eigenvalue problem has a solution w when λ satisfies

$$\tan(\lambda) = -\mu d\lambda + \frac{Bg(u_0^*)||V_0||^2(u_0^*)P'(u_0^*)}{\lambda}. \tag{2.66}$$

The solutions of this equation in conjunction with (2.62) determine the stability of the perturbation w; if $Re(\lambda^2) > 0 (< 0)$, then the steady state u_0^* is linearly stable (unstable).

We shall first show that λ^2 is real. To demonstrate this, we multiply (2.63) by the complex conjugate of w, integrate the resulting expression from 0 to 1, apply the boundary conditions (2.64),(2.65), and solve for λ^2. The result is

$$\lambda^2 = \frac{||w'||^2 + Bg(u_0^*)||V_0||^2(u_0^*)P'(u_0^*)}{||w||^2 + \mu d|w(0)|^2} \tag{2.67}$$

where the norm $||\,||$ is as defined in (2.54) with the limits of integration replaced by 0 and 1. Since the right hand side of (2.67) is a real number, λ^2 is too, and we may conclude that λ is either purely real or purely imaginary. We further note that (2.63) with $\lambda = 0$ shows that zero is not an eigenvalue.

We shall now show that the steady state solutions corresponding to the upper and lower branches of the S-shaped curve are stable, i.e., $\lambda^2 > 0$. This follows from (2.67) and the fact that $P'(u_0^*) > 0$ on these branches, as can be seen from Figure 2.2.

For steady-state solutions lying on the middle branch we see from Figure 2.2 that $P'(u_0^*) < 0$. These solutions will be unstable if the numerator of (2.67) is negative. If this is the case, then $\lambda = ia$ and (2.66) becomes

$$\tanh(a) = -\mu da - \frac{Bg(u_0^*)||V_0||^2(u_0^*)P'(u_0^*)}{a}. \tag{2.68}$$

Equation (2.68) admits real roots, hence the middle branch is unstable. This is clear; for as a tends to zero (infinity) the right hand side tends to positive (negative) infinity and intersects the graph of $\tanh(a)$.

2.5 Dynamics of the Reduced System

In the previous section we analyzed the linear stability of our steady state solutions. The linear stability analysis yields a local result, in this subsection we explore the global behavior of solutions by considering the dynamics of our reduced system. In particular we use results due to Londen [10], and Roberts and Mann [11] to show that bounded solutions of (2.56)-(2.59) monotonically approach the stable steady-state solutions found in the previous subsection.

We begin by recasting the problem (2.56)-(2.59) as a nonlinear Volterra integral equation. This technique has been exploited by Mann and Wolf [12], Chambre [13] and others in the field of heat transfer, and in such diverse areas as superfluidity, population dynamics [14], and shape memory alloys [15]. To derive this integral equation we apply the Laplace transform to the system (2.56)-(2.59), solve the resulting ordinary differential equation, use the convolution theorem to invert, and obtain

$$u_0(x,t) = \int_0^t F(u_0(0,\tau))H(x,t-\tau)d\tau \tag{2.69}$$

where F and H are given by:

$$F(u) = BPg(u)\,||V_0||^2 - BL(u), \tag{2.70}$$

$$H(x,t-\tau) = \frac{1}{1+\mu d} + \sum_{n=0}^{\infty} \frac{2e^{-\alpha_n^2(t-\tau)}\cos(\alpha_n(1-x))}{\cos\alpha_n(1+\mu d+(\mu d\alpha_n))^2} \tag{2.71}$$

and the $\alpha_n's$ are the solutions of

$$\tan(\alpha) = -\mu d\alpha. \tag{2.72}$$

Finally, we evaluate (2.69) at $x = 0$ and obtain the Volterra equation

$$y(t) = \int_0^t F(y(\tau))\kappa(t-\tau)d\tau \tag{2.73}$$

where $\kappa(t-\tau) = H(0,t-\tau)$ and $y(t) = u_0(0,t)$, the temperature at the susceptor-ceramic boundary.

Noting that $\kappa(t)$ is bounded, nonincreasing, and fails to be $L_1(0,\infty)$, while F is continuous on the whole real line, we see that Londen's first theorem applies and we may conclude that any bounded solution of (2.73) satisfies

$$\lim_{t\to\infty} F(y(t)) = 0. \tag{2.74}$$

Therefore bounded solutions of (2.69) approach one of the steady states found in the previous subsection.

Next, we wish to show monotonicity. First, differentiate (2.73) with respect to t and obtain

$$y'(t) = \kappa(0)F(y(t)) + \int_0^t F(y(\tau))\kappa'(t-\tau)d\tau. \tag{2.75}$$

Denote the first zero of F by y_e, we shall prove by contradiction that the solution is trapped between $y = 0$ and $y = y_e$. To see this, assume $y > y_e$ for some time t_1, then by continuity there exists a smallest time t_0 with $t_0 < t_1$ such that $y(t_0) = y_e$ and $y < y_e$ on $[0, t_0)$. But evaluating (2.75) at $t = t_0$ yields $y'(t_0) < 0$, this contradiction implies that $y < y_e$ for all t. Next, note that $y(0) = 0$ and $y'(0) > 0$ and assume $y < 0$ for some time t_1. Then there exists a smallest time $t_0 > 0$ such that $y(t_0) = 0$. Then evaluating (2.73) at $t = t_0$ yields

$$0 = \int_0^{t_0} F(y(\tau))\kappa(t-\tau)d\tau. \tag{2.76}$$

But we have just shown $y < y_e$, hence $F(y(t)) > 0$ on $[0, t_0]$ which implies the integrand of (2.74) is positive, a contradiction.

Since we have shown that y is bounded between zero and the first zero of F, the first theorem of Roberts and Mann [11] applies and we conclude that bounded solutions of (2.73) increase monotonically. Combining the two results we may conclude that bounded solutions of our reduced equations monotonically approach the steady state solutions u_0^* investigated in the previous section.

2.6 Analysis for a Related Geometry

Thus far, we have considered a low-loss ceramic surrounded by lossy susceptors. In applications the converse situation often occurs. That is in Figure 2.1 we take the two outer slabs to be low-loss ceramics and the middle slab to be lossy. In this situation the outer slabs may be referred to as 'insulators' while the inner slab is called the 'target.' Again we adopt this convention. If we make the same symmetry assumptions as above, scale the governing equations in the same manner, and perform the same asymptotic analysis we again obtain a reduced system of equations which represent a leading order asymptotic approximation to the temperatures of the slabs. We note that the scaling is done with regards to the low-loss material. In particular, the length scale is always chosen based on the length of the low-loss material. Our reduced system for this heating problem is

$$\frac{\partial u}{\partial t} = \frac{\partial^2 u}{\partial x^2}, \qquad -1 < x < 0 \tag{2.77}$$

$$\frac{\partial u}{\partial x} = BL(u), \qquad x = -1 \tag{2.78}$$

$$\mu d \frac{\partial u}{\partial t} + \frac{\partial u}{\partial x} = BPG(u), \qquad x = 0 \tag{2.79}$$

$$u(x, 0) = 0. \tag{2.80}$$

Here u is the leading order term of the asymptotic expansion for the solution in the insulator, V is the leading order term for the electric field in the target, and

$$G(u) = g(u) \int_0^d |V|^2 \, dx. \tag{2.81}$$

An expression for V is derived in Appendix B.

We shall briefly analyze the steady state solutions, their related stability, and the dynamical solutions of this system in the following section.

2.7 Steady-State Solutions

We begin by seeking steady-state solutions to our initial boundary value problem (2.77)-(2.80). Setting the time derivatives equal to zero there, integrating the resulting ordinary differential equation, and applying the boundary conditions we find that the steady-state temperature u^* is a linear function of position

$$u^*(x) = a_0 x + a_1 \tag{2.82}$$

where the coefficients a_0 and a_1 satisfy:

$$a_0 = BL(a_1 - a_0) \tag{2.83}$$

$$a_0 = PBG(a_1). \tag{2.84}$$

Here the norm of the electric field in G is evaluated using the temperature in the target, $u^*(0)$. We again assume that g is the exponential function with an appropriate value of β_1.

We may eliminate a_0 from equations (2.83),(2.84) and obtain

$$P = \frac{L(a_1 - PBG(a_1))}{G(a_1)} \tag{2.85}$$

which is reminiscent of the power-response curve derived for the susceptor-ceramic. Since a_1 is the temperature in the target, equation (2.85) represents a power-response curve for the target. In Figure 2.3 we plot equation (2.85) and again obtain an S-shaped curve. The linear profile may be recovered from equation (2.84).

The linear stability of these steady-state solutions will now be analyzed. Towards this end we let

$$u = u^*(x) + w(x)e^{-\lambda^2 t}, \qquad -1 < x < 0 \tag{2.86}$$

where again the perturbation $|w| << 1$. Inserting this ansatz into (2.77)-(2.80), expanding the nonlinear terms in Taylor series, and omitting quadratic and higher

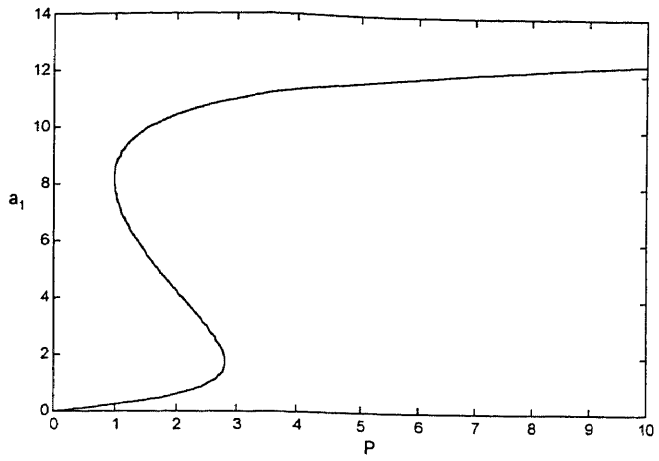

Figure 2.3 Power-response curve for insulated target.

order terms in w, we obtain the linear eigenvalue problem

$$\frac{d^2w}{dx^2} + \lambda^2 w = 0, \qquad -1 < x < 0 \tag{2.87}$$

$$w'(-1) = BL'(u^*(-1))w(-1) \tag{2.88}$$

$$-\mu d\lambda^2 w(0) + w'(0) = PBG'(u^*(0))w(0). \tag{2.89}$$

Solving for w and applying the boundary conditions we find that λ satisfies

$$\tan(\lambda) = -\lambda \frac{BPG'(a_1) - BL'(a_1 - a_0) + \mu d\lambda^2}{\mu d\lambda^2 BL'(a_1 - a_0) + B^2 PL'(a_1 - a_0)G'(a_1) + \lambda^2}. \tag{2.90}$$

The solutions of (2.90) in conjunction with (2.86) determine the stability of the perturbation w; if $Re(\lambda^2) > 0 (< 0)$, then the steady state u_0^* is stable (unstable).

We shall first demonstrate that λ^2 is real. To demonstrate this, we multiply (2.87) by the complex conjugate of w, integrate the resulting expression from -1 to 0, apply the boundary conditions (2.88),(2.89), and solve for λ^2. The result is

$$\lambda^2 = \frac{||w'||^2 + |w(-1)|^2 BL'(a_1 - a_0) - |w(0)|^2 PBG'(a_1)}{\mu d|w(0)|^2 + ||w'||^2}. \tag{2.91}$$

Here the norm on w is over the interval $(-1, 0)$. Since the right hand side of equation (2.91) is real we can again conclude that λ is either purely real or purely imaginary.

A straightforward but tedious analysis shows that real solutions to (2.91) exist for all points on our S-shaped curve. Hence stability is determined by imaginary solutions. If we set $\lambda = ia$ and insert this into (2.90), we obtain

$$\tanh(a) = -a\frac{BPG'(a_1) - BL'(a_1 - a_0) - \mu da^2}{-\mu da^2 BL'(a_1 - a_0) + B^2PL'(a_1 - a_0)G'(a_1) - a^2}. \tag{2.92}$$

Again the analysis of this equation is straightforward but tedious. We do not repeat it here, rather we simply note that for points along the middle branch of our S-shaped curve, equation (2.92) always has a real solution, hence the middle branch is unstable. Further, it may be shown that for points on the upper or lower branches of the S-shaped curve, equation (2.92) never has a real solution, hence these branches are stable.

2.8 Dynamics for the Insulated-Target

In the previous section we investigated the linear stability of steady-state solutions for the insulated-target configuration. We would like to extend this local analysis to determine the global behavior of solutions, i.e., do solutions of our reduced system approach the steady-state solutions found in the previous section? If we again attempt to apply the Laplace transform to our reduced system and convert to an integral equation, we do not arrive at a single non-linear integral equation, but a coupled pair of non-linear Volterra integral equations. The analysis of such systems is daunting and here we resort to numerical techniques.

We apply an explicit finite-difference time-domain scheme to equations (2.77)-(2.80). Some sample solutions are shown in Figures 2.4 and 2.5. We note that if the initial conditions are identically zero, the target temperature monotonically approaches either the upper or lower branch of the S-shaped curve according as the value of the power, P. If the initial conditions are not identically zero, the target temperature need not be a monotonic function of time. For example, if the

initial conditions are constant with a value slightly above a stable branch the target temperature will initially increase before reversing direction and decreasing to the temperature of the nearest point on a stable branch. (See Figures 2.6 and 2.7.) This occurs because losses occur a finite distance away from the target, hence it takes finite time for the effect of those losses to be felt at the target. This is in contrast to the susceptor-ceramic configuration where the effect of losses was felt immediately and the temperature was always a monotonic function of time. Finally, we note that whether monotonically or not, the target temperature always approaches the nearest stable branch of the S-shaped curve.

2.9 Discussion

In order to interpret the results of our analysis it is useful to compare the heating of the composite structures considered above with the heating of solitary lossy and low-loss targets. The heating of solitary targets has been considered by several researchers, here we rely upon the results of Kriegsmann [7, 9], for purposes of comparison. Using an asymptotic analysis based on the assumption of a small Biot number, Kriegsmann derived a steady-state power-response curve for the heating of a solitary slab. Allowing θ to denote the temperature in the solitary slab, E the electric field, and assuming an expansion of the form

$$\theta \sim \theta_0 + B\theta_1 + \cdots \tag{2.93}$$

where B is the Biot number, Kriegsmann found that $\theta_0 = \theta_0(t)$ which in the steady-state satisfies

$$p = \frac{L(\theta_0)}{h(\theta_0)||E_0||^2} \tag{2.94}$$

where here E_0 is the leading order term in the expansion of the electric field and the norm is taken over the single slab. The function L and the parameter p are as in our

model, and h is a non-dimensional conductivity function identical in meaning to our functions g and f.

First, we compare the results for the susceptor-ceramic model with the heating of a solitary low-loss ceramic. Recall that the response curve for the present susceptor-ceramic-susceptor laminate is given by (2.60) under the assumption of an expansion of the form $u \sim u_0 + \delta^{1/2}u_1 + \cdots$. Since u_0 was found to depend only on time, any gradients within the low-loss ceramic must be $O(\delta^{1/2})$ in the steady-state. From (2.93) we see that for a solitary low-loss ceramic thermal gradients are $O(B)$ in the steady-state. For real materials $\delta^{1/2} << B$ which implies that the susceptor acts to smooth thermal gradients. Next, from (2.60) we note that for the laminate case the power axis is in terms of P, while from (2.94) we see that for the solitary low-loss target the power axis is scaled with p or equivalently $P\delta$. This implies that less power is necessary to reach a given temperature when a susceptor is used. This result is in agreement with qualitative experimental observations, [1, 2, 3, 4]. Finally, in Figure 2.8, we plot our power response curve for the laminate configuration for various values of the relative thickness, d. We make two observations. First, as the susceptor thickness is increased the power requirements decrease. This is as expected from our comparison with the heating of a solitary low-loss target. Second, we note that the upper branch of the S-shaped curve is lower for larger d. This may have implications for thermal runaway. If initially the upper branch is above the desired processing temperature the addition of a thicker susceptor may bring the branch down to desired processing temperatures. This may allow thermal runaway to be avoided, however the height of the upper branch also depends on material properties and these must be taken into account in any experimental situation. Again, these observations agree with qualitative experimental observations, [1, 2, 3, 4].

Finally, we compare the results for the insulated target with those of a solitary lossy target. The decreased power requirements and smoother thermal gradients

follows from the same observations made in the susceptor-ceramic case. In Figure 2.9, we plot our power response curve for the insulated target for various values of the relative thickness d. We again note that increased insulation lowers the power requirements. Further we note that the upper branch of the S-shaped curve is again lower for larger d. If for a given thickness of insulation, the upper branch is at the processing temperature, this may imply that the addition of additional insulation may actually increase the power requirements.

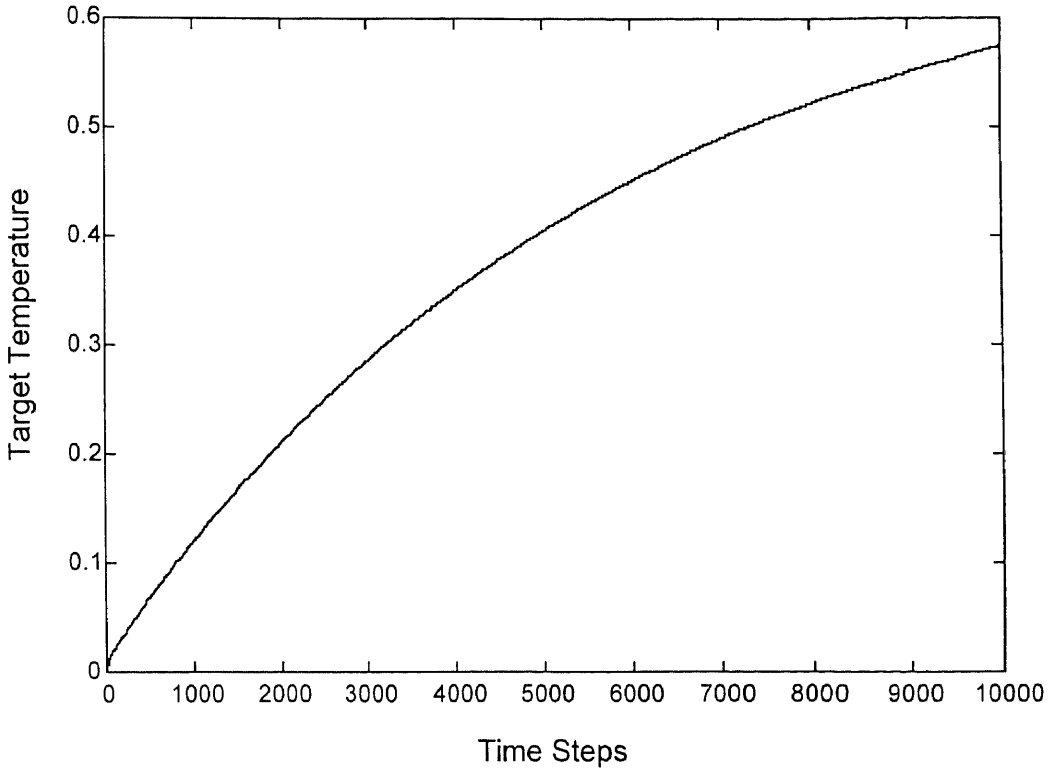

Figure 2.4 Sample solution for insulated target.

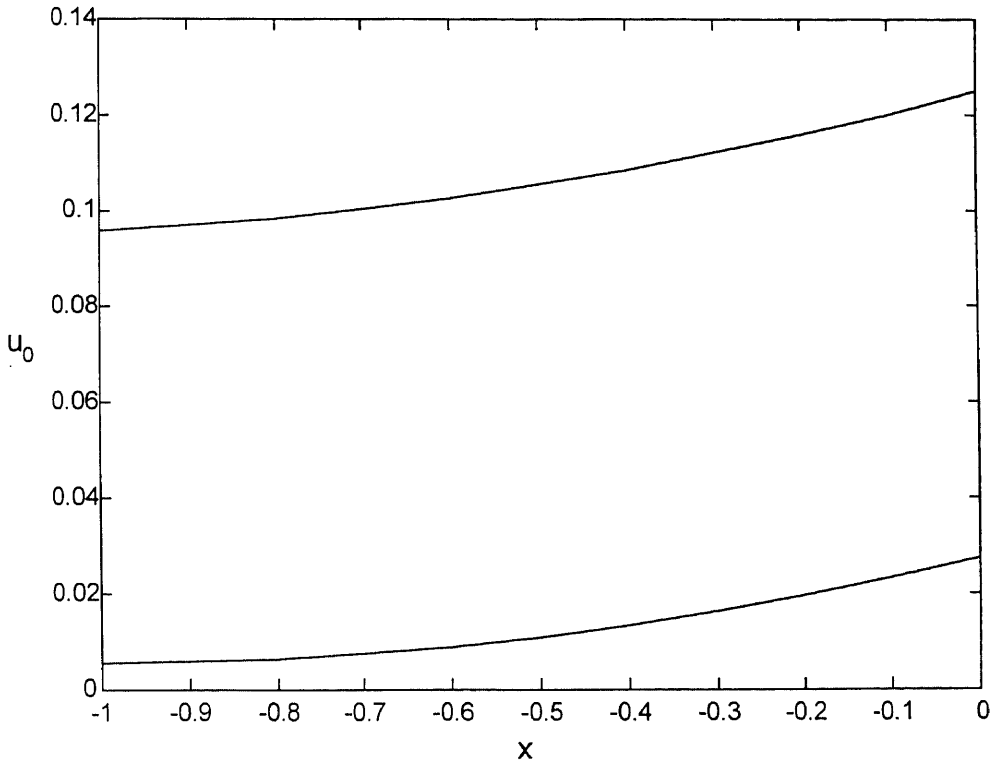

Figure 2.5 Sample solution for insulated target, insulation temperature.

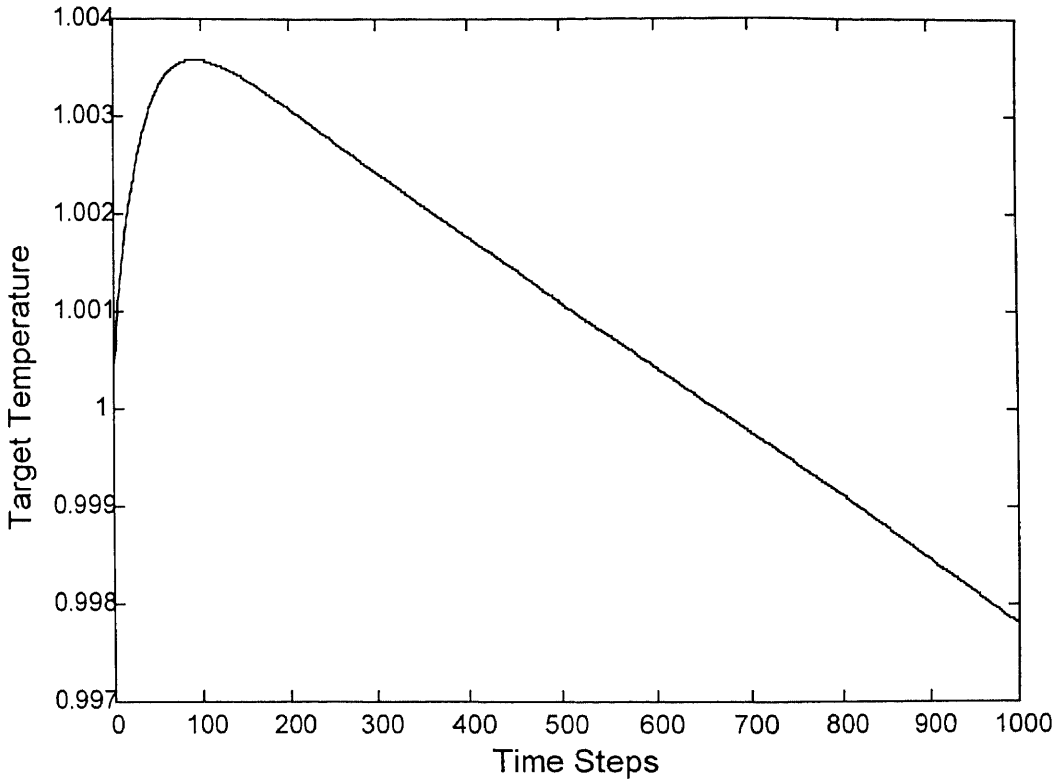

Figure 2.6 Sample solution for insulated target.

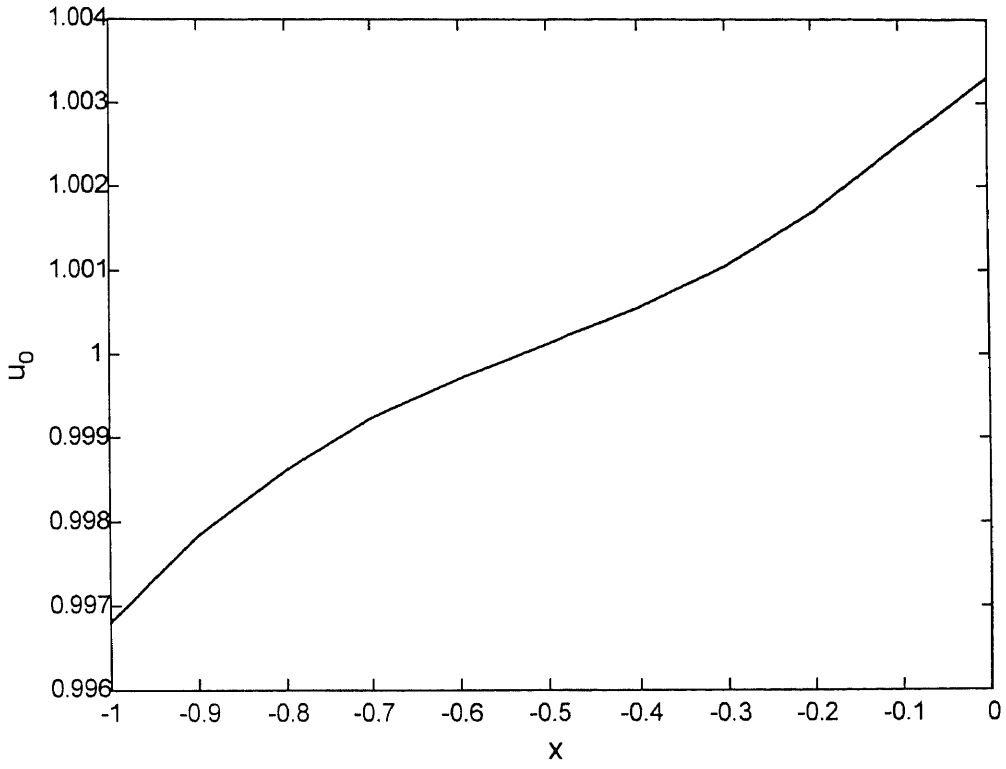

Figure 2.7 Sample solution for insulated target, insulation temperature.

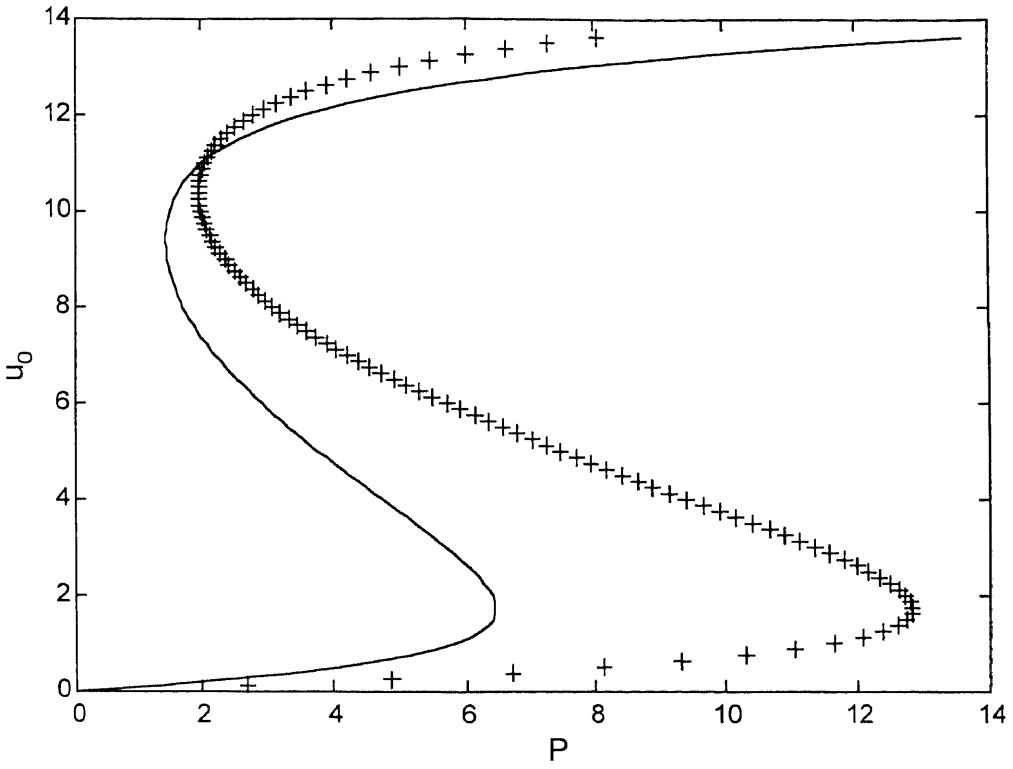

Figure 2.8 Power response curves for susceptor configuration.

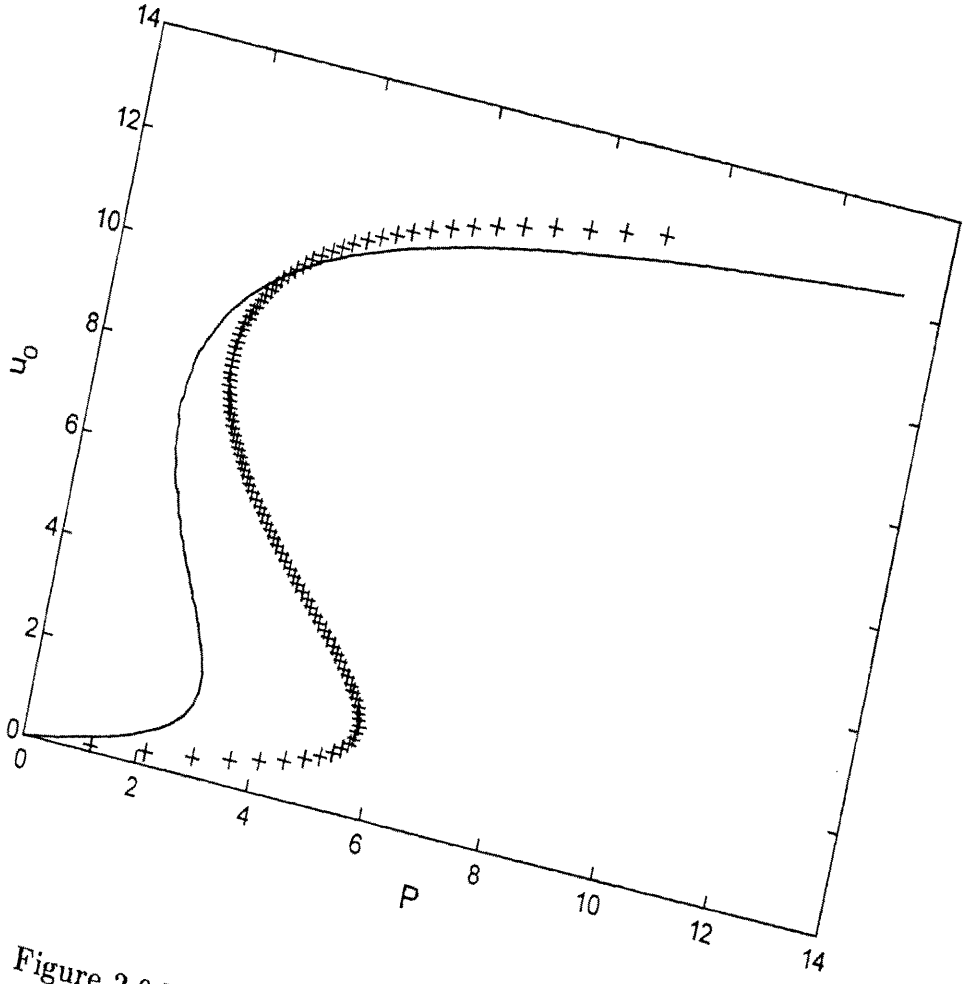

Figure 2.9 Power response curves for insulated target.

CHAPTER 3
MICROWAVE HEATING OF CERAMIC COMPOSITES

In this chapter, we explore another class of hybrid heating schemes. Some investigators have attempted to enhance the microwave absorption of low-loss materials by embedding many small lossy particles in a low-loss ceramic cement or matrix, [5]. With this approach, desirable properties of the low-loss cement, such as formability and strength, may be combined with the strong microwave absorption of the lossy material, to manufacture products with a range of useful features. In order to realize this goal, it is necessary to understand the microwave heating of such composites. In this chapter we construct and analyze a model of these types of composites.

First, in Section 3.1, we formulate the model. The model consists of $M+1$ non-linear partial differential equations, where M is the number of embedded particles. In typical experiments, M is $O(10^3 - 10^{11})$. A non-linear term enters into the governing equations through the temperature dependence of each materials effective electrical conductivity. In general, for ceramics, this is an exponential function of temperature. Non-dimensional variables are then introduced and the equations are written in non-dimensional form. In Section 3.2, we physically interpret the non-dimensional parameters which arise. It is assumed that two parameters may be considered small and of the same order. In particular, the Biot number, which characterizes the relative strengths of convection away from the composite's surface and conduction within the composite is assumed small. In addition, a non-dimensional version of the contact conductance, which characterizes the rate of heat transfer from the embedded particles to the matrix is assumed small. With these two assumptions, an asymptotic theory is developed. The set of $M + 1$ non-linear partial differential equations is reduced to a set of $M + 1$ non-linear first order ordinary differential equations. In Section 3.3, we study these equations. First, we assume that all of the embedded particles are identical. In this case, the system of $M + 1$ equations may

be reduced to a system of two equations. We show that qualitative agreement with experiment is a feature of this model. In particular we study the variation of steady-state temperature with varying particle radii and fixed microwave power. Finally, we study the power-response curve which characterizes heating of these composites.

3.1 Formulation of the Model

We consider the microwave heating of a ceramic composite comprised of M small lossy particles embedded in a low-loss ceramic cement. It is assumed that the particles are uniformly distributed throughout the body, that none of the particles are in direct contact, and that none of the particles are exposed to the external environment. That is, each particle is completely surrounded by the matrix. We denote the ceramic region by Ω', and its outer boundary by ∂'_c, while each particle's region is denoted by Ω'_i, and its outer boundary by ∂'_i. Next, we assume that the electric field is known and constant throughout the sample. This assumption is valid provided the sample size is smaller than an electromagnetic wavelength and it allows us to focus on the thermal aspects of the problem. At typical microwave frequencies, a wavelength is on order of ten centimeters. So, our results are valid for samples characterized by a length scale on order of one to two centimeters.

With these assumptions in mind, we first formulate the equation governing temperature evolution in the cement, i.e. in the region Ω'. The temperature in this region, T_c satisfies:

$$\rho_c c_c \frac{\partial T_c}{\partial t'} = \kappa_c \nabla'^2 T_c + \frac{|E_c|^2}{2} \zeta_c(T_c) \quad \text{in} \quad \Omega' \tag{3.1}$$

where ρ_c denotes density, c_c specific heat, κ_c thermal conductivity, $|E_c|^2$ electric field intensity, ζ_c the effective electrical conductivity, and ∇'^2 is the Laplace operator. Similarly, labeling the temperature in the ith particle by T_i the temperature in

region Ω_i' satisfies:

$$\rho_i c_i \frac{\partial T_i}{\partial t'} = \kappa_i \nabla'^2 T_i + \frac{|E_i|^2}{2}\zeta_i(T_i) \quad \text{in} \quad \Omega_i' \tag{3.2}$$

Here, of course, the parameters and variables have the same meaning as above but refer to the material occupying the ith region.

Next, we formulate the boundary conditions for our problem. Thermal energy is assumed to be convected and radiated at the surface of the sample, hence we assume:

$$\kappa_c \frac{\partial T_c}{\partial n'} + h(T_c - T_A) + s\epsilon(T_c^4 - T_A^4) = 0 \quad \text{on} \quad \partial_c'. \tag{3.3}$$

Here, n' denotes the outward unit normal to the surface, h is a convective heat-transfer coefficient, s is the Stefan-Boltzmann constant, ϵ is the emissivity, and T_A is the ambient temperature of the surrounding environment. Each particle is assumed to be in imperfect thermal contact with the surrounding matrix. Hence on each particle boundary we impose:

$$\kappa_i \frac{\partial T_i}{\partial n_i'} = -\kappa_c \frac{\partial T_c}{\partial n_c'} \quad \text{on} \quad \partial_i' \tag{3.4}$$

$$\kappa_i \frac{\partial T_i}{\partial n_i'} = -k_i(T_i - T_c) \quad \text{on} \quad \partial_i' \tag{3.5}$$

where here, k_i denotes the contact conductance of each boundary region, and the normals are outward unit normals. Finally, we assume that initially the entire sample is at the ambient temperature and impose:

$$T_c(\vec{x}', 0) = T_i(\vec{x}', 0) = T_A. \tag{3.6}$$

Next, we choose dimensionless temperature and length scales, scale the electric field with a reference field amplitude, and rewrite the conductivities as their values at the ambient temperature multiplied by a dimensionless function of the scaled temperature. Further, we scale time with respect to the diffusive time of the cement. This yields the new variables:

$$\theta = \frac{T_c - T_A}{T_A}, \qquad \phi_i = \frac{T_i - T_A}{T_A}, \qquad e_c = \frac{E_c}{E_0}, \qquad e_i = \frac{E_i}{E_0},$$

$$\zeta_c = \sigma_c f(\theta), \qquad \zeta_i = \sigma_i g_i(\phi_i), \qquad t = \frac{\kappa_c t'}{\rho_c c_c L^2}, \qquad \vec{x} = \frac{\vec{x}'}{L}.$$

We have assumed that the sample is characterized by a single length scale, L. When these dimensionless variables are introduced into our governing equations, we obtain:

$$\frac{\partial \theta}{\partial t} = \nabla^2 \theta + pBf(\theta)\,|e_c|^2 \quad \text{in} \quad \Omega \tag{3.7}$$

$$\mu_i \gamma_i \frac{\partial \phi_i}{\partial t} = \nabla^2 \phi_i + \frac{pB\gamma_i}{\delta_i} g_i(\phi_i)\,|e_i|^2 \quad \text{in} \quad \Omega_i \tag{3.8}$$

$$\frac{\partial \theta}{\partial n} + BL(\theta) = 0 \quad \text{on} \quad \partial_c \tag{3.9}$$

$$L(\theta) = \theta + R[(\theta+1)^4 - 1] \tag{3.10}$$

$$\frac{\partial \phi_i}{\partial n} = \gamma_i \frac{\partial \theta}{\partial n} \quad \text{on} \quad \partial_i \tag{3.11}$$

$$\frac{\partial \phi_i}{\partial n} + B_i(\phi_i - \theta) = 0 \quad \text{on} \quad \partial_i \tag{3.12}$$

$$\theta(\vec{x}, 0) = \phi_i(\vec{x}, 0) = 0. \tag{3.13}$$

Here, the unprimed symbols denoting regions or boundaries refer to scaled versions of these regions, similarly unprimed normals are dimensionless outward pointing unit normals. Further, the parameters in the above equations are defined as:

$$\mu_i = \frac{\rho_i c_i}{\rho_c c_c}, \qquad \gamma_i = \frac{\kappa_c}{\kappa_i}, \qquad p = \frac{E_0^2 \sigma_c L}{2hT_A}, \qquad \delta_i = \frac{\sigma_c}{\sigma_i},$$

$$B = \frac{hL}{\kappa_c}, \qquad R = \frac{s\epsilon T_A^3}{h}, \qquad B_i = \frac{k_i L}{\kappa_i}.$$

3.2 An Asymptotic Theory

In this section, we develop an asymptotic theory which allows us to reduce our set of $M+1$ non-linear pde's to a set of $M+1$ non-linear ode's. First, let us consider the non-dimensional parameters which arose when we scaled the governing equations. The parameter μ_i may be interpreted as a relative heat capacity as it is simply a ratio of the heat capacity of the ith particle to the heat capacity of the cement. Similarly,

γ_i is a relative thermal conductivity, appearing as a ratio of the thermal conductivity in the cement to the thermal conductivity in the ceramic. The parameter p is a non-dimensional power. In particular it is a ratio of a reference microwave power absorbed by the cement to a reference power lost at the surface due to convection. The parameter δ_i is the ratio of room temperature electrical conductivities in the cement and the ith material, hence it is simply a relative electrical conductivity. The parameter B, which is known as the Biot number, measures the relative strengths of convection and conduction. The parameter R is simply the radiative equivalent of the Biot number. Finally, the parameter B_i is similar to the Biot number, but measures the relative strengths of conduction across a particle surface to conduction within the particle.

Next, in order to develop an asymptotic theory, we need to order our parameters. Since we would like our model to be general enough to include materials which are not too disparate thermally or electrically, we take the parameters μ_i,γ_i and δ_i to be $O(1)$. Further, the power p, and the radiative Biot number, R, are also assumed to be $O(1)$. The first assumption implies that power absorbed is the same order of magnitude as power lost, the second allows the effects of radiation and convection to be weighted equally in our model. Next, we assume that the Biot number B is a small parameter. This is equivalent to assuming that the composite is well insulated, which is true in typical experimental situations, [5]. Finally, we assume that the parameters B_i, are small and are the same order as the Biot number. We rescale by setting $B_i = \beta_i B$, where the β_i are $O(1)$. Here, we are assuming that it is easier to transport heat through a particle than it is to transport heat through the particles surface.

With these assumptions, we attempt a regular perturbation expansion, by assuming power series solutions in the form:

$$\theta \sim \theta_0 + B\theta_1 + \cdots$$

$$\phi_i \sim \phi_{i0} + B\phi_{i1} + \cdots.$$

Inserting these into our governing equations, (3.7)-(3.13), expanding the non-linear terms in Taylor series, and equating to zero the coefficients of the powers of B, we obtain an infinite set of equations which sequentially should determine the θ_n and ϕ_{in}. A quick glance at our governing equations however, shows that this approach is flawed. In particular it is easy to see that the leading order solutions will be identically zero, while the $O(B)$ solutions will depend linearly on time. To rectify this situation, we rescale the time variable with the Biot number, $\tau = Bt$, and employ the technique of asymptotic matching. Here, since the leading order solutions are identically zero, the matching is trivial. That is, the long time behavior of the leading order solution on the t time scale gives the initial conditions for the leading order solution on the τ time scale, but here the initial conditions do not change, i.e. this boundary layer in time is empty. So, we may proceed to analyze our rescaled equations, these are:

$$B\frac{\partial\theta}{\partial\tau} = \nabla^2\theta + pBf(\theta)\,|e_c|^2 \quad \text{in} \quad \Omega \tag{3.14}$$

$$B\mu_i\gamma_i\frac{\partial\phi_i}{\partial\tau} = \nabla^2\phi_i + \frac{pB\gamma_i}{\delta_i}g_i(\phi_i)\,|e_i|^2 \quad \text{in} \quad \Omega_i \tag{3.15}$$

$$\frac{\partial\theta}{\partial n} + BL(\theta) = 0 \quad \text{on} \quad \partial_c \tag{3.16}$$

$$L(\theta) = \theta + R[(\theta+1)^4 - 1] \tag{3.17}$$

$$\frac{\partial\phi_i}{\partial n} = \gamma_i\frac{\partial\theta}{\partial n} \quad \text{on} \quad \partial_i \tag{3.18}$$

$$\frac{\partial\phi_i}{\partial n} + B\beta_i(\phi_i - \theta) = 0 \quad \text{on} \quad \partial_i \tag{3.19}$$

$$\theta(\vec{x},0) = \phi_i(\vec{x},0) = 0. \tag{3.20}$$

Technically, we should relabel our dependent variables, as they are now functions of τ; to avoid confusing notation, we shall simply remember that this is true and leave the variable names alone. Now, we again attempt an expansion in the form:

$$\theta \sim \theta_0 + B\theta_1 + \cdots$$

$$\phi_i \sim \phi_{i0} + B\phi_{i1} + \cdots.$$

Inserting these into our rescaled equations, (3.14)-(3.20), expanding non-linear terms in a Taylor series, and equating to zero coefficients of powers of B, we obtain:

$$\nabla^2\theta_0 = 0 \quad \text{in} \quad \Omega \tag{3.21}$$

$$\nabla^2\phi_{i0} = 0 \quad \text{in} \quad \Omega_i \tag{3.22}$$

$$\frac{\partial\theta_0}{\partial n} = 0 \quad \text{on} \quad \partial_c \tag{3.23}$$

$$\frac{\partial\phi_{i0}}{\partial n} = \gamma_i\frac{\partial\theta_0}{\partial n} \quad \text{on} \quad \partial_i \tag{3.24}$$

$$\frac{\partial\phi_{i0}}{\partial n} = 0 \quad \text{on} \quad \partial_i \tag{3.25}$$

$$\theta_0(\vec{x},0) = \phi_{i0}(\vec{x},0) = 0. \tag{3.26}$$

and

$$\frac{\partial\theta_0}{\partial\tau} = \nabla^2\theta_1 + pf(\theta_0)\left|e_c\right|^2 \quad \text{in} \quad \Omega \tag{3.27}$$

$$\mu_i\gamma_i\frac{\partial_0\phi_i}{\partial\tau} = \nabla^2\phi_{i1} + \frac{p\gamma_i}{\delta_i}g_i(\phi_{i0})\left|e_i\right|^2 \quad \text{in} \quad \Omega_i \tag{3.28}$$

$$\frac{\partial\theta_1}{\partial n} + L(\theta_0) = 0 \quad \text{on} \quad \partial_c \tag{3.29}$$

$$\frac{\partial\phi_{i1}}{\partial n} = \gamma_i\frac{\partial\theta_1}{\partial n} \quad \text{on} \quad \partial_i \tag{3.30}$$

$$\frac{\partial\phi_{i1}}{\partial n} + \beta_i(\phi_{i0} - \theta_0) = 0 \quad \text{on} \quad \partial_i \tag{3.31}$$

$$\theta_1(\vec{x},0) = \phi_{i1}(\vec{x},0) = 0 \tag{3.32}$$

where we have only given the first two sets of equations, these are sufficient to determine the leading order behavior.

We begin our analysis by noting that equations (3.21)-(3.26) immediately imply that $\theta_0 = \theta_0(\tau)$ and $\phi_{i0} = \phi_{i0}(\tau)$, that is our leading order solutions are functions of time only. Next, we derive a system of ordinary differential equations which

determine the evolution of θ_0 and ϕ_{i0}. We integrate equation (3.27) over the volume Ω to obtain:

$$V_c \frac{d\theta_0}{d\tau} = \int_\Omega \nabla^2 \theta_1 + pf(\theta_0) \, ||e_c||^2 \tag{3.33}$$

where here:

$$||e_c||^2 = \int_\Omega |e_c|^2 \tag{3.34}$$

and V_c denotes the volume of the cement. Now, we use the divergence theorem to rewrite the integral as a surface integral and apply the boundary conditions (3.29)-(3.31) to obtain:

$$\int_\Omega \nabla^2 \theta_1 = -S_c L(\theta_0) + \sum_i \frac{\beta_i S_i}{\gamma_i} (\phi_{i0} - \theta_0) \tag{3.35}$$

where here, S_c is the surface area of the cement, S_i is the surface area of the ith particle, and the summation is over all M particles. Inserting equation (3.35) into equation (3.33) yields:

$$V_c \frac{d\theta_0}{d\tau} = pf(\theta_0) \, ||e_c||^2 - S_c L(\theta_0) + \sum_i \frac{\beta_i S_i}{\gamma_i} (\phi_{i0} - \theta_0). \tag{3.36}$$

Next, integrating equation (3.28) over Ω_i, using the divergence theorem in the same manner as above, and using the boundary conditions, (3.29)-(3.31), we obtain:

$$\mu_i \gamma_i V_i \frac{d\phi_{i0}}{d\tau} = \frac{p\gamma_i}{\delta_i} g_i(\phi_{i0}) \, ||e_i||^2 - \beta_i S_i (\phi_{i0} - \theta_0) \tag{3.37}$$

where here V_i denotes the volume of the ith particle. Equations (3.36) and (3.37) together with the appropriate initial conditions constitute a set of $M + 1$ non-linear coupled ordinary differential equations for the leading order behavior of the temperature in the cement and in each particle.

3.3 Analysis of the Reduced System

In the previous section we developed an asymptotic theory based on a small Biot number and small contact conductance assumption. This allowed us to reduce our

system of non-linear pde's to the following system of non-linear ode's:

$$V_c \frac{d\theta_0}{d\tau} = pf(\theta_0) \left|\left|e_c\right|\right|^2 - S_c L(\theta_0) + \sum_i \frac{\beta_i S_i}{\gamma_i}(\phi_{i0} - \theta_0) \tag{3.38}$$

$$\mu_i \gamma_i V_i \frac{d\phi_{i0}}{d\tau} = \frac{p\gamma_i}{\delta_i} g_i(\phi_{i0}) \left|\left|e_i\right|\right|^2 - \beta_i S_i(\phi_{i0} - \theta_0). \tag{3.39}$$

These equations are still completely general, that is, each particle is allowed to have unique material properties, size etc. In typical experiments, only one or two species of particles are used. In this section, we further simplify our system of equations by making assumptions about the variety of particles embedded in our cement; namely, throughout this section, we will assume that all of the embedded particles are identical. Then, recalling our assumption that the electric field is constant throughout the entire sample, and that the initial conditions are the same for all particles, our set of $M+1$ equations may be reduced to two equations. First, equation (3.38) simplifies to:

$$V_c \frac{d\theta_0}{d\tau} = pV_c f(\theta_0) - S_c L(\theta_0) + \frac{\beta S_p}{\gamma}(\phi_0 - \theta_0) \tag{3.40}$$

where here S_p denotes the total surface area of all the embedded particles, subscripts on β and γ have been dropped to indicate that they refer to the properties of any given particle, and ϕ_{i0} has been replaced by ϕ_0 to indicate that we need only track the temperature of one particle. To obtain an equation for ϕ_0 we may select any one of the M equations, (3.39), selecting any one of these and multiplying by M for convenience yields:

$$\mu\gamma V_p \frac{d\phi_0}{d\tau} = \frac{pV_p\gamma}{\delta} g(\phi_0) - \beta S_p(\phi_0 - \theta_0) \tag{3.41}$$

where here, V_p denotes the total volume of all the embedded particles and subscripts have been dropped to indicate that the material properties are identical for all particles. In the remainder of this section, we study equations (3.40) and (3.41) in a variety of situations.

3.3.1 A Linear Model

In this subsection we further simplify our model to arrive at a linear system of ordinary differential equations. Although our assumptions are not strictly valid in most experimental situations, it is useful to examine this simplified theory to illuminate specific effects observed in experiment, and to illustrate the role played by key parameters in controlling these effects.

To obtain a linear theory we make several assumptions. First, we assume that $R = 0$, hence $L(\theta_0) = \theta_0$. Next, we assume that $g(\phi_0) = 1$. Then, we assume that $p = P\delta$ and take the limit as $\delta \to 0$. Physically, we are considering the limit where the cement is microwave transparent and the conductivity of the particles is constant. This yields:

$$V_c \frac{d\theta_0}{d\tau} = -S_c\theta_0 + \frac{\beta S_p}{\gamma}(\phi_0 - \theta_0) \tag{3.42}$$

$$\mu\gamma V_p \frac{d\phi_0}{d\tau} = PV_p\gamma - \beta S_p(\phi_0 - \theta_0). \tag{3.43}$$

We begin our analysis of this system by locating the stationary or critical points. Setting the time derivatives to zero, we find this system has a unique stationary point, (θ_0^*, ϕ_0^*), located at:

$$\theta_0^* = \frac{PV_p}{S_c}, \qquad \phi_0^* = PV_p(\frac{1}{S_c} + \frac{\gamma}{\beta S_p}).$$

We notice that the steady-state temperatures of the particles and the cement are different. This leads us to inquire as to what temperature is actually measured experimentally. Since the diameter of a typical thermocouple inserted into the sample is much larger than a particle diameter, it seems reasonable to assume that the experimentally measured temperature is some weighted average of particle and cement temperatures.

If we multiply equation (3.43) by γ^{-1} and add our two equations, we obtain:

$$\frac{d}{d\tau}(V_c\theta_0 + \mu V_p\phi_0) = PV_p - S_c\theta_0. \tag{3.44}$$

The right hand side is simply the net power into the sample, this suggests that we define:

$$\psi = \frac{V_c\theta_0 + \mu V_p\phi_0}{V_c + \mu V_p} \tag{3.45}$$

as the mean sample temperature. We note that this can be rewritten as:

$$\psi = \frac{\theta_0 + (C_p/C_c)\phi_0}{1 + (C_p/C_c)} \tag{3.46}$$

where C_p and C_c are the total heat capacities of the particles and cement respectively. Then, the mean steady-state temperature is given by:

$$\psi^* = \frac{PV_p}{S_c} + \frac{PV_p\gamma}{\beta S_p}\frac{(C_p/C_c)}{(1 + (C_p/C_c))}. \tag{3.47}$$

Now, we may make some qualitative comparisons with experiment. As mentioned in the introduction, it has been observed that the steady-state temperature of the sample decreases with decreasing particle radii, [5]. It is important to note that in these experiments the total mass of the embedded particles is held constant. This implies that in equation (3.47) only the parameter S_p varies with particle radii. Recall that this is a scaled version of the total particle surface area. With the total mass held constant, this parameter increases with decreasing particle radii, hence the mean steady-state temperature decreases with decreasing particle radii, in agreement with experimental observations. Further experiments were carried out in which it was observed that the steady-state temperature increased as additional particles were added to the matrix. We may rewrite our steady-state temperature in terms of the number of particles:

$$\psi^* = \frac{PMV_i}{S_c} + \frac{PV_i\gamma}{\beta S_i}\frac{(Mc_p/C_c)}{(1 + (Mc_p/C_c))} \tag{3.48}$$

where here c_p is the heat capacity of a single particle. Equation (3.48) is easily seen to be an increasing function of M, again in agreement with experimental observations.

Next, we investigate the stability of the steady-state solution. To do so, we rewrite our equations in matrix form:

$$\frac{d}{d\tau}\begin{bmatrix}\theta_0\\ \phi_0\end{bmatrix} = \begin{bmatrix}-(\frac{\beta S_p}{\gamma V_c}+\frac{S_c}{V_c}) & \frac{\beta S_p}{\gamma V_c}\\ \frac{\beta S_p}{\mu\gamma V_p} & -\frac{\beta S_p}{\mu\gamma V_p}\end{bmatrix}\begin{bmatrix}\theta_0\\ \phi_0\end{bmatrix} + \begin{bmatrix}0\\ \frac{P}{\mu}\end{bmatrix}. \tag{3.49}$$

Stability of the steady-state solution will be determined by the eigenvalues of the above matrix. These are easily seen to satisfy:

$$\lambda^2 + \left(\frac{\beta S_p}{\gamma V_c}+\frac{S_c}{V_c}+\frac{\beta S_p}{\mu\gamma V_p}\right)\lambda + \frac{\beta S_p S_c}{\mu\gamma V_c V_p} = 0. \tag{3.50}$$

Since all coefficients are positive, both eigenvalues have a negative real part. Hence, our steady-state solution is stable. We may further inquire as to whether this critical point is a sink or a focus. By examining the discriminant of the eigenvalue equation, we see that the eigenvalues will be strictly real provided that:

$$\frac{C_p}{C_c} \leq 1.$$

If this condition is satisfied, the approach to the steady-state is monotonic. If it is violated, the approach to the steady-state becomes oscillatory. In typical experiments this condition is satisfied. Finally, in Figure 3.1, we plot ψ as a function of time for various values of S_p. We again note that the solutions approach the steady-state monotonically, and that the final value is dependent on S_p.

3.3.2 A Simplified Non-Linear Theory

In this subsection, we consider our two equation model with two non-linear terms retained. As in the previous subsection, we assume $p = P\delta$ and let $\delta \to 0$, but here we do not assume $R = 0$ nor that $g = 1$. That is, we consider:

$$V_c\frac{d\theta_0}{d\tau} = -S_c L(\theta_0) + \frac{\beta S_p}{\gamma}(\phi_0 - \theta_0) \tag{3.51}$$

$$\mu\gamma V_p\frac{d\phi_0}{d\tau} = PV_p\gamma g(\phi_0) - \beta S_p(\phi_0 - \theta_0). \tag{3.52}$$

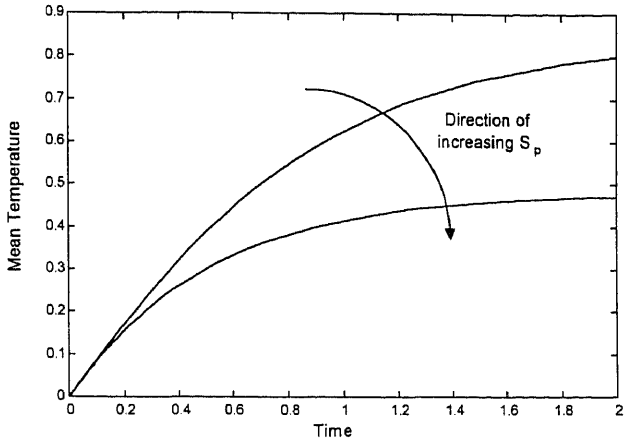

Figure 3.1 Mean temperature, linear theory.

Physically, we are assuming that the cement is essentially microwave transparent at all temperatures, i.e. it is low-loss. However, we are including radiative losses and the temperature dependence of the particle's electrical conductivity.

Again, we begin our analysis by looking for stationary solutions, (θ_0^*, ϕ_0^*). We find that stationary solutions must satisfy:

$$\frac{\beta S_p}{\gamma}(\phi_0^* - \theta_0^*) - S_c L(\theta_0^*) = 0$$

$$P\gamma V_p g(\phi_0^*) - \beta S_p(\phi_0^* - \theta_0^*) = 0.$$

We may solve the first of these equations for ϕ_0^* and eliminate in favor of θ_0^* in the second to obtain:

$$P = \frac{S_c L(\theta_0^*)}{V_p g(\theta_0^* + \frac{\gamma S_c}{\beta S_p} L(\theta_0^*))}. \tag{3.53}$$

This is reminiscent of a typical power-response curve for a homogenous material, [9]. In order to pursue the analysis further, we must choose a specific form for the function g. Recall that g is the non-dimensional electrical conductivity function for the particles. Examination of conductivity data [8] reveals that this is typically an

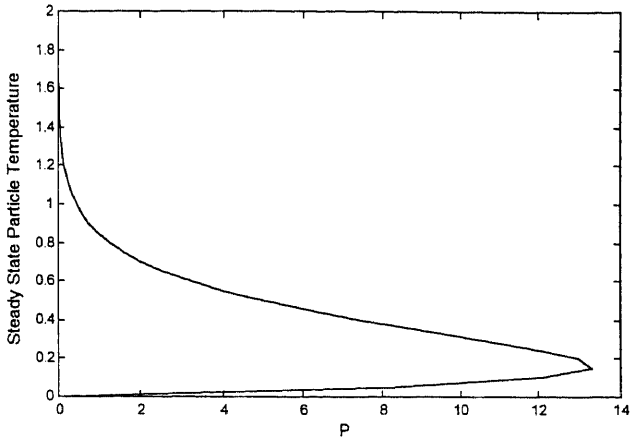

Figure 3.2 Power response curve, non-linear theory.

exponential function of temperature. Thus we take:

$$g(\phi_0^*) = e^{\alpha\phi_0^*} \tag{3.54}$$

where the constant α, depends upon the nature of the particular material. In general we cannot explicitly solve (3.53) for θ_0^* as a function of P. However, this analysis can be done graphically as shown in Figure 3.2, where P is plotted as a function of θ_0^* and the axis are reversed. Note that this power response curve has only two branches, in contrast to the typical S-shaped power-response curves usually observed. Recall that we have assumed that the electric field is a constant, in [9] it was shown that for homogeneous materials temperature variations of the electric field produces a skin effect which causes the upper branch of the S-shaped curve. In addition, in the previous chapter it was shown that a similar phenomenon occurs in the heating of ceramic laminates composed of two electrically disparate materials. We do not do this here, rather we simply conjecture that our upper branch will be restored if the full electric field was computed as a function of temperature. That is, we conjecture that temperature variations of the electric field will produce a skin effect and add an upper branch to our power-response curve.

We may study the stability of our steady-state solutions by linearizing our governing equations near each critical point. We carry this out by first inserting the ansatz:

$$\theta_0 = \theta_0^* + Ae^{\lambda\tau}$$

$$\phi_0 = \phi_0^* + Be^{\lambda\tau}$$

into our governing equations and expanding non-linear terms in a Taylor series. We find that λ satisfies:

$$\lambda^2 + \left(\frac{\beta S_p}{\gamma V_c} + \frac{S_c L'(\theta_0^*)}{V_c} + \frac{\beta S_p}{\mu\gamma V_p} - \frac{Pg'(\phi_0^*)}{\mu}\right)\lambda + \frac{\beta S_p g(\phi_0^*) P'(\theta_0^*)}{\mu\gamma V_p V_c} = 0. \tag{3.55}$$

Here P' denotes differentiation of P as a function of θ_0^*, g' differentiation of g as a function of ϕ_0^*, and L' differentiation of L as a function of θ_0^*. As can be seen in Figure 3.2, $P'(\theta_0^*)$ is negative on the upper branch, this immediately implies that solutions on the upper branch are unstable saddle points. Points on the lower branch are stable if and only if the coefficient of λ is positive. If $C_p/C_c \leq 1$, as is typically the case, then:

$$\frac{S_c L'(\theta_0^*)}{V_c(C_p/C_c)} - \frac{Pg'(\phi_0^*)}{\mu} \leq \frac{S_c L'(\theta_0^*)}{V_c} - \frac{Pg'(\phi_0^*)}{\mu}. \tag{3.56}$$

However, we find that:

$$\frac{S_c L'(\theta_0^*)}{V_c(C_p/C_c)} - \frac{Pg'(\phi_0^*)}{\mu} = \frac{P'(\theta_0^*)g(\phi_0^*)}{\mu} + \frac{Pg'(\phi_0^*)L'(\theta_0^*)S_c\gamma}{\mu\beta S_p}. \tag{3.57}$$

Hence, on the lower branch, we have a positive lower bound on two terms in the coefficient of λ. The remaining terms are already positive, hence solutions on the lower branch are stable.

Again, we note that the steady-state solutions for θ_0^* and ϕ_0^* are different. Combining our governing equations as in the previous subsection, we obtain:

$$\frac{d}{d\tau}(V_c\theta_0 + \mu V_p\phi_0) = PV_p g(\phi_0) - S_c L(\theta_0). \tag{3.58}$$

This again suggests that we again define a mean temperature of the sample as:

$$\psi = \frac{\theta_0 + (C_p/C_c)\phi_0}{1 + (C_p/C_c)} \tag{3.59}$$

and hypothesize that this is the temperature observed in experiment. In the same manner as described above, a power-response curve may be plotted for ψ. If again, we hold the total mass of embedded particles fixed, while varying their radii we may study variations in this power-response curve. An example is shown in Figure 3.3. We note that the height of the lower branch decreases with decreasing particle radii, while the height of the upper branch increases. If we assume that the lower branch is stable, as discussed above, we again see that steady-state temperatures of the sample decrease with decreasing particle radii. Finally, in Figure 3.4, we plot numerical solutions for ψ as a function of τ for various values of S_p.

3.3.3 Non-Transparent Cement

In this subsection, we consider the case where the cement is not transparent to microwaves. Thus, we retain all terms, that is we consider:

$$V_c \frac{d\theta_0}{d\tau} = pV_c f(\theta_0) - S_c L(\theta_0) + \frac{\beta S_p}{\gamma}(\phi_0 - \theta_0) \tag{3.60}$$

$$\mu\gamma V_p \frac{d\phi_0}{d\tau} = \frac{pV_p\gamma}{\delta} g(\phi_0) - \beta S_p(\phi_0 - \theta_0). \tag{3.61}$$

We begin by looking for steady-state solutions, which now must satisfy:

$$pV_c f(\theta_0^*) - S_c L(\theta_0^*) + \frac{\beta S_p}{\gamma}(\phi_0^* - \theta_0^*) = 0$$

$$\frac{pV_p\gamma}{\delta} g(\phi_0^*) - \beta S_p(\phi_0^* - \theta_0^*) = 0.$$

We can rewrite as:

$$\phi_0^* = \theta_0^* + \frac{\gamma S_c}{\beta S_p} L(\theta_0^*) - p\frac{\gamma V_c}{\beta S_p} f(\theta_0^*)$$

$$p = \frac{S_c L(\theta_0^*)}{V_c f(\theta_0^*) + \frac{V_p}{\delta} g(\phi_0^*)}.$$

Note that in contrast to our previous results, we cannot write p as an explicit function of θ_0^*. This makes our steady-state solution difficult to analyze in general. Here, we consider a special case.

We assume that the conductivity of the particles is a very weak function of temperature and take $g = 1$. This simplifies our steady-state solutions and allows us to write:

$$\phi_0^* = \theta_0^* + \frac{pV_P\gamma}{\delta\beta S_p}$$

$$p = \frac{S_c L(\theta_0^*)}{V_c f(\theta_0^*) + \frac{V_p}{\delta}}.$$

In the same manner as discussed in the previous subsection, we can now sketch a power-response curve by regarding p as a function of θ_0^*. We do this in Figure 3.5. Note that this power-response curve has the same form as those previously considered, however here it is the variation of the cement conductivity with temperature that provides us with the upper branch. Once again we investigate the stability of these solutions by inserting the ansatz:

$$\theta_0 = \theta_0^* + Ae^{\lambda\tau}$$

$$\phi_0 = \phi_0^* + Be^{\lambda\tau}$$

into our governing equations and expanding non-linear terms in a Taylor series. Here, we find that λ satisfies:

$$\lambda^2 + \left(\frac{\beta S_p}{\mu\gamma V_p} + \frac{\beta S_p}{\gamma V_c} + p'(\theta_0^*)(f(\theta_0^*) + \frac{V_p}{\delta V_c})\right)\lambda + \frac{\beta S_p}{\mu\gamma V_p}(f(\theta_0^*) + \frac{V_p}{\delta V_c})p'(\theta_0^*) = 0 \quad (3.62)$$

where the prime on p denote differentiation with respect to θ_0^*. Now, by noting that p' is positive on the lower branch and negative on the upper branch, we immediately see that the lower branch is stable, while the upper branch is unstable.

Finally, we note that as in the previous examples, the same mean temperature, ψ, may be defined as:

$$\psi = \frac{\theta_0 + (C_p/C_c)\phi_0}{1 + (C_p/C_c)} \tag{3.63}$$

and again hypothesize that this is the experimentally observed temperature. Numerical solutions for ψ are shown in Figure 3.6, again illustrating variations with varying particle radii.

3.4 Discussion

In this chapter we began by constructing a model of the microwave heating of a ceramic composite consisting of many lossy ceramic particles embedded within a low-loss ceramic cement. This model was simplified asymptotically. Two key assumptions were made. First, we assumed that the Biot number was small. That this is the regime of interest is clear; in most experiments the samples are well insulated. We also assumed that the non-dimensional contact conductance, B_i, was a small parameter. That this should be true is not as obvious. Further, there are very few measured values of contact conductance available. We note however, that this assumption is strongly suggested by experimental evidence combined with a mathematical observation. As discussed previously, steady-state temperatures are observed to vary strongly with particle radii, even as the total mass of the embedded particles is held constant. Discounting the electric field, which should not vary significantly under these circumstances, the only parameter varied in these experiments is the total surface area of the embedded particles, S_p. So, in any correct model, the leading order approximation to the steady-state temperature should vary with S_p. In the limit of perfect thermal contact, these variations disappear from the solution. This suggests that B_i is not large. Further, if B_i is taken to be $O(1)$, then to leading order, the temperature is constant throughout the sample and again variations with

S_p disappear from the leading order solution. That suggests that B_i is indeed a small parameter.

Next, we studied our reduced equations in various simplified situations. We began by considering the limit where the cement was microwave transparent, the conductivity of the particles was constant, and radiative effects could be ignored. We noted that there was a need to define a mean temperature and we hypothesized that this was the temperature measured in experiment. We saw that observed experimental results, could be explained as a geometric effect; variations in the total surface area of the embedded particles correspond to the observed behavior for varying particle radii.

In Subsection 3.3.2, we again considered the cement to be microwave transparent, but incorporated the nonlinear temperature dependence of the particle's conductivity. We saw that a multi-valued power-response curve was the result. Solutions on the upper branch were always unstable, while solutions on the lower branch were stable. It is interesting to consider this power-response curve in the context of thermal runaway. In homogeneous materials, sudden uncontrolled heating of the material occurs once the power is turned past some critical value. On any of our power response curves, this would correspond to turning the power past the 'nose' of the curve. Here, the same phenomena occurs. However, we see that by varying particle properties, the location of this 'nose' may be varied. In particular, by simply increasing S_p, i.e. by using smaller particles, the 'nose' moves up an to the right. This allows stable heating of the composite at higher temperatures.

In Subsection 3.3.3, we considered the case where the particle conductivity could be regarded as constant, while the cement conductivity was an exponential function of temperature. We noted that the structure of the power-response curve was now controlled by the cement. Here again, we observed that steady-state temperatures could be controlled by varying particle radii.

Finally, we note that we have barely scratched the surface in analyzing our system of $M + 1$ non-linear ordinary differential equations. Here, we have used simplified versions of our full model to explain qualitatively various observed physical phenomena. If in these simple cases, the quantitative validity of this model could be confirmed, i.e. if extensive enough experimental data becomes available so that such an analysis could be carried out, we would suggest that this model might be useful in designing composites with tailor made microwave heating properties.

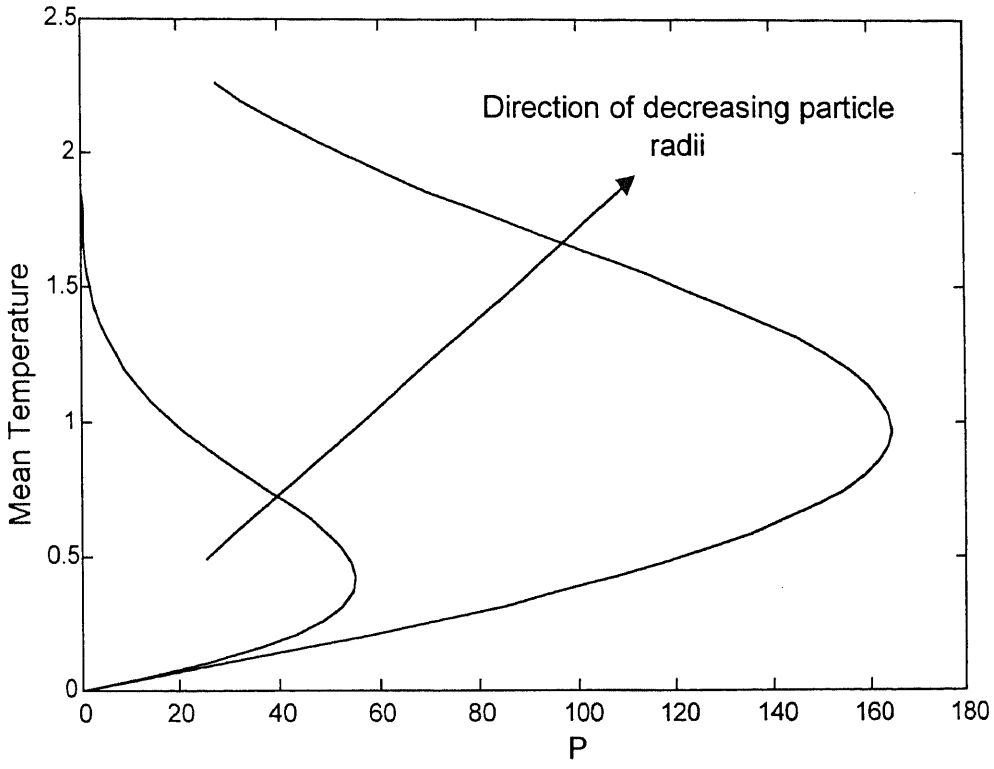

Figure 3.3 Variation in power-response curve with particle radii.

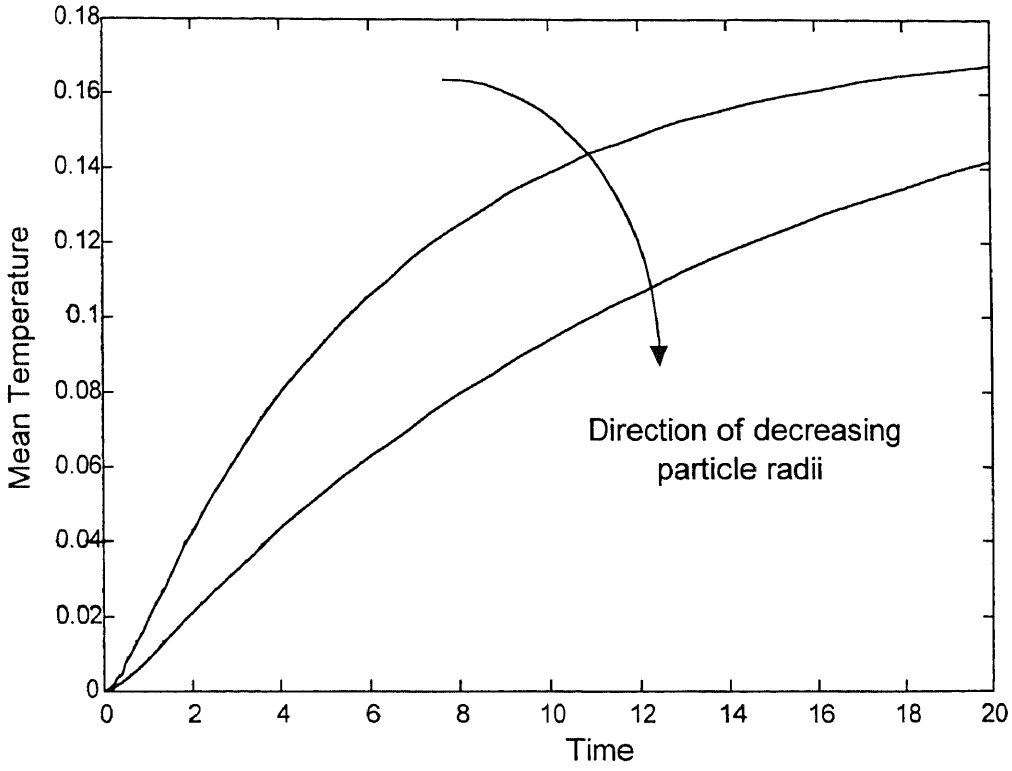

Figure 3.4 Variation of mean temperature with particle radii.

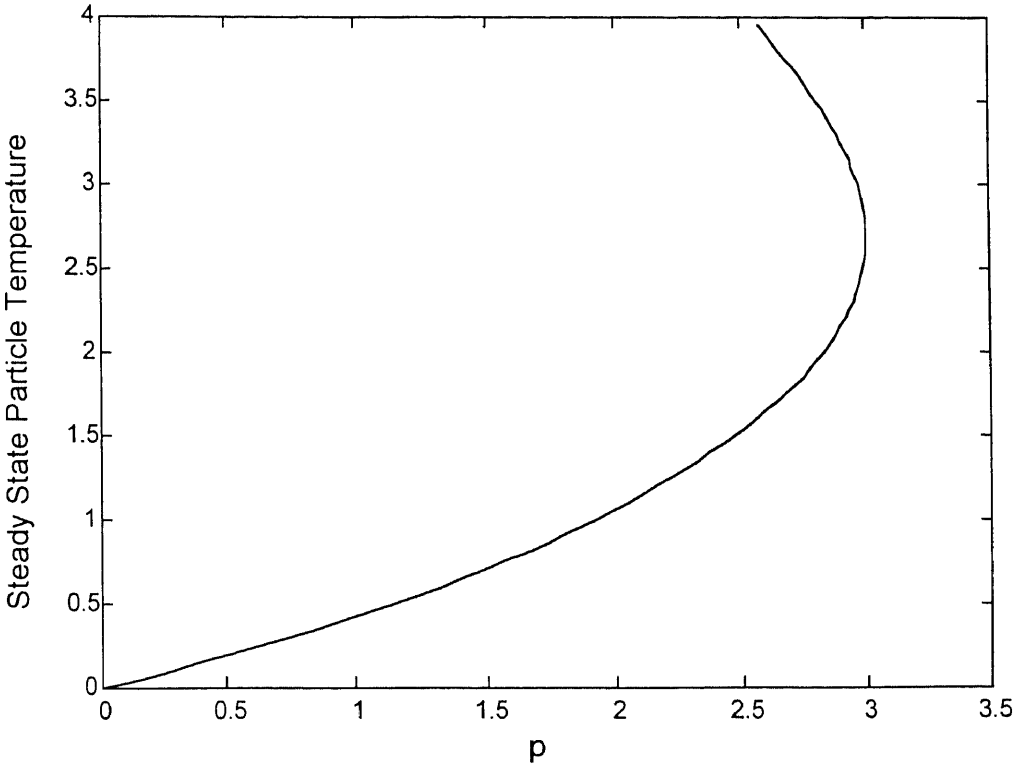

Figure 3.5 Power-response curve for non-transparent cement.

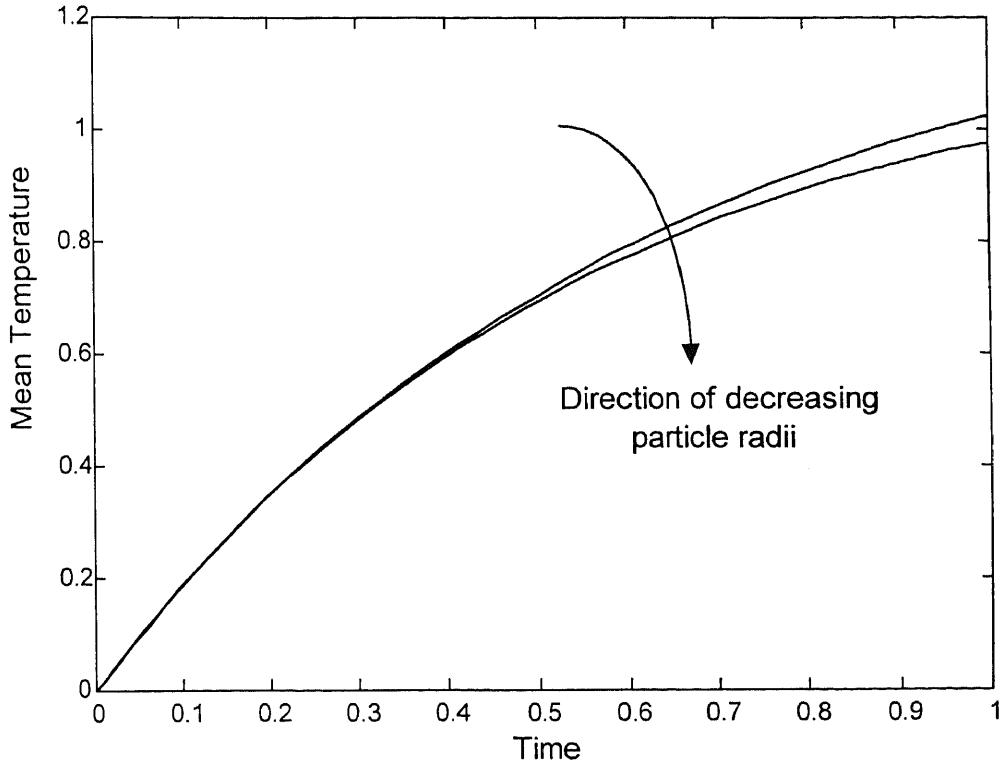

Figure 3.6 Variation of mean temperature, non-transparent cement.

CHAPTER 4

THERMOMECHANICAL INTERACTION IN A SIMPLE OSCILLATOR

The mass-spring oscillator is as ubiquitous in mechanics as the piston-cylinder system is in thermodynamics. In this chapter we investigate the dynamics of a coupled mass-spring oscillator and piston-cylinder system. In this investigation the piston head serves as both the mass in the mass-spring oscillator and the piston head in the piston-cylinder system. (See Figure 4.1.) Our intent is to model and gain insight into the coupling between coherent mechanical and incoherent internal or thermal energy. The bulk of our investigation shall center upon the mass-spring piston-cylinder oscillator, although in the end we shall show that by linking many such oscillators and taking the appropriate limits, a continuum model may be derived. This continuum model is seen to be a one-dimensional version of the equations of thermoelasticity.

We begin in Section 4.1 with a derivation of the equations governing our system. Hooke's law, the ideal gas law, and Newton's law of cooling are taken as constitutive laws and used in conjunction with Newton's second law and the law of conservation of energy. In Section 4.2 these equations are put in non-dimensional form and the parameters which arise are physically interpreted. In Section 4.3 we linearize our governing equations and investigate the dynamics of the resulting linear system. We pay particular attention to the parameters governing the rate of decay of mechanical energy. In Section 4.4, we return to the non-linear system. We show that the entropy places severe restrictions on the dynamics of the system. This restricted region of phase space is explored analytically and numerically. Finally, in Section 4.5 we derive a continuum model by stringing together many mass-spring piston-cylinder oscillators. The linearization of this model is seen to yield the familiar equations of one-dimensional linear thermoelasticity.

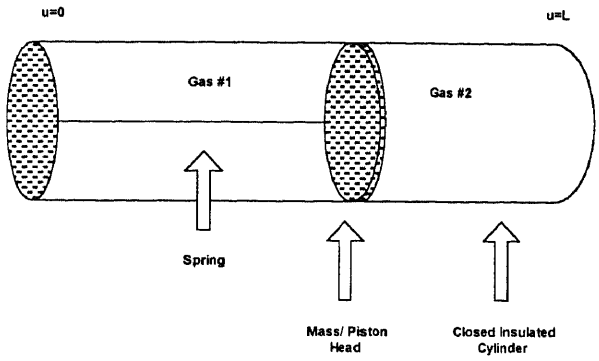

Figure 4.1 The mass-spring piston-cylinder oscillator.

4.1 Derivation of the Model

Consider the system pictured in Figure 4.1. We assume the piston head of mass m moves without friction and is impermeable to the gasses which occupy the left and right chambers of the cylinder. The cylinder of length L is closed at both ends and is assumed to have constant cross-section A. Then, applying Newton's second law to the mass we obtain:

$$m\ddot{u} = -k(u - L/2) + A(p_1 - p_2). \tag{4.1}$$

Here p_i is the pressure in the ith chamber, $L/2$ is the equilibrium length of the spring, dots denote differentiation with respect to time and u is the displacement of the piston head from the left end of the cylinder. Now, we assume each chamber is filled with N moles of an ideal gas, and apply the ideal gas law in the form:

$$p_i V_i = NRT_i \tag{4.2}$$

where again the subscript denotes the ith gas, V_i is the volume occupied by the gas, T_i is the temperature of the gas and R is the ideal gas constant. We can express the volume of each chamber in terms of the cross-sectional area and the piston head's displacement:

$$V_1 = Au \qquad V_2 = A(L - u). \tag{4.3}$$

Now, eliminating p_i and V_i in favor of T_i and u, equation (4.1) becomes:

$$m\ddot{u} + k(u - L/2) = NR(\frac{T_1}{u} - \frac{T_2}{L-u}). \tag{4.4}$$

We have eliminated in favor of the temperature, but the temperature of each gas is allowed to vary as the piston head oscillates. Thus, we need equations governing T_1 and T_2 in order to close the system. We derive these equations by applying the first law of thermodynamics to the ith gas. The infinitesimal form of the first law may be written:

$$dU_i = \hat{d}Q_i + \hat{d}W_i. \tag{4.5}$$

Here, dU_i is an exact differential representing the change in internal energy, $\hat{d}Q_i$ and $\hat{d}W_i$ are process dependent differentials representing changes in heat energy and work respectively. We consider a small displacement of the system which takes the ith gas from state 1 to state 2 and integrate over this process:

$$\int_1^2 dU_i = \int_1^2 \hat{d}Q_i + \int_1^2 \hat{d}W_i. \tag{4.6}$$

Now, we parameterize this process by assuming it begins at some time t and ends at some time $t + \delta t$. Consider the first integral:

$$\int_1^2 dU_i = \int_t^{t+\delta t} \frac{dU_i}{dt} dt = U_i(t + \delta t) - U_i(t). \tag{4.7}$$

Similarly the second integral may be written:

$$\int_1^2 \hat{d}Q_i = \int_t^{t+\delta t} \frac{\hat{d}Q_i}{dt} dt. \tag{4.8}$$

We assume the cylinder is perfectly insulated from the external environment, but that heat is exchanged between the gasses through the piston head. We assume this exchange of heat is governed by Newton's law of cooling so that we may write:

$$\frac{\hat{d}Q_i}{dt} = -hA(T_i - T_j) \tag{4.9}$$

where h is the heat transfer coefficient, and $j \neq i$. Then:

$$\int_1^2 \hat{d}Q_i = -hA \int_t^{t+\delta t} (T_i - T_j)dt. \tag{4.10}$$

We next apply the integral form of the mean value theorem to (4.10) and obtain:

$$\int_1^2 \hat{d}Q_i = -hA(T_i(\tilde{t}) - T_j(\tilde{t}))\delta t \tag{4.11}$$

where $\tilde{t}$ is some time between t and $t + \delta t$. Now, in considering the third integral we make the assumption that the change of state is reversible. That is, we are assuming that the change is sufficiently slow so that the system is effectively in equilibrium throughout. This allows us to express the change in the work as $-p_i dV_i$. Again applying the mean value theorem we obtain:

$$\int_1^2 \hat{d}W_i = -\int_t^{t+\delta t} p_i \frac{dV_i}{dt} dt = -p_i(\tilde{t})(V_i(t + \delta t) - V_i(t)). \tag{4.12}$$

Inserting (4.7), (4.11) and (4.12) into (4.6), dividing by δt and taking the limit as δt approaches zero we obtain:

$$\dot{U}_i = -hA(T_i - T_j) - p_i\dot{V}_i. \tag{4.13}$$

For an ideal gas U_i may be expressed in terms of the temperature:

$$U_i = KNRT_i \tag{4.14}$$

where K is related to the number of degrees of freedom of the gas molecules. Since we are assuming K takes on the same value for each gas, we are assuming that the same type of gas occupies each chamber. Finally, using this expression, the ideal gas law, and equation (4.3) we obtain:

$$KNR\dot{T}_1 + hA(T_1 - T_2) = \frac{-NRT_1}{u}\dot{u} \tag{4.15}$$

$$KNR\dot{T}_2 + hA(T_2 - T_1) = \frac{NRT_2}{L - u}\dot{u}. \tag{4.16}$$

Equations (4.4), (4.15), and (4.16) together with appropriate initial conditions represent a closed system for the displacement u and the temperatures T_1 and T_2. However, as we shall see it is useful to introduce the entropy, S, and carry it along in our calculations. The time rate of change of the entropy of our entire system is given by:

$$\frac{dS}{dt} = \frac{1}{T_1}\frac{\hat{d}Q_1}{dt} + \frac{1}{T_2}\frac{\hat{d}Q_2}{dt}. \tag{4.17}$$

Using equation (4.11) this reduces to:

$$\dot{S} = hA\frac{(T_1 - T_2)^2}{T_1 T_2}. \tag{4.18}$$

An alternate representation may be obtained by multiplying equation (4.15) by T_1^{-1}, equation (4.16) by T_2^{-1} and adding:

$$\dot{S} = KNR\frac{\dot{T}_1}{T_1} + KNR\frac{\dot{T}_2}{T_2} + NR\frac{\dot{u}}{u} - NR\frac{\dot{u}}{L-u}. \tag{4.19}$$

We divide by NR and integrate this equation from 0 to t to obtain:

$$\frac{S(t) - S(0)}{NR} = K\log(\frac{T_1 T_2}{T_1(0)T_2(0)}) + \log(\frac{u(L-u)}{u(0)(L-u(0))}). \tag{4.20}$$

Finally, we define the change in the entropy as $\Delta S = S(t) - S(0)$ and exponentiate to obtain:

$$\exp(\frac{\Delta S}{NR}) = (\frac{T_1 T_2}{T_1(0)T_2(0)})^K(\frac{u(L-u)}{u(0)(L-u(0))}). \tag{4.21}$$

4.2 Scaling

Our coupled system consists of the following three equations:

$$m\ddot{u} + k(u - L/2) = NR(\frac{T_1}{u} - \frac{T_2}{L-u}) \tag{4.22}$$

$$KNR\dot{T}_1 + hA(T_1 - T_2) = \frac{-NRT_1}{u}\dot{u} \tag{4.23}$$

$$KNR\dot{T}_2 + hA(T_2 - T_1) = \frac{NRT_2}{L-u}\dot{u}. \tag{4.24}$$

In addition, we have the following expressions for the time rate of change of entropy:

$$\dot{S} = hA\frac{(T_1 - T_2)^2}{T_1 T_2} \tag{4.25}$$

and the total change in entropy:

$$\exp(\frac{\Delta S}{NR}) = (\frac{T_1 T_2}{T_1(0)T_2(0)})^K(\frac{u(L-u)}{u(0)(L-u(0))}). \tag{4.26}$$

We introduce non-dimensional variables by scaling u with the length L, T_i with some reference temperature T_0, and time with the characteristic frequency of the mass-spring:

$$w = (u - L/2)/L, \qquad \theta = \frac{T_1}{T_0}, \qquad \phi = \frac{T_2}{T_0}, \qquad \tau = \sqrt{\frac{k}{m}}t.$$

This yields:

$$\ddot{w} + w = \alpha(\frac{\theta}{w + 1/2} + \frac{\phi}{w - 1/2}) \tag{4.27}$$

$$\dot{\theta} + \beta(\theta - \phi) = -\frac{1}{K}\frac{\theta\dot{w}}{w + 1/2} \tag{4.28}$$

$$\dot{\phi} + \beta(\phi - \theta) = -\frac{1}{K}\frac{\phi\dot{w}}{w - 1/2}. \tag{4.29}$$

Here, K is a pure number, dots now denote differentiation with respect to τ and:

$$\alpha = \frac{NRT_0}{kL^2}, \qquad \beta = \frac{hA}{KNR}\sqrt{\frac{m}{k}}.$$

We also define a non-dimensional version of the change in entropy:

$$\Delta s = \frac{\Delta S}{NR}. \tag{4.30}$$

Our scalings then yield:

$$\dot{s} = \frac{K\beta(\theta - \phi)^2}{\theta\phi} \tag{4.31}$$

$$\exp(\Delta s) = C_0(\theta\phi)^K(1/4 - w^2) \tag{4.32}$$

where here:

$$C_0 = (\frac{T_0^2}{T_1(0)T_2(0)})^K(\frac{L^2}{u(0)(L-u(0))}). \tag{4.33}$$

Before we delve into the dynamics of our system, let us attempt to find a physical interpretation of the dimensionless parameters α and β. Using the ideal gas law and our definition of volume we may rewrite α as:

$$\alpha = \frac{NRT_0}{kL^2} = \frac{p_0 A}{kL}$$

where p_0 is the pressure in a cylinder of length L held at temperature T_0. From this representation we see that α is the ratio of a reference pressure force to a reference spring force. That is α provides a measure of the gas's ability to stretch or compress the spring. For this reason, α may be thought of as a non-dimensional coefficient of thermal expansion or as a coupling constant, measuring the relative strengths of pressure and spring forces. Anticipating a connection with linear thermoelasticity, we note that it is reasonable to expect α to be a small parameter. That is, the physically relevant case is the one in which the spring is strong compared to the pressure within the gasses. Next, to interpret β we note that:

$$[\sqrt{\frac{m}{k}}] = \text{time} \qquad [\frac{hA}{KnR}] = \frac{1}{\text{time}}.$$

Hence β is a ratio of two time scales in the problem. The first is a characteristic oscillation time of the spring, while the second is a characteristic thermal transport time. That is, β is a ratio of the rate at which oscillations of the mass-spring occur to the rate at which thermal energy is exchanged between the gasses.

4.3 A Linear Model

Our governing equations are non-linear. In this section, we linearize these equations and analyze the dynamics of the resulting system of linear equations. First, we note that the system has a physical equilibrium solution given by $w = 0$, and $\theta = \phi$. We linearize by first assuming that w is small, hence we expand:

$$\frac{1}{w + 1/2} \approx 2(1 - 2w) \tag{4.34}$$

$$\frac{1}{w-1/2} \approx -2(1+2w). \tag{4.35}$$

Further, we assume that T_1 and T_2 remain near to the reference temperature T_0, hence we introduce:

$$\hat{\theta} = 1-\theta, \qquad \hat{\phi} = 1-\phi$$

and assume that $\hat{\theta}$ and $\hat{\phi}$ are small. Introducing these approximations into our governing equations and ignoring products of dependent variables yields the linear system:

$$\ddot{w} + (1+8\alpha)w = 2\alpha(\theta-\phi) \tag{4.36}$$

$$\dot{\theta} + \beta(\theta-\phi) = -\frac{2\dot{w}}{K} \tag{4.37}$$

$$\dot{\phi} + \beta(\phi-\theta) = \frac{2\dot{w}}{K}. \tag{4.38}$$

We see immediately that a first integral exists, i.e. $\dot{\theta}+\dot{\phi}=0$, hence we can reduce this to a third order system. We do so by introducing a deviation from thermal equilibrium, ψ, defined as $\psi = \theta - \phi$. We obtain:

$$\ddot{w} + (1+8\alpha)w = 2\alpha\psi \tag{4.39}$$

$$\dot{\psi} + 2\beta\psi = -\frac{4\dot{w}}{K}. \tag{4.40}$$

Defining $v = \dot{w}$, we then rewrite this as a first order system:

$$\begin{bmatrix} \dot{w} \\ \dot{v} \\ \dot{\psi} \end{bmatrix} = \begin{bmatrix} 0 & 1 & 0 \\ -(1+8\alpha) & 0 & 2\alpha \\ 0 & -4/K & -2\beta \end{bmatrix} \begin{bmatrix} w \\ v \\ \psi \end{bmatrix}. \tag{4.41}$$

This system has a single equilibrium point located at the origin; that it is stable follows immediately by defining a Lyapanov function V, [16]:

$$V = \frac{v^2}{2} + (1+8\alpha)\frac{w^2}{2} + \frac{\alpha K \psi^2}{4} \tag{4.42}$$

and noting:

$$V \geq 0 \qquad \dot{V} = -\alpha\beta K\psi^2 \leq 0. \tag{4.43}$$

We have implicitly assumed that α, β, and K are positive real parameters. This, of course, is the physical region of parameter space. This Lyapanov function has a physical interpretation. The first two terms in V represent the mechanical energy of the system, the third term is the distance from thermal equilibrium. Hence, the result that $\dot{V} \leq 0$ simply says that mechanical energy is dissipated and the system approaches thermal equilibrium.

Although we have shown that our equilibrium point is stable, we have not gained any insight into how rapidly solutions decay towards the origin, or equivalently how rapidly mechanical energy is converted into thermal energy. We can estimate this rate of decay by determining the eigenvalues of the matrix in equation (4.41). In particular solutions of our linearized system have the form $\exp(\lambda\tau)$ where λ is a solution of the characteristic equation:

$$\lambda^3 + 2\beta\lambda^2 + (1 + 8\alpha + 8\alpha/K)\lambda + 2\beta(1 + 8\alpha) = 0. \tag{4.44}$$

In principle we may find these eigenvalues exactly; but the expressions for the roots are cumbersome. By our analysis above we know that all eigenvalues have negative real part for positive values of our parameters. Considering the physical interpretation of our parameters and noting that $K \geq 3/2$, it appears reasonable to assume that α/K is small and expand the roots of our characteristic polynomial in powers of α/K. We find:

$$\lambda \approx -2\beta + \frac{16\alpha\beta}{K(1 + 8\alpha + 4\beta^2)}$$

$$\lambda \approx \pm i\sqrt{1 + 8\alpha}(1 + \frac{4\alpha}{K(1 + 4\beta^2)}) - \frac{8\alpha\beta}{K(1 + 4\beta^2)}$$

where we have retained the first two terms in the expansion. Hence for small α/K we see that one root is strictly negative and real, while the other two are a complex conjugate pair with a negative real part. Since we are interested in the decay of mechanical energy in the spring into thermal energy, we may focus on the smallest negative real part. This is the negative real part of the complex conjugate pair. Now

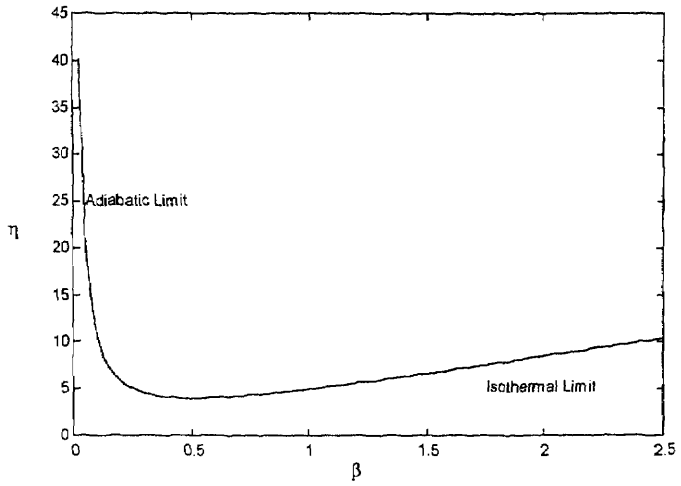

Figure 4.2 Non-dimensional decay time.

it is easy to see that mechanical oscillations will decay like:

$$\exp(-\frac{8\alpha\beta}{K(1+4\beta^2)}\tau).$$

Next, we fix α and define a slow time variable:

$$\eta = \frac{8\alpha\tau}{K}.$$

Now, we may investigate decay on the η time scale as a function of β. We find that mechanical energy has decayed by a factor of e^{-1} when:

$$\eta = 4\beta + \frac{1}{\beta}.$$

We plot this decay time as a function of β in Figure 4.2. First, we note that this curve has a global minimum at $\beta = 1/2$. That is, there is some optimal ratio of the characteristic frequency of the mass spring and the heat transfer rate across the piston head which maximizes the rate of conversion of mechanical into thermal energy. Next, we note that as $\beta \to 0$, the decay time becomes infinite. This is the adiabatic isentropic limit, i.e. both $\hat{d}Q$ and $\dot{s}$ are identically zero. In this limit, no

heat is transferred across the piston head, however each gas still exerts a force on the mass. The motion of the piston head becomes periodic, all work done on the gas during compression is recovered during expansion. In the opposite limit where $\beta \to \infty$, decay time also becomes infinite. This is the isothermal limit, i.e. the two chambers are always in thermal equilibrium. In this limit, the motion of the piston head is also periodic. We note that in each of these limits, the mass-spring system has a different characteristic frequency. In the adiabatic isentropic limit, the frequency is $(1 + 8\alpha + 8\alpha/K)^{-1/2}$, while in the isothermal limit the frequency is $(1 + 8\alpha)^{-1/2}$. We conclude that not only does β affect the decay rate, but that β also affects the characteristic frequency of oscillation.

An interesting historical parallel arises in theory of sound waves in gasses, see Lin & Segel [17]. Newton and Euler each calculated the speed of sound in air by assuming that air maintained a constant temperature during compression. Later, Laplace recomputed the speed of sound by assuming the compression was adiabatic rather than isothermal. For sound waves in air, it was found that the adiabatic limit leads to the most accurate result. These limits are of course analogous to the limits on β and the results concerning frequency discussed above.

Finally, we note that as $\alpha \to 0$, the system becomes uncoupled and again decay time becomes infinite. In this limit, the gas is unable to affect the motion of the mass-spring. Examining our eigenvalues, we see that the rate of conversion of mechanical to thermal energy is directly proportional to α.

4.4 Return to the Non-Linear System

In the previous section, we linearized our governing equations and analyzed the resulting system. The nature of the solutions was consistent with our intuition, i.e. over time oscillations of the spring decayed. However, our original system of governing equations was non-linear and it is natural to ask whether or not the

non-linear system behaves similarly. Recall that our governing equations in non-dimensional form are:

$$\ddot{w} + w = \alpha(\frac{\theta}{w+1/2} + \frac{\phi}{w-1/2}) \tag{4.45}$$

$$\dot{\theta} + \beta(\theta - \phi) = -\frac{1}{K}\frac{\theta\dot{w}}{w+1/2} \tag{4.46}$$

$$\dot{\phi} + \beta(\phi - \theta) = -\frac{1}{K}\frac{\phi\dot{w}}{w-1/2}. \tag{4.47}$$

In addition, we computed the rate of entropy production and the entropy:

$$\dot{s} = \frac{K\beta(\theta-\phi)^2}{\theta\phi} \tag{4.48}$$

$$\exp(\Delta s) = C_0(\theta\phi)^K(1/4 - w^2). \tag{4.49}$$

Now, we realize that physically the system should be restricted to the region of phase space where both θ and ϕ are strictly positive, and w lies in the open interval $(-1/2, 1/2)$. It is intuitive that if our solution begins in this region, it should remain in this region. The veracity of this statement may be demonstrated with the aid of the entropy. First, note that if initial conditions are such that the solution begins in the physical region of phase space, then the constant C_0 is positive. Now, the left hand side of equation (4.49) is real and positive, the constant K is restricted to the sequence $3/2, 5/2, 7/2, \cdots$, hence it immediately follows that θ and ϕ must always have the same sign. Note, the restriction on K follows from the well known expression for the energy in an ideal gas. Now, if initially both θ and ϕ are positive, they must remain positive or cross into the non-physical region at the origin. But, if either θ or ϕ becomes zero, the rate of entropy production, $\dot{s}$, becomes infinite, and consequently equation (4.49) could not be satisfied. We conclude that if θ and ϕ start in the physical region of phase space they remain there. Now, this having been established, equation (4.49) immediately tells us that w is restricted to the open interval $(-1/2, 1/2)$. Hence, solutions beginning in the physical region of phase space remain there.

Next, our system is isolated and we expect energy to be conserved. Multiplying equation (4.45) by $\dot{w}$ and adding our three governing equations we obtain a first integral which is in fact the energy:

$$E = \frac{\dot{w}^2}{2} + \frac{w^2}{2} + \alpha K(\theta + \phi). \tag{4.50}$$

Of course, $\dot{E}$ is identically zero. The first term on the right is the kinetic energy of the mass, the second term is the potential energy stored in the spring, and the third term is the sum of thermal energy in each gas. Hence solutions in our four dimensional phase space are further restricted to move on level sets defined by equation (4.50).

Now, we note that our governing equations admit three steady solutions, i.e. there are three critical points. The first is defined by $w = 0$, $\dot{w} = 0$ and $\theta = \phi$. The other two solutions lie outside the physical domain when α is positive and will not be considered further. To envision the dynamics, it is useful to think in terms of an 'energy space.' Since θ and ϕ are positive, we may define a total thermal energy $\psi^2 = 2\alpha K(\theta + \phi)$. Then equation (4.50) becomes:

$$E = \frac{\dot{w}^2}{2} + \frac{w^2}{2} + \frac{\psi^2}{2}. \tag{4.51}$$

This defines a sphere in our three dimensional energy space. If we place w on the x axis, $\dot{w}$ on the y axis, and ψ on the z axis then our critical point lies at the north pole of this energy sphere. Solutions are then restricted to the northern hemisphere. We expect solutions to simply spiral into the north pole, our linear analysis in the previous section established that this is true in some neighborhood of the north pole. It is clear that this result does not hold globally, i.e. our energy space is divided into three regions which are separated by the singularitys in the governing equations at $w = \pm 1/2$. That is, solutions in any of these three regions cannot cross into any other. However, we expect solutions in the physical region of energy space to spiral into the north pole. This is difficult to establish rigorously from a mathematical point of view, however we can argue physically and supplement our results with

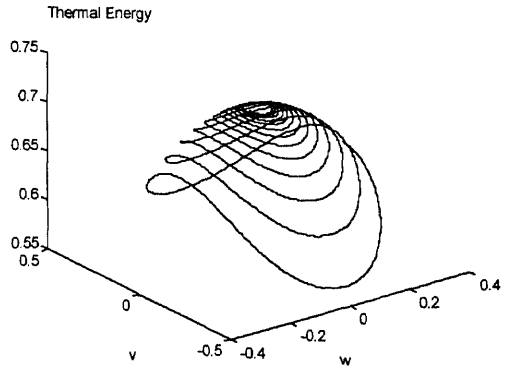

Figure 4.3 Typical trajectory in energy space.

numerical simulations. The argument is simply an application of the second law of thermodynamics to our system, i.e. entropy tends towards a maximum. From equation (4.48) we see that this maximum occurs when $\theta = \phi$. Once the maximum is attained, no further change is possible, i.e. any further change would cause a decrease in entropy. The only such point is at $w = \dot{w} = 0$ and $\theta = \phi$. A numerical solution of these equations, with trajectories plotted in energy space, is shown in Figure 4.3.

It is also worthwhile to consider limiting values of our parameters as was done in the previous section. First, we note that in the limit $\alpha \to 0$ our governing equations once again become uncoupled. In this limit, the spring oscillates with its own natural frequency and simply drives temperature variations in the gasses. The limit where $\beta \to 0$ again is the adiabatic isentropic limit. In this limit equations (4.46) and (4.47) may be integrated and the results used to eliminate θ and ϕ from equation (4.45). This yields the non-linear oscillator:

$$\ddot{w} + w = \alpha\left(\frac{1}{(w+1/2)^{\frac{K+1}{K}}} + \frac{1}{(w-1/2)^{\frac{K+1}{K}}}\right). \tag{4.52}$$

It is clear that in this limit, mechanical energy does not decay. In the limit where $\beta \to \infty$ we have that $\theta = \phi$. Again, the temperature may be eliminated from

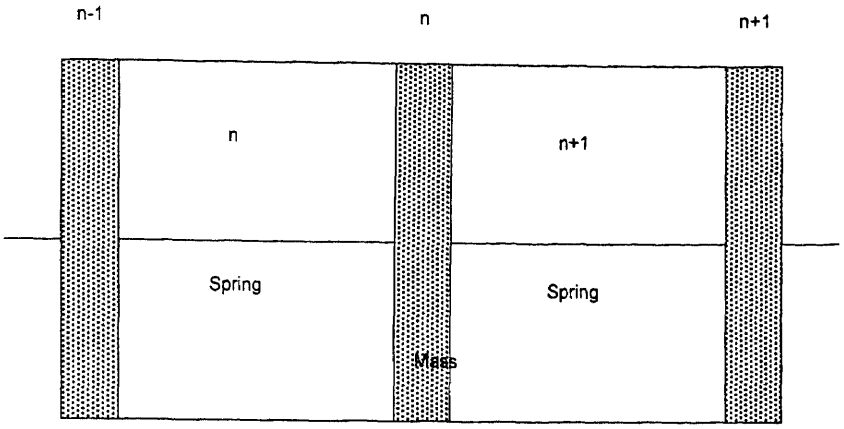

Figure 4.4 Many coupled oscillators.

equation (4.45) and an equation for a non-linear oscillator derived. This is the isothermal limit, and again it is clear that mechanical oscillations will not decay. Examining these two limits, and noting that $\dot{s}$ is proportional to β leads us to the same conclusion regarding the influence of β on decay time and frequency that was obtained through our linear analysis. In particular, we expect there to be an optimal β which maximizes the rate of decay of mechanical into thermal energy. Finally, we note that β will influence the frequency of the oscillations. That is, as was true in the limiting cases considered above, different values for β lead to different characteristic frequencies of mechanical oscillation.

4.5 A Continuum Model

Having considered a single mass-spring piston-cylinder system, it is natural to inquire as to what happens when many such systems are strung together and a continuum limit is taken. We imagine a long cylinder with many piston heads attached to each other by springs. Referring to Figure 4.4 we first consider the motion of the nth mass. Proceeding as in Section 4.2 we may write:

$$m\ddot{u}_n = k(u_{n+1} - 2u_n + u_{n-1}) - A(p_{n+1} - p_n). \tag{4.53}$$

Where now, the subscripts denote the nth mass, nth volume etc. In addition, all masses are taken to be identical, as are all springs and gasses. Now, using the ideal gas law as in Section 4.2 we obtain:

$$m\ddot{u}_n = k(u_{n+1} - 2u_n + u_{n-1}) + \frac{NR}{L}\left(\frac{T_n}{1+\frac{u_n-u_{n-1}}{L}} - \frac{T_{n+1}}{1+\frac{u_{n+1}-u_n}{L}}\right). \tag{4.54}$$

Now, we assume that:

$$\frac{T_n}{1+\frac{u_n-u_{n-1}}{L}} \approx T_n\left(1 - \frac{u_n - u_{n-1}}{L}\right) \tag{4.55}$$

and that:

$$T_n = T_A(1+\theta) \tag{4.56}$$

where $\theta \ll 1$, and T_A is some reference temperature. Inserting these approximations into (4.54) and ignoring products of dependent variables we obtain:

$$m\ddot{u}_n = (k + \frac{NRT_A}{L^2})(u_{n+1} - 2u_n + u_{n-1}) - \frac{NR}{L}(T_{n+1} - T_n). \tag{4.57}$$

Now, we divide by L and take the limit as $L \to 0$ in such a way that:

$$\frac{m}{L} \to \rho, \qquad kL \to E,$$

$$\frac{NRT_A}{kL^2} \to 0, \qquad \frac{NR}{L} \to \alpha_0 E,$$

where here ρ is a linear density, E is a Young's modulus, and α_0 is the coefficient of thermal expansion. The assumption that $\frac{NRT_A}{kL^2}$ tends to zero may be understood by rewriting as:

$$\frac{NRT_A}{kL^2} = \frac{p_A A}{kL} = \frac{\text{pressure force}}{\text{spring force}}$$

hence, the spring force dominates the pressure force in this limit. Similarly, if we rewrite:

$$\frac{NR}{L} = \frac{p_A A/T_A}{kL}kL = \frac{\text{pressure force/unit temp}}{\text{spring force}}$$

we retain changes in the pressure force with respect to the spring force, i.e. we retain the effect of thermal expansion. Then we have:

$$\rho\frac{\partial^2 u}{\partial t^2} = E\frac{\partial^2 u}{\partial x^2} - E\alpha_0\frac{\partial T}{\partial x}. \tag{4.58}$$

Next, as in Section 4.2 we derive an energy equation. Making the same assumptions as in Section 4.2, evaluating the integrals in the same manner, and linearizing as in Section 4.3 we arrive at:

$$KNR(T_n^{t+\delta t} - T_n^t) = hA\delta t(T_{n+1}^t - 2T_n^t + T_{n-1}^t) - \frac{NRT_A}{L}(u_n^{t+\delta t} - u_{n-1}^{t+\delta t} - u_n^t + u_{n-1}^t). \tag{4.59}$$

For notational convenience we have used superscripts to denote time. Now dividing by $L\delta t$ and taking the appropriate limits we arrive at:

$$C_p\frac{\partial T}{\partial t} = \kappa\frac{\partial^2 T}{\partial x^2} - E\alpha_0 T_A\frac{\partial^2 u}{\partial x \partial t}. \tag{4.60}$$

Again the constants are limits of the constants in our discrete equation. In particular, KNR/L approaches the linear heat capacity C_p, hAL approaches the linear thermal conductivity κ, and the remaining constant is re-expressed in terms of constants which arose in the previous equation. So, our continuum model is:

$$\rho\frac{\partial^2 u}{\partial t^2} = E\frac{\partial^2 u}{\partial x^2} - E\alpha_0\frac{\partial T}{\partial x} \tag{4.61}$$

$$C_p\frac{\partial T}{\partial t} = \kappa\frac{\partial^2 T}{\partial x^2} - E\alpha_0 T_A\frac{\partial^2 u}{\partial x \partial t}. \tag{4.62}$$

These are, of course, a one-dimensional version of the equations of linear thermoelasticity. We note that while arriving at the same point, our approach to this continuum model varies significantly from the modern derivation of these equations, such as can be found in Boley & Weiner [18]. Most significantly, our treatment has rested upon classical equilibrium thermodynamics while a modern approach utilizes non-equilibrium thermodynamics. That is, at each time step we have assumed that the relations of equilibrium thermodynamics apply, strictly speaking they do not.

Nonetheless, our model produces the same equations and provides an intuitive framework in which to understand them.

4.6 Discussion

In this chapter we have tried to illuminate the process of thermomechanical exchange by studying a simple mass-spring piston-cylinder oscillator. At the outset, we stated that it was our goal to gain insight into the coupling between mechanical and thermal energy. First, let us review.

We began by applying conservation of momentum and conservation of energy to the single mass-spring piston-cylinder system. We derived a coupled set of non-linear ode's. By scaling and linearizing these ode's, we saw how two dimensionless parameters govern the interchange of mechanical and thermal energy. In particular, by fixing one parameter, our thermal expansion coefficient, and varying the second, we begin to understand how the decay of mechanical energy varies. We saw that, in this limit, it is the ratio of the rates of mechanical energy transport and thermal energy transport which governs this decay. We found that decay time, as a function of this parameter, becomes infinite in two limits. Thermodynamically, we identified these as the adiabatic and isothermal limits.

Next, we returned to the non-linear system. We saw how the entropy restricts the dynamics in phase space. We noted that the dynamics were further restricted by the existence of an energy integral. By applying the second law of thermodynamics, we conjectured that in the physical region of phase space, solutions approach the sole equilibrium point. Again, we investigated the relationship between β and decay of mechanical energy.

In Section 4.5 we considered the case of many mass-spring piston-cylinder systems linked together. By taking the appropriate limits we arrived at a continuum model. This continuum limit was seen to yield the one-dimensional equations of linear

thermoelasticity. Because of this connection, we gain insight into the processes taking place in thermoelastic phenomena by studying our simple system. Recognizing that a Fourier transform in space of the thermoelastic equations yields ode's of the form that we studied earlier, we realize that the time behavior of elastic waves will mirror the behavior of our simple system. Perhaps the most pertinent result is that the rate of decay of mechanical energy depends strongly on how quickly thermal energy may be transported away from a wave-front. In our piston-cylinder model this rate appeared as β, the non-dimensional rate of exchange of thermal energy across the piston head. In the thermoelastic case the corresponding key parameter will be the thermal conductivity, κ. Decay time will behave as a function of κ just as it behaved as a function of β in our model.

Finally, we note that this model has numerous possible extensions. Of particular interest might be the temperature dependence of parameters appearing in the model. By studying the effects for our simple oscillator we can hope to gain further knowledge of how such variations might affect the behavior of solutions to the full equations of thermoelasticity.

CHAPTER 5

SINGLE PULSE ELECTRON BEAM JOINING

The integration of advanced engineering materials, such as high temperature metals, ceramics, and composites, into engineering structures compels the development of new joining processes, [19, 20]. In the case of metals, it is necessary to develop a joining process which avoids damaging carefully tailored microstructures. This demands that the joining process act locally, i.e. the heat treated region must be restricted to the joint itself. Ceramics, on the other hand, are brittle materials and as such are vulnerable to thermal shock damage as well as cracking induced by residual stresses which result from the joining process. This demands that the joining process be tailored to minimize such stresses. Further, in order to be widely applicable, the joining method must be capable of creating joints at buried interfaces. In Chapters 5 through 9, we study a method proposed by Mako et. al., [6], which utilizes a single-pulse high-energy electron beam in an attempt to join similar and dissimilar advanced engineering materials at buried interfaces.

The joining method proposed by Mako et. al., [6], is applicable to the joining of ceramics and metals as well as ceramics and ceramics. The process begins by forming a three layer composite, consisting of the two materials to be joined and a third brazing material, or interlayer. The composite is arranged as shown in Figure 5.1. The sample is then placed in a vacuum chamber, and a single-pulse high-energy electron beam is directed towards the surface of the ceramic workpiece. The beam deposits energy in each material, but due to differences in heat capacities, the materials are heated to different temperatures. In particular, the interlayer is chosen so that its heat capacity is considerably lower than those of the two materials to be joined; hence it is heated to a higher temperature. In this way, the interlayer is heated to joining temperatures, and a joint is formed.

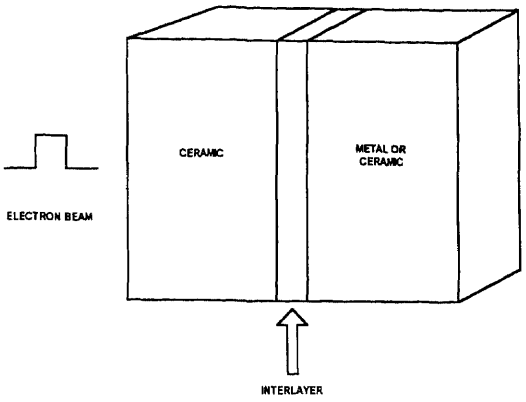

Figure 5.1 Sketch of the experimental setup

In order to utilize the proposed method, numerous difficulties must be overcome. Foremost among these is the control of thermal stress waves created during the process. As mentioned above, if these stresses are too large, they can lead to cracking or spalling of the ceramic, deformation of the metal, changes in microstructure, and result in weak joints. We focus our attention on understanding these stresses, i.e. we focus on the thermoelastic aspect of the process.

That thermal energy can cause mechanical motion was known by the ancient Greeks. A colossal statue near Thebes in Egypt, said to represent Memnon, but more probably representing the Egyptian pharaoh Amenophis, bears the inscription: Every morning, when the rays of the rising sun touched the statue, it gave forth musical sounds like the twang of a harp string, [21]. The ancient Greeks interpreted this music as Memnon singing out to his mother after having been slain by Achilles. As such, the equations governing thermoelastic behavior remained unformulated until 1835. In 1835, Duhamel, formulated the equations of linear thermoelasticity [22]. For the next one hundred and fifteen years, these equations were studied in the quasi-static or thermal stress formulation. Finally, in 1950, Danilowskaya began the study of dynamic thermoelasticity by considering the thermal stress waves generated in an elastic half-space which is suddenly heated on its boundary, [23].

In order to classify our problem as a thermal stress or thermoelastic problem, it is useful to briefly consider the equations of linear thermoelasticity, and discuss the standard simplifications. In Chapter 4, we presented the equations in one dimension. Here, we restate the equations of linear thermoelasticity, derived from a three dimensional theory, under the assumption of zero displacements and zero temperature gradients in two directions:

$$\rho c_v \frac{\partial T}{\partial t} = \kappa \frac{\partial^2 T}{\partial x^2} - (3\lambda + 2\mu)\alpha T_A \frac{\partial^2 u}{\partial x \partial t} + S(x,t) \tag{5.1}$$

$$\frac{\partial \sigma}{\partial x} = \rho \frac{\partial^2 u}{\partial t^2} \tag{5.2}$$

$$\sigma = (\lambda + 2\mu)\frac{\partial u}{\partial x} - (3\lambda + 2\mu)\alpha(T - T_A). \tag{5.3}$$

Equation (5.1) is an energy equation, governing the temperature T. The dependent variable u, is the elastic displacement in the x direction, and S is a source term. The second equation, (5.2), is the equation of motion. Here, σ is the stress in the x direction. The third equation, (5.3), is the stress-strain law or Duhamel-Neumann relation.

All thermoelastic problems are characterized by at least three time scales. First, in the presence of a thermal source, there is the energy deposition time scale, t_p. Next, there is a characteristic time for thermal diffusion, t_D. Finally, there is a characteristic mechanical time, t_M, defined by the wave speed of the elastic medium. In most engineering problems, $t_M \ll t_p \sim t_D$. Under this assumption it is permissible to make the uncoupled quasi-static approximation. That is, in equation (5.1), the second term on the right may be ignored, and further, if equations (5.2) and (5.3) are combined to yield a wave equation:

$$(\lambda + 2\mu)\frac{\partial^2 u}{\partial x^2} - (3\lambda + 2\mu)\alpha \frac{\partial T}{\partial x} = \rho \frac{\partial^2 u}{\partial t^2} \tag{5.4}$$

the inertial term, i.e. the term on the right hand side, may be ignored. For a full discussion of the validity of these approximations see Boley, [18].

It is evident that the uncoupled and quasi-static approximations greatly simplify the analysis of thermoelastic problems. However, in the electron beam joining process we wish to consider, the energy deposition time scale is very rapid. In particular we are interested in a single pulse with pulse width on order of 10^{-7} to 10^{-6} seconds. This implies that $t_p \sim t_M$, hence at the very least, inertial terms must be retained. That is, the wavelike nature of thermal stresses is important. As we shall show, it will still be permissible to make the uncoupled approximation when we are interested in short time solutions. However, in order to bring thermoelastic decay back into our problem, we will need to retain the coupling term in the heat equation.

Numerous authors have considered thermoelastic problems in the parameter range in which the inertial term must be retained. Most notably, the laser heating of elastic materials has been considered by many authors, [24, 25, 26]. Further, many authors have considered these types of problems without reference to a specific application. For example, Boley and Tolins considered the coupled form of Danilowskay's problem, [27], Soler and Brull developed perturbation techniques for coupled problems, [28], and Achenbach, Stickler and Nickell, developed approximate techniques for replacing the coupling term with a delta function in the neighborhood of a wavefront, [29, 30] . Although some authors have studied thermoelastic effects due to heating by a low-power density, multiply pulsed electron beam, [31, 32], relatively little has been done to further our understanding of single-pulse high-energy electron beam heating.

The most important research in single-pulse high-energy electron beam heating has been done by Turman et. al., Mako et. al., and most notably by Bailey, [33, 6, 34]. Since much of our work will be focused on improving engineering stress estimates given by Bailey, it is useful to briefly state Bailey's most important results. Bailey identified the key parameter in electron beam joining experiments, $\tau_0 = ct_p/L$. Here,

c is the elastic wave speed of the medium, t_p is the beam energy deposition time, and L is a characteristic length scale in the problem. In the limit where $\tau_0 \gg 1$, Bailey's expression for the peak propagating stress is given by:

$$\sigma_{\max} = \frac{\Gamma J V}{2c} \tag{5.5}$$

where here, Γ is the Gruneisen parameter, J the beam current density, and V the beam kinetic energy. Further, in the limit $\tau_0 \ll 1$, Bailey identified the peak propagating stress as:

$$\sigma_{\max} = \frac{\rho \Gamma E}{2m} \tag{5.6}$$

where here ρ is the density of the elastic media, E is the total energy deposited, and m is a reference mass. Bailey further noted that rarefaction waves formed at free boundaries could significantly reduce these estimates.

In the remaining chapters, we shall consider a sequence of models whose analysis will further our understanding of thermoelastic behavior in the electron beam joining process. We shall focus on several aspects of this problem. First, much of our analysis will be directed towards refining Bailey's estimates for the peak propagating stress. That is, we seek to determine the maximum stresses which are formed while the beam acts. In the design of electron beam joining experiments such estimates are of the utmost importance. Designing high-energy accelerators with long-pulse lengths is expensive; a detailed understanding of the variation of stress amplitude with pulse length translates into an economic advantage. Next, we seek to understand how stress waves propagate once the beam has been turned off. Since such waves may constructively interfere, propagation may significantly effect maximum stress amplitudes. Finally, we consider the question of thermoelastic decay. An understanding of decay rates may be considered a refinement of our understanding of stress wave propagation.

We begin in Chapter 6 by revisiting the simple oscillator discussed in Chapter 4. In the context of the oscillator, we introduce much of the mathematical machinery that will be used in later sections. Further, we use this simple setting to clarify the role played by mechanical and thermal relaxation of stresses. Next, in Chapter 7, we consider the electron beam joining process in a homogeneous infinite elastic slab. We carefully formulate the model of the source term in the heat equation. This allows us to relate stress estimates to beam parameters. These estimates are compared to those of Bailey in the appropriate limits. Then, in Chapter 8, we consider the problem in a single finite slab. Here, in addition to deriving short time stress estimates, we also consider thermoelastic decay and clarify the importance of various parameters in determining decay rates. Further, we consider numerical solutions to this problem, and illustrate the role played by rarefaction waves and constructive interference of stress waves. Next, in Chapter 9 we investigate the electron beam joining process in multiple layers. To simplify the analysis, we make use of boundary layer theory to obtain the thermal field, and utilize the disparity in length scales between the interlayer and the surrounding layers. The solutions are given in 'travelling-wave' form, which has the advantage that for finite time, it consists of a finite number of terms. These solutions are studied, and shown to capture thermal expansion mismatch, diffusion at interfaces, and variations in stress due to varying material properties. Finally, the problem is investigated numerically, and illustrative examples are shown.

For the convenience of the reader this work has been divided into five distinct chapters, in particular to simplify equation numbering. We note however that Chapters 5 through 9 should be viewed intellectually as a single chapter.

CHAPTER 6

THE OSCILLATOR AS A MODEL OF ELECTRON BEAM JOINING

In the previous chapter we discussed a proposed method for employing high-energy single-pulse electron beams in the joining of ceramics to metals. We noted the importance of understanding the creation and propagation of thermal stresses which are created during this process. As a first step towards understanding these stresses, we revisit the simple oscillator introduced in Chapter 4. By adding a thermal source to the equations governing our oscillator, we obtain a primitive model of the electron beam joining process. Even though the model lacks the complexity necessary to fully understand the process, analysis of the model yields insight into the effect of pulse length on stress amplitude, the decay of thermal stress, and the mathematical machinery necessary for dealing with these types of problems.

6.1 Formulation of the Model

We begin by adding a source term to the equations governing our mass-spring piston-cylinder oscillator. Recall that the beam acts for a finite time and deposits its energy in a localized region. The source term we introduce takes the form of a thermal pulse, acting on only one of the chambers, and lasting for a finite time. This models an electron beam incident upon an elastic solid. The source term which we introduce is $pG(t/t_p)$, where p has the units of energy per unit time, and G is a dimensionless function defined by:

$$G(t/t_p) = H(t'/t_p) - H(t'/t_p - 1), \tag{6.1}$$

where H denotes the Heaviside function. Note that our source only acts over the interval $(0, t_p)$, where here t_p will be referred to as the pulse length. Our governing equations are then:

$$\ddot{u} + k(u - L/2) = NR(\frac{T_1}{u} - \frac{T_2}{L-u}) \tag{6.2}$$

$$KNR\dot{T}_1 + hA(T_1 - T_2) = -\frac{NRT_1}{u}\dot{u} + pG(t/t_p) \tag{6.3}$$

$$KNR\dot{T}_2 + hA(T_2 - T_1) = -\frac{NRT_2}{L-u}\dot{u} \tag{6.4}$$

$$u(0) = L/2 \qquad T_1(0) = T_2(0) = T_A \tag{6.5}$$

where we have assumed quiescent initial conditions. Now, in the electron beam problem we are primarily interested in thermal stresses. Here, we introduce F, the total force acting on the piston head, which is the analog of stress.

$$F = -k(u - L/2) + NR(\frac{T_1}{u} - \frac{T_2}{L-u}). \tag{6.6}$$

Next, we introduce the same dimensionless variables as in Chapter 4:

$$w = \frac{u - L/2}{L}, \quad \theta = \frac{T_1}{T_A}, \quad \phi = \frac{T_2}{T_A}, \quad \tau = \sqrt{\frac{k}{m}}t.$$

In terms of these variables our governing equations become:

$$\ddot{w} + w = \alpha(\frac{\theta}{w + 1/2} + \frac{\phi}{w - 1/2}) \tag{6.7}$$

$$\dot{\theta} + \beta(\theta - \phi) = -\frac{1}{K}\frac{\theta\dot{w}}{w + 1/2} + PG(\tau/\tau_0) \tag{6.8}$$

$$\dot{\phi} + \beta(\phi - \theta) = -\frac{1}{K}\frac{\phi\dot{w}}{w - 1/2}. \tag{6.9}$$

Here, K is a pure number, dots denote differentiation with respect to τ and:

$$\alpha = \frac{NRT_0}{kL^2}, \qquad \beta = \frac{hA}{KNR}\sqrt{\frac{m}{k}}, \qquad P = \frac{p}{KNRT_A}\sqrt{\frac{m}{k}}, \qquad \tau_0 = t_p\sqrt{\frac{k}{m}}.$$

We also define a dimensionless force or stress:

$$\Sigma = -\frac{F}{kL}$$

which yields:

$$\Sigma = w - \alpha(\frac{\theta}{w + 1/2} + \frac{\phi}{w - 1/2}). \tag{6.10}$$

We note that the parameters α and β have the same physical interpretation as in the previous chapter, while P may be interpreted as a dimensionless power, and τ_0 as a dimensionless measure of pulse length.

Next, we develop a linear theory. Proceeding as in Chapter 4 we linearize and obtain:

$$\ddot{w} + (1 + 8\alpha)w = 2\alpha(\theta - \phi) \tag{6.11}$$

$$\dot{\theta} + \beta(\theta - \phi) = -\frac{2\dot{w}}{K} + PG(\tau/\tau_0) \tag{6.12}$$

$$\dot{\phi} + \beta(\phi - \theta) = \frac{2\dot{w}}{K}. \tag{6.13}$$

Adding equations (6.12) and (6.13), and defining $\psi = \theta - \phi$, we reduce this system to a system of two equations:

$$\ddot{w} + (1 + 8\alpha)w = 2\alpha\psi \tag{6.14}$$

$$\dot{\psi} + 2\beta\psi = -\frac{4\dot{w}}{K} + PG(\tau/\tau_0) \tag{6.15}$$

$$\Sigma = (1 + 8\alpha)w - 2\alpha\psi. \tag{6.16}$$

We note that equation (6.16) is the analog of the Duhamel-Neumann relation. Now, in realistic problems involving thermoelastic media, the non-dimensional coefficient of thermal expansion or coupling coefficient is typically a small parameter. Here, we make the analogous assumption that α is a small parameter. We then make the approximation:

$$\frac{1}{1 + 8\alpha} \approx 1.$$

Additionally, for convenience, we rescale Σ and rename several parameters:

$$\sigma = \frac{\Sigma}{2\alpha}, \qquad \epsilon = \frac{8\alpha}{K}, \qquad D = 2\beta.$$

Now, introducing this approximation, the rescaling, the new parameters, and eliminating w from our linearized equations yields:

$$\ddot{\sigma} + \sigma = -\ddot{\psi} \tag{6.17}$$

$$\dot{\psi} + D\psi = -\epsilon(\dot{\sigma} + \dot{\psi}) + PG(\tau/\tau_0) \tag{6.18}$$

$$\sigma(0) = \psi(0) = 0 \tag{6.19}$$

$$\dot{\sigma}(0) = -\dot{\psi}(0). \tag{6.20}$$

Equations (6.17)-(6.20) are the equations we will study throughout the remainder of this chapter. We make two observations. First, the displacement has been eliminated in terms of a measure of the total force acting on the piston head. This is the analog of the stress in a elastic problem and we will refer to σ as stress. Second, we note, without demonstrating it here, that these equations are actually more than an analog to linear thermoelasticity. We will see later that these equations are identical to the spatially Fourier transformed linear thermoelastic equations.

6.2 Analysis During the Pulse

Equations (6.17)-(6.20) represent a third order non-autonomous linear system of coupled ordinary differential equations. In principle there is nothing mysterious or difficult about such a system, i.e. it may be solved exactly. In practice, such a solution is often difficult to obtain and not necessarily useful once it has been obtained. So, rather than looking back and carrying out an analysis similar to that of Chapter 4, we look forward and use this simple setting to develop approximate methods of solution which will be applicable to more complicated models.

We begin our analysis by applying the Laplace transform to our governing equations. If the transform variable is s, and we denote transformed functions by hats, we have:

$$(s^2 + 1)\hat{\sigma} = -s^2\hat{\psi} \tag{6.21}$$

$$(s + D)\hat{\psi} = -s\epsilon(\hat{\sigma} + \hat{\psi}) + P\hat{G}. \tag{6.22}$$

We may solve for $\hat{\sigma}$ to obtain:

$$\hat{\sigma} = \frac{-s^2 P\hat{G}}{s^3 + Ds^2 + (1+\epsilon)s + D}. \tag{6.23}$$

The time behavior of the solution is then determined by the roots of the characteristic equation:

$$s^3 + Ds^2 + (1+\epsilon)s + D = 0. \tag{6.24}$$

Since ϵ is a small parameter we may expand the roots in powers of ϵ to obtain:

$$s \sim \pm i(1 + \frac{\epsilon}{2(1+D^2)}) - \frac{\epsilon D}{2(1+D^2)}$$

$$s \sim -D + \frac{\epsilon D}{D^2+1}.$$

We find, as in Chapter 4, that two of our roots are a complex conjugate pair with a small negative real part, while the third root is negative and real. Solutions will behave like $e^{s\tau}$, hence we may determine the effect of ignoring $O(\epsilon)$ terms by simply considering the largest $O(\epsilon)$ correction to the roots. This is the term:

$$\frac{\epsilon D}{D^2+1}.$$

Now, we would like to develop a short time solution, i.e. one that is valid until the end of the pulse. The order epsilon correction term becomes important when:

$$\tau \sim \frac{(1+D^2)}{\epsilon D}.$$

Hence, if the dimensionless pulse length satisfies:

$$\tau_0 \ll \frac{(1+D^2)}{\epsilon D}$$

then we may obtain a good approximation to the exact solution, valid up until $\tau = \tau_0$, by simply ignoring terms of $O(\epsilon)$. That is, for short times the exact equations may be replaced by the approximate system:

$$\ddot{\sigma}_s + \sigma_s = -\ddot{\psi}_s \tag{6.25}$$

$$\dot{\psi}_s + D\psi_s = PG(\tau/\tau_0) \tag{6.26}$$

$$\sigma_s(0) = \psi_s(0) = 0 \tag{6.27}$$

$$\dot{\sigma}_s(0) = -\dot{\psi}_s(0) \tag{6.28}$$

where we have labeled our dependent variables with the subscript s to indicate that this solution is valid only for short times. In particular we shall only use this solution up till $\tau = \tau_0$, although it is clearly valid for somewhat longer times. Now, the solution of equations (6.25)-(6.28) is straightforward and we find immediately:

$$\psi_s(\tau) = P\int_0^\tau G(\zeta/\tau_0)e^{-D(\tau-\zeta)}d\zeta \tag{6.29}$$

$$\sigma_s(\tau) = -\psi_s(\tau) + \int_0^\tau \psi_s(\zeta)\sin(\tau-\zeta)d\zeta. \tag{6.30}$$

Or if we carry out the integrations, assuming that $\tau \leq \tau_0$, we obtain:

$$\psi_s(\tau) = \frac{P}{D}(1 - e^{-D\tau}) \tag{6.31}$$

$$\sigma_s(\tau) = \frac{PD}{D^2+1}(e^{-D\tau} - \cos(\tau)) - \frac{P\sin(\tau)}{D^2+1}. \tag{6.32}$$

6.3 Analysis After the Pulse

In the previous section, we developed a solution valid at least until $\tau = \tau_0$. In this section, we develop a solution valid on the interval (τ_0, ∞). Our method is based on a simple observation. At $\tau = \tau_0$, our source turns off. Hence our problem reduces to solving:

$$\ddot{\sigma} + \sigma = -\ddot{\psi} \tag{6.33}$$

$$\dot{\psi} + D\psi = -\epsilon(\dot{\sigma} + \dot{\psi}) \tag{6.34}$$

with initial conditions imposed at $\tau = \tau_0$. If we had the exact solution on $(0, \tau_0)$, and we computed values of ψ, σ and $\dot{\sigma}$ at τ_0 using this exact solution, then imposed these as initial conditions on equations (6.33)-(6.34), we would be making no error

at all. But, we do not have the exact solution on $(0, \tau_0)$, we have the approximate solution ψ_s and σ_s. However, we know that the error in this solution is $O(\epsilon D\tau_0)$, hence we can impose:

$$\psi(\tau_0) = \psi_s(\tau_0) + O(\epsilon D\tau_0) \tag{6.35}$$

$$\sigma(\tau_0) = \sigma_s(\tau_0) + O(\epsilon D\tau_0) \tag{6.36}$$

$$\dot{\sigma}_s(\tau_0) = \dot{\sigma}_s(\tau_0) + O(\epsilon D\tau_0). \tag{6.37}$$

Now, we wish to develop an approximate solution on (τ_0, ∞). We note that a regular perturbation expansion in ϵ fails, i.e. it becomes non-uniform in time. To remove this secularity we employ the method of multiple scales.

We begin by redefining our time variable as $\tau' = \tau - \tau_0$. This shifts our initial conditions to the origin. So we will study:

$$\ddot{\sigma} + \sigma = -\ddot{\psi} \tag{6.38}$$

$$\dot{\psi} + D\psi = -\epsilon(\dot{\sigma} + \dot{\psi}) \tag{6.39}$$

$$\psi(0) = \psi_s(\tau_0) + O(\epsilon D\tau_0) \tag{6.40}$$

$$\sigma(0) = \sigma_s(\tau_0) + O(\epsilon D\tau_0) \tag{6.41}$$

$$\dot{\sigma}(0) = \dot{\sigma}_s(\tau_0) + O(\epsilon D\tau_0) \tag{6.42}$$

where dots on ψ and σ denote differentiation with respect to τ' and dots on ψ_s and σ_s denote differentiation with respect to τ. Now, we let $\eta = \epsilon\tau'$, and seek solutions as functions of the two time variables η and τ' in the form of a power series solution in epsilon:

$$\psi \sim \psi_0(\tau', \eta) + \epsilon\psi_1(\tau', \eta) + \cdots$$

$$\sigma \sim \sigma_0(\tau', \eta) + \epsilon\sigma_1(\tau', \eta) + \cdots.$$

We also replace our time derivative by:

$$\frac{d}{d\tau'} \longrightarrow \frac{\partial}{\partial\tau'} + \epsilon\frac{\partial}{\partial\eta}.$$

Now, inserting our power series expansion into equations (6.38)-(6.39), and equating to zero coefficients of powers of epsilon we obtain an infinite set of equations for the ψ_n and σ_n. We list the first two:

$$\frac{\partial^2\sigma_0}{\partial\tau'^2} + \sigma_0 = -\frac{\partial^2\psi_0}{\partial\tau'^2} \tag{6.43}$$

$$\frac{\partial\psi_0}{\partial\tau'} + D\psi_0 = 0 \tag{6.44}$$

$$\psi_0(0) = \psi_s(\tau_0) \tag{6.45}$$

$$\sigma_0(0) = \sigma_s(\tau_0) \tag{6.46}$$

$$\frac{\partial\sigma_0}{\partial\tau'}(0) = \dot{\sigma_s}(\tau_0) \tag{6.47}$$

and

$$\frac{\partial^2\sigma_1}{\partial\tau'^2} + \sigma_1 = -\frac{\partial^2\psi_1}{\partial\tau'^2} - 2\frac{\partial^2\psi_0}{\partial\tau'\partial\eta} - 2\frac{\partial\sigma_0}{\partial\tau'\partial\eta} \tag{6.48}$$

$$\frac{\partial\psi_1}{\partial\tau'} + D\psi_1 = -\frac{\partial\psi_0}{\partial\eta} - \frac{\partial\sigma_0}{\partial\tau'} - \frac{\partial\sigma_0}{\partial\tau'} \tag{6.49}$$

$$\psi_1(0) = O(\epsilon D\tau_0) \tag{6.50}$$

$$\sigma_1(0) = O(\epsilon D\tau_0) \tag{6.51}$$

$$\frac{\partial\sigma_1}{\partial\tau'}(0) + \frac{\partial\sigma_0}{\partial\eta} = O(\epsilon D\tau_0). \tag{6.52}$$

Next, we integrate the leading order equations to find:

$$\sigma_0(\tau', \eta) = C_0(\eta)e^{-D\tau'} \tag{6.53}$$

$$\sigma_0(\tau', \eta) = A(\eta)\cos(\tau') + B(\eta)\sin(\tau') - \frac{D^2C_0(\eta)}{D^2+1}e^{-D\tau'}. \tag{6.54}$$

Next, we examine the right hand side of our equation for ψ_1. We note that any term on the right which is a constant multiple of $e^{-D\tau}$ will lead to a secular term. We require that such terms vanish and thereby obtain an equation for C_0:

$$C_0'(\eta) - \frac{D}{D^2+1}C_0(\eta) = 0 \tag{6.55}$$

where the prime denotes differentiation with respect to η. Solving this ode we find:

$$C_0(\eta) = C_0(0)\exp(\frac{D\eta}{D^2+1}) \tag{6.56}$$

and hence:

$$\psi_0(\tau',\eta) = C_0(0)\exp(\frac{D\eta}{D^2+1})\exp(-D\tau'). \tag{6.57}$$

Now, we still need the solution for ψ_1, but now ψ_1 satisfies:

$$\frac{\partial\psi_1}{\partial\tau'} + D\psi_1 = A(\eta)\sin(\tau') - B(\eta)\cos(\tau') \tag{6.58}$$

and the solution may be written as:

$$\psi_1(\tau',\eta) = C_1(\eta)e^{-D\tau'} + \int_0^{\tau'}(A(\eta)\sin(\zeta) - B(\eta)\cos(\zeta))e^{-D(\tau'-\zeta)}d\zeta. \tag{6.59}$$

Next, we examine the right hand side of the equation for σ_1. We note that any term on the right which is a constant multiple of $\sin(\tau')$ or $\cos(\tau')$ will lead to a secular term. Requiring these terms to vanish yields a system of ordinary differential equations for A and B:

$$\begin{bmatrix} A'(\eta) \\ B'(\eta) \end{bmatrix} = \begin{bmatrix} \frac{-D}{2(D^2+1)} & \frac{1}{2(D^2+1)} \\ \frac{-1}{2(D^2+1)} & \frac{-D}{2(D^2+1)} \end{bmatrix} \begin{bmatrix} A \\ B \end{bmatrix} \tag{6.60}$$

which is easily solved:

$$\begin{bmatrix} A(\eta) \\ B(\eta) \end{bmatrix} = \exp(\frac{-D\eta}{2(D^2+1)}) \begin{bmatrix} \cos(\frac{\eta}{2(D^2+1)}) & -\sin(\frac{\eta}{2(D^2+1)}) \\ \sin(\frac{\eta}{2(D^2+1)}) & \cos(\frac{\eta}{2(D^2+1)}) \end{bmatrix} \begin{bmatrix} A(0) \\ B(0) \end{bmatrix}. \tag{6.61}$$

We note that the initial conditions yield:

$$C_0(0) = \psi_s(\tau_0) \tag{6.62}$$

$$A(0) = \sigma_s(\tau_0) + \frac{D^2\psi_s(\tau_0)}{D^2+1} \tag{6.63}$$

$$B(0) = \dot{\sigma}_s(\tau_0) - \frac{D^3\psi_s(\tau_0)}{D^2+1}. \tag{6.64}$$

Finally, we write our leading order solution for ψ and σ in terms of τ:

$$\psi_0(\tau) = \psi_s(\tau_0)\exp(\frac{\epsilon D(\tau-\tau_0)}{D^2+1})\exp(-D(\tau-\tau_0)) \tag{6.65}$$

$$\begin{aligned}\sigma_0(\tau) &= A(\epsilon(\tau-\tau_0))\cos(\tau-\tau_0) + B(\epsilon(\tau-\tau_0))\sin(\tau-\tau_0) - \\ &\quad \frac{D^2\psi_s(\tau_0)}{D^2+1}\exp(\frac{\epsilon D(\tau-\tau_0)}{D^2+1})\exp(-D(\tau-\tau_0))\end{aligned} \tag{6.66}$$

where A and B are given by equations (6.61),(6.63) and (6.64).

6.4 Discussion

In this chapter we have considered a simple model of our electron beam joining process. We obtained this model by adding a source term to our mass-spring piston-cylinder oscillator, linearizing, and rewriting our equations in terms of a 'stress.' This yielded a coupled system of non-autonomous linear ordinary differential equations. We developed an approximate method which allowed us to construct solutions to this system. First, we should comment on our mathematical method. The method is based upon a simple observation. After a finite time, our source turns off. This allows us to separate our problem into two pieces, the first on the interval $(0, \tau_0)$ where the source is on, and the second on the interval (τ_0, ∞) where the source is off. The exact solution may be obtained by solving the problem in each region and patching the solutions together through initial conditions on the problem in the second region. However, we recognized that we have a small parameter in our problem. By exploiting this small parameter in the first region, we obtained an uncoupled system of ordinary differential equations which were easy to solve. We realized that this solution is not valid for all time, but was certainly valid up until the end of the pulse, i.e. until the start of the second region. So, we used this solution to provide initial conditions for the problem in the second region. In the second region, we then had an autonomous system of ordinary differential equations with non-zero

initial conditions. In order to exploit our small parameter in this region, we were forced to employ the method of multiple scales. This allowed us to develop a uniform approximation to the solution valid on (τ_0, ∞). It is natural to inquire as to why the method of multiple scales was not employed right at the start. We note that for this problem, this could indeed be done. However, for the more complicated problems we will face in later chapters, this approach becomes exceedingly difficult and often impossible. Here we have taken advantage of this simple setting to introduce our mathematical method.

We introduced this model with the hope of learning something about the electron-beam joining process. Although the model is too simple to allow quantitative statements, we can make qualitative statements and observations which later may be of some use. The most important conclusions we can draw concern the development of the stress during the pulse. Recall that our solution for the stress on the interval $(0, \tau_0)$ is:

$$\sigma_s(\tau) = \frac{PD}{D^2+1}(e^{-D\tau} - \cos(\tau)) - \frac{P\sin(\tau)}{D^2+1}. \tag{6.67}$$

Now, we wish to study variations in the maximum stress as a function of dimensionless pulse length, τ_0. In the actual electron beam joining process, the power P is varied with τ_0 to maintain a constant total amount of energy deposited. If we denote the dimensionless form of this energy by E, we may then write $P\tau_0 = E$. Rewriting the stress in terms of E we then have:

$$\sigma_s(\tau) = \frac{ED}{\tau_0(D^2+1)}(e^{-D\tau} - \cos(\tau)) - \frac{E\sin(\tau)}{\tau_0(D^2+1)}. \tag{6.68}$$

Next, we note that the relevant limit for our electron beam joining process is the limit where $D \to 0$. That is, the case where heat is transported on a time scale longer than that on which mechanical oscillations occur is the physical limit of interest. We begin by considering this limit. Then, our expression for the stress on the interval

$(0, \tau_0)$ reduces to:

$$\sigma_s(\tau) = -\frac{E\sin(\tau)}{\tau_0}. \tag{6.69}$$

Now, provided that $\tau_0 \leq \pi/2$, (6.69) has an extrema on the interval $(0, \tau_0)$ when $\tau = \tau_0$. That is, in amplitude, the maximum stress occurs at $\tau = \tau_0$ for all $\tau_0 \leq \pi/2$. For the moment, we restrict our attention to this range for τ_0. Then, the maximum stress amplitude is given by:

$$|\sigma_m| = \left|\frac{E\sin(\tau_0)}{\tau_0}\right|. \tag{6.70}$$

We may draw several conclusions from equation (6.70). First, the maximum stress amplitude is a monotonic decreasing function of τ_0. In the worst case, i.e. when $\tau_0 = 0$, the maximum stress amplitude is given by E. This would correspond to a delta function heat source in time. We note, that in order to capture variations of maximum stress with pulse length, we cannot model the source as a delta function. Next, as τ_0 is increased, the maximum stress amplitude decreases. Physically, we are seeing stress relaxation during the pulse. In our oscillator model, this simply means that the piston head begins to move on the time interval in which the source acts. We note that, if τ_0 is allowed to increase beyond $\pi/2$, then the maximum stress amplitude need not occur at the end of the pulse. Next, we write our maximum stress amplitude for non-zero D:

$$|\sigma_m| = \left|\frac{E}{\tau_0(D^2+1)}(-\sin(\tau_0) - D\cos(\tau_0) + De^{-D\tau_0})\right|. \tag{6.71}$$

If we plot our two expressions for the maximum stress amplitude as a function of τ_0, as is done in Figure 6.1, we see the effect of heat transport is to relieve the stress. That is, the maximum stress amplitude decreases as D is increased. Or, more simply, for fixed τ_0, the maximum stress amplitude is a monotonic decreasing function of D.

We stated at the outset that one of our most important goals was to understand how variations in pulse length and material properties affect the maximum stresses

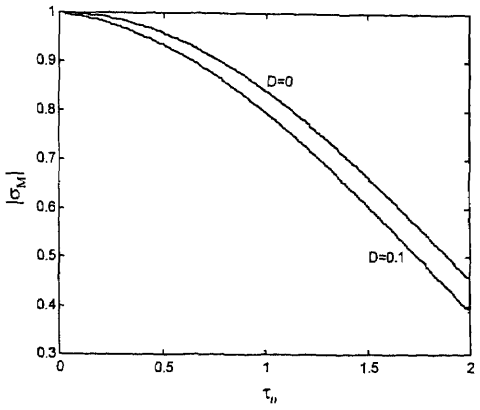

Figure 6.1 Stress amplitude vs. pulse length

which form during the joining process. We see from our simple model that there are at least two effects of which we must be aware. First, there is mechanical stress relaxation. That is, stresses are decreased when the pulse length is increased because the system has time to respond to internal forces. Second, there is thermal stress relaxation. That is, the smoothing of thermal gradients acts to relieve stresses. The magnitude of this thermal effect is governed by the ratio of a characteristic mechanical time to a characteristic thermal time and is a higher order effect compared to mechanical stress relaxation. Nonetheless, as we shall see, in the presence of sharp thermal gradients, diffusion becomes an important effect. Each of these effects depends upon system specific, or material, properties. In the remaining chapters we will refine these observations, and more clearly delineate the role played by variations in material properties.

CHAPTER 7

A MODEL IN AN INFINITE DOMAIN

In this chapter we take the next step toward understanding our electron beam joining process. In particular, we formulate the equations of linear thermoelasticity in an infinite domain with a source term which models the electron beam. We scale these equations and physically interpret the dimensionless parameters which arise. Then, we consider the uncoupled version of these equations and obtain solutions valid for small time. In this way, we derive expressions for the maximum stress formed during the pulse. These results are compared with those of Bailey, [34], in the appropriate limits.

7.1 Formulation of the Model

We begin by restating the equations of linear thermoelasticity applicable to a one-dimensional problem. First, we have the heat or energy equation which governs the temperature T:

$$\rho c_E \frac{\partial T}{\partial t'} = \kappa \frac{\partial^2 T}{\partial x^2} - \alpha T_A (3\lambda + 2\mu) \frac{\partial^2 u'}{\partial x' \partial t'} + S(x', t') \tag{7.1}$$

where here ρ denotes density, c_E specific heat at constant deformation, κ is thermal conductivity, α is the coefficient of thermal expansion, λ and μ are the Lame constants, u' is the displacement, T_A is a reference temperature, and S is a source term to be specified later. Next, we have a wave equation governing the stress, σ', in the x' direction:

$$(\lambda + 2\mu) \frac{\partial^2 \sigma'}{\partial x'^2} - (3\lambda + 2\mu) \rho \alpha \frac{\partial^2 T}{\partial t'^2} = \rho \frac{\partial^2 \sigma'}{\partial t'^2}. \tag{7.2}$$

In addition, we have the Duhamel-Neumann relation which connects the displacement and the stress:

$$\sigma' = (\lambda + 2\mu) \frac{\partial u'}{\partial x'} - (3\lambda + 2\mu) \alpha (T - T_A). \tag{7.3}$$

Finally, we assume quiescent initial conditions, that is:

$$T(x',0) = T_A \tag{7.4}$$

$$\sigma'(x',0) = 0 \tag{7.5}$$

$$\frac{\partial \sigma'}{\partial t'}(x',0) = -(3\lambda + 2\mu)\alpha \frac{\partial T}{\partial t'}(x',0). \tag{7.6}$$

Equations (7.1)-(7.6) supplemented with the appropriate boundary conditions and source term S, form the basis for all of the models of the electron beam joining process which we will study.

Now, we must consider how to choose the source term S. In essence, S models the electron beam. We would like to choose this source in such a way that the results of our analysis may be related to known beam parameters. The key beam parameters are the beam energy ε, the current I, the pulse length t_p, and the beam radius r_b. We may express the power, P, in terms of these parameters:

$$P = \varepsilon I.$$

Similarly, assuming a circular beam, we can compute the power density, P_d:

$$P_d = \frac{\varepsilon I}{\pi r_b^2}.$$

Now, the spatial variation in the source term S is given by the change in power density with respect to x', i.e. the energy lost by the beam and converted to thermal energy within the material. To account for the temporal variation, we include a function, G, which is only non-zero on the interval $(0, t_p)$. So:

$$S(x',t') = \frac{I}{\pi r_b^2} \frac{d\varepsilon}{dx'} G(t'/t_p). \tag{7.7}$$

As was mentioned in Chapter 5, spatial variations in the temperature profile are due to variations in heat capacity. This manifests itself in the source term once we recognize that the quantity:

$$\frac{1}{\rho} \frac{d\varepsilon}{dx'} \tag{7.8}$$

is essentially constant for all materials and beam energies of interest, [6]. We introduce the density into our source term to reflect this fact:

$$S(x',t') = \frac{I\rho}{\pi r_b^2}\frac{1}{\rho}\frac{d\varepsilon}{dx'}G(t'/t_p). \tag{7.9}$$

Now, since we are assuming a single material, this source term would be constant throughout all space. As was discussed in Chapter 5, when we seek to join different materials, variations in heat capacity cause a spatial variation in the thermal field. To capture this in our single slab model we artificially introduce spatial variation:

$$S(x',t') = \frac{I\rho}{\pi r_b^2}\frac{1}{\rho}\frac{d\varepsilon}{dx'}\phi(x'/L)G(t'/t_p) \tag{7.10}$$

and assume that L is some characteristic length of this spatial variation. Numerous authors have computed values of our source term for a wide variety of materials, [6, 35, 36, 37], typically through extensive Monte-Carlo type simulations of electron interaction with a specified material. Finally, we assume that the function G is given, as before, by a difference of Heaviside functions:

$$G(t'/t_p) = H(t'/t_p) - H(t'/t_p - 1). \tag{7.11}$$

7.2 Scaling

In this section we introduce dimensionless variables in order to recast our governing equations in non-dimensional form. For the convenience of the reader we restate our governing equations and include the boundary conditions appropriate for the study of an infinite slab:

$$\rho c_E\frac{\partial T}{\partial t'} = \kappa\frac{\partial^2 T}{\partial x^2} - \alpha T_A(3\lambda+2\mu)\frac{\partial^2 u'}{\partial x'\partial t'} + \frac{I\rho}{\pi r_b^2}\frac{1}{\rho}\frac{d\varepsilon}{dx'}\phi(x'/L)G(t'/t_p) \tag{7.12}$$

$$(\lambda+2\mu)\frac{\partial^2\sigma'}{\partial x'^2} - (3\lambda+2\mu)\rho\alpha\frac{\partial^2 T}{\partial t'^2} = \rho\frac{\partial^2\sigma'}{\partial t'^2} \tag{7.13}$$

$$\sigma' = (\lambda+2\mu)\frac{\partial u'}{\partial x'} - (3\lambda+2\mu)\alpha(T-T_A) \tag{7.14}$$

$$|T| \to 0 \quad \text{as} \quad |x'| \to \infty \tag{7.15}$$

$$|\sigma'| \to 0 \quad \text{as} \quad |x'| \to \infty \tag{7.16}$$

$$T(x', 0) = T_A \tag{7.17}$$

$$\sigma'(x', 0) = 0 \tag{7.18}$$

$$\frac{\partial \sigma'}{\partial t'}(x', 0) = -(3\lambda + 2\mu)\alpha \frac{\partial T}{\partial t'}(x', 0). \tag{7.19}$$

Now, we scale the temperature with respect to the initial temperature of the medium, the stress with respect to the Lame constants, the displacement and the spatial coordinate with respect to a characteristic length L defined by the deposition profile, and the time with the elastic wave speed:

$$\theta = \frac{T - T_A}{T_A}, \quad \Sigma = \frac{\sigma'}{\lambda + 2\mu}, \quad u = u'/L, \quad x = x'/L, \quad t = \frac{ct'}{L},$$

where:

$$c^2 = \frac{\lambda + 2\mu}{\rho}$$

and c is the speed of propagation of elastic waves in the medium of interest. Introducing these scalings into our governing equations yields:

$$\frac{\partial \theta}{\partial t} = D\frac{\partial^2 \theta}{\partial x^2} - \Gamma \frac{\partial^2 u}{\partial x \partial t} + p\phi(x)G(t/\tau_0) \tag{7.20}$$

$$\frac{\partial^2 \Sigma}{\partial t^2} = \frac{\partial^2 \Sigma}{\partial x^2} - \delta \frac{\partial^2 \theta}{\partial t^2} \tag{7.21}$$

$$\Sigma = \frac{\partial u}{\partial x} - \delta\theta \tag{7.22}$$

$$|\theta| \to \quad \text{as} \quad |x| \to \infty \tag{7.23}$$

$$|\Sigma| \to \quad \text{as} \quad |x| \to \infty \tag{7.24}$$

$$\theta(x, 0) = 0 \tag{7.25}$$

$$\Sigma(x, 0) = 0 \tag{7.26}$$

$$\frac{\partial \Sigma}{\partial t}(x, 0) = -\delta \frac{\partial \theta}{\partial t}(x, 0) \tag{7.27}$$

where here:

$$D = \frac{\kappa}{\rho c_E L c}, \quad \Gamma = \frac{\alpha}{\rho c_E}(3\lambda + 2\mu), \quad p = \frac{I}{\pi r_b^2 c_E T_A c}\frac{1}{\rho}\frac{d\varepsilon}{dx},$$

$$\delta = \frac{3\lambda + 2\mu}{\lambda + 2\mu}\alpha T_A, \quad \tau_0 = \frac{ct_p}{L}.$$

We further define $\epsilon = \Gamma\delta$ and rescale:

$$\sigma = \Sigma/\delta, \quad v = u/\delta.$$

Introducing these rescalings into our governing equations and eliminating the displacement in favor of the stress we arrive at:

$$\frac{\partial\theta}{\partial t} = D\frac{\partial^2\theta}{\partial x^2} - \epsilon(\frac{\partial\sigma}{\partial t} + \frac{\partial\theta}{\partial t}) + p\phi(x)G(t/\tau_0) \tag{7.28}$$

$$\frac{\partial^2\sigma}{\partial t^2} = \frac{\partial^2\sigma}{\partial x^2} - \frac{\partial^2\theta}{\partial t^2} \tag{7.29}$$

$$\sigma = \frac{\partial v}{\partial x} - \theta \tag{7.30}$$

$$|\theta| \to \quad \text{as} \quad |x| \to \infty \tag{7.31}$$

$$|\sigma| \to \quad \text{as} \quad |x| \to \infty \tag{7.32}$$

$$\theta(x, 0) = 0 \tag{7.33}$$

$$\sigma(x, 0) = 0 \tag{7.34}$$

$$\frac{\partial\sigma}{\partial t}(x, 0) = -\frac{\partial\theta}{\partial t}(x, 0). \tag{7.35}$$

It is worthwhile to pause and consider the physical interpretation of the five dimensionless parameters which arise in our scaled version of the governing equations. First, we notice that τ_0 is Bailey's parameter which was identified as important for assessing the magnitude of stress waves in electron beam joining experiments. As τ_0 is a ratio of pulse length to a characteristic mechanical oscillation time, τ_0 may be thought of as a dimensionless pulse length, measuring the relative speed of heat input to elastic wave propagation. The parameter Γ is known as the Gruneisen parameter

and measures the change in pressure in a medium due to thermal excitation. The Grueneisen parameter also possesses a thermodynamic definition, $\rho\Gamma = \Delta P/\Delta E$. Where here, ΔP is a change in pressure and ΔE is a change in internal energy. The parameter δ is a non-dimensional version of the coefficient of thermal expansion. The product of δ and Γ, which we have labeled ϵ, is typically referred to as the coupling constant. We note that for most engineering materials ϵ is a small parameter. Next, the parameter p may be interpreted as a dimensionless power. For high-energy electron beams p is an order one quantity. Finally, we note that D is a ratio of two time scales in the problem. In particular, it is a ratio of a characteristic mechanical time, L/c, to a characteristic thermal time $(\rho c_E L^2)/\kappa$. Consequently, D plays the same role as did the parameter β in Chapter 4. We note that D is typically a small parameter, that is, elastic waves propagate on a time scale shorter than that on which heat diffuses.

7.3 Short Time Analysis, $D \to 0$

As in the previous chapter, we note that during the pulse the uncoupled approximation is valid. That is, for short times, we recognize that the effects of thermoelastic decay are minimal. Hence, we set ϵ to zero, and consider the uncoupled equations. As was shown earlier, this approximation is valid provided that $t \ll (\epsilon D)^{-1}$. Further, as was noted above, D is typically a small parameter. We further simplify our governing equations by considering the limit $D \to 0$. Now, while sending ϵ to zero limits the validity in time of our solution, sending D to zero restricts the validity of our solution both in time and in space. First, if we view sending D to zero as a regular perturbation expansion of our solutions to heat equation, we recognize that this expansion becomes non-uniform it time. In particular, our solution viewed in this manner will only be valid provided that $t \ll D^{-1}$. Next, we recognize that D multiplies the highest order derivative in the heat equation, hence this is really

a singular perturbation problem in space. In regions where the deposition profile, ϕ, undergoes rapid change, the diffusion term will become non-negligible. That is, we recognize, that by sending D to zero, we may in fact be introducing boundary layers into the solution. These boundary layers may be treated in one of two ways. First, we could assume that ϕ is sufficiently smooth, so that no boundary layers arise. Or, we could identify the location of these boundary layers and use boundary layer theory to obtain a spatially uniform approximation to the solution. In Chapter 9, we develop such a solution. In this section, we take neither approach. Rather, we simply note these difficulties and study the following simplified equations:

$$\frac{\partial \theta}{\partial t} = p\phi(x)G(t/\tau_0) \tag{7.36}$$

$$\frac{\partial^2 \sigma}{\partial t^2} = \frac{\partial^2 \sigma}{\partial x^2} - \frac{\partial^2 \theta}{\partial t^2} \tag{7.37}$$

$$\sigma = \frac{\partial v}{\partial x} - \theta \tag{7.38}$$

$$|\theta| \to \quad \text{as} \quad |x| \to \infty \tag{7.39}$$

$$|\sigma| \to \quad \text{as} \quad |x| \to \infty \tag{7.40}$$

$$\theta(x,0) = 0 \tag{7.41}$$

$$\sigma(x,0) = 0 \tag{7.42}$$

$$\frac{\partial \sigma}{\partial t}(x,0) = -\frac{\partial \theta}{\partial t}(x,0). \tag{7.43}$$

We begin by integrating equation (7.36) with respect to t and applying the initial condition (7.41) to obtain:

$$\theta(x,t) = p\phi(x)\int_0^t G(\zeta/\tau_0)d\zeta. \tag{7.44}$$

Now, using this solution for θ and applying the spatial Fourier transform to equations (7.37,7.42,7.43) we obtain:

$$\frac{d^2\hat{\sigma}}{dt^2} + \omega^2\hat{\sigma} = -p\hat{\phi}(\delta(t) - \delta(t-\tau_0)) \tag{7.45}$$

$$\hat{\sigma}(\omega, 0) = \hat{\sigma}_t(\omega, 0) = 0 \tag{7.46}$$

where here hat's denote transformed functions, ω is the Fourier transform variable, and $\delta(t)$ is the Dirac delta function. Next, we apply the Laplace transform in time, denote the doubly transformed functions with a bar, and solve for $\bar{\sigma}$ to obtain:

$$\bar{\sigma} = \frac{p\hat{\phi}}{s^2 + \omega^2}(e^{-s\tau_0} - 1) \tag{7.47}$$

where here s is the Laplace transform variable. Now, the inversion with respect to the Laplace transform variable may be easily carried out to obtain:

$$\hat{\sigma} = \frac{p\hat{\phi}}{\omega}(H(t - \tau_0)\sin(\omega(t - \tau_0)) - \sin(\omega t)). \tag{7.48}$$

Then, with the aid of the convolution theorem for Fourier transforms we may invert this to obtain:

$$\sigma(x, t) = -\frac{p}{2}\int_{x-t}^{x+t} \phi(\zeta)d\zeta + \frac{p}{2}H(t - \tau_0)\int_{x-t+\tau_0}^{x+t-\tau_0} \phi(\zeta)d\zeta. \tag{7.49}$$

Finally, for $t \leq \tau_0$ we state the solutions for both θ and σ:

$$\theta(x, t) = p\phi(x)t \tag{7.50}$$

$$\sigma(x, t) = -\frac{p}{2}\int_{x-t}^{x+t} \phi(\zeta)d\zeta. \tag{7.51}$$

7.4 Discussion

In this chapter we derived short time solutions, valid during the electron beam pulse, for the thermoelastic response of a single infinite elastic slab. We took care to relate the source term in the heat equation to known beam parameters. This allows us to compare our results with known expressions for stresses formed in electron beam joining experiments. Our governing equations were subjected to several simplifications. First, throughout this chapter, we have considered only the uncoupled approximation. We again note that this implies that our solutions are valid only

when $t \ll (\epsilon D)^{-1}$. As we are interested in stresses formed during the pulse, this presents no real difficulty. Next, in Section 7.3, we made the additional assumption that D was small, and set D to zero. We noted that this restricted the validity of our solutions in both time and space. In particular, our solutions thus obtained are only valid for $t \ll D^{-1}$, and for smooth deposition profiles. However, as we shall see, these crude approximations yield the standard stress estimates given by Bailey, [34]. Now, let us examine our solutions, and use them to study the electron beam joining process.

We begin with solutions obtained in Section 7.3, that is when D was set equal to zero. In this case, we found that for $t \leq \tau_0$ the stress field was given by:

$$\sigma(x,t) = -\frac{p}{2}\int_{x-t}^{x+t} \phi(\zeta)d\zeta. \tag{7.52}$$

Now, in order to compare with Bailey, we need to choose a specific form for the deposition profile, ϕ. We note that Bailey assumed a triangular deposition profile with compact support in the interior of an infinite slab. However, we can show, that any deposition profile, properly scaled, with compact support, leads directly to Bailey's results. Recall that we have assumed that the deposition profile is characterized by some length scale L. Further, we scaled our spatial variables with respect to L. Hence, it is appropriate to assume that ϕ is only non-zero on the interval $(-1/2, 1/2)$. In addition, to be compatible with Bailey's analysis, we must require that the total energy deposited be independent of ϕ. Hence we assume:

$$\int_{-\infty}^{\infty} \phi(x)dx = 1. \tag{7.53}$$

With these assumptions, we evaluate (7.52) at the end of the pulse, i.e. at $t = \tau_0$, and consider the limit $\tau_0 \gg 1$ for fixed finite x. Then we find:

$$\sigma(x,\tau_0) \to -\frac{p}{2}. \tag{7.54}$$

If we scale the change in electron energy per unit length with respect to beam energy, and rewrite in terms of dimensional variables we find:

$$|\sigma'| = \frac{\Gamma J \varepsilon_0}{2c} \tag{7.55}$$

where here J is the current density and ε_0 is the beam energy. This is the result obtained by Bailey, [34], for long pulse lengths. Next, we consider the limit where $\tau_0 \to 0$. Then:

$$\sigma(x, \tau_0) \to -p\tau_0\phi(x). \tag{7.56}$$

If we evaluate at the maximum of ϕ, assumed to be scaled to one, and rewrite in dimensional variables we find:

$$|\sigma'| = \frac{\rho \Gamma E}{2m} \tag{7.57}$$

where here, $E = I\varepsilon_0 t_p$, $V = \pi r_0^2 L$, $m = \rho V$, and we multiplied by a factor of $1/2$ to be compatible with Bailey's propagating stress estimates. This result then agrees with Bailey's result for short pulse lengths.

Thus far, we have shown that our expression for the stress reduces to those obtained by Bailey in the appropriate limits. Further, we have shown that in the long and short pulse length limits, Bailey's results are independent of the deposition profile, provided the deposition profile has compact support. Next, we would like to use our expression to study the variation in the stress as a function of pulse length for fixed total energy deposited. Rather than choosing a deposition profile with compact support, which is somewhat unrealistic, we choose a deposition profile which is piecewise constant. In particular, we assume:

$$p\phi(x) = p_1 + (p_2 - p_1)H(x + 1/2) + (p_3 - p_2)H(x - 1/2). \tag{7.58}$$

This choice simulates an interlayer of width L, located between $-L/2$ and $L/2$, and surrounded by two different materials. We further restrict our attention to the stress at a particular point in space. Speculating that the maximum stress should occur

within the interlayer, we consider the stress at $x = 0$. We have two cases. If $\tau_0 < 1/2$ then:

$$\sigma(0, \tau_0) = -p_2 \tau_0. \tag{7.59}$$

If $\tau_0 > 1/2$ then:

$$\sigma(0, \tau_0) = -\frac{p_2}{2} - \frac{(p_1 + p_3)(\tau_0 - 1/2)}{2}. \tag{7.60}$$

Now, we imagine that our goal is to heat the interlayer to some joining temperature. That is, it is necessary to fix the quantity $p_2\tau_0$. We define $E = p_2\tau_0$, and note that p_1 and p_3 also scale with E. That is, we let $p_1\tau_0 = aE$ and $p_3\tau_0 = bE$. We immediately observe that for $\tau_0 < 1/2$, the stress at $x = 0$ does not vary with pulse length when the energy deposited in the interlayer, E, is held fixed. For $\tau_0 > 1/2$ we find:

$$\sigma(0, \tau_0) = -\frac{E}{2\tau_0} - \frac{E(a+b)(\tau_0 - 1/2)}{2\tau_0}. \tag{7.61}$$

We observe that stress decreases with increasing pulse length. In the case where no energy is deposited outside of the interlayer, i.e. $p_1 = p_3 = 0$, the stress tends to zero as τ_0 tends to infinity. In this case, the stress generated in the interlayer is able to propagate freely into the surrounding regions. If p_1 and p_3 are not identically zero, then thermal stresses are being generated everywhere within the slab. In this case, as τ_0 tends to infinity, we find that there is a non-zero stress remaining and that it is equal to:

$$\sigma(0, \tau_0) \to -\frac{E(a+b)}{2}. \tag{7.62}$$

Note that this represents an average of the stresses being generated in the outer regions, and can be interpreted as a restriction on how much stress can be propagated out of the interlayer.

Finally, we note that our results thus far compare favorably with those obtained in the previous chapter. In particular, we again observed mechanical stress relaxation by considering the limit where diffusion tends to zero. In addition, in this chapter we have begun to incorporate spatial variations due to the presence of multiple slabs

into our stress analysis. We note that even this simplistic analysis begins to yield possible design criteria. Most striking is the result that, to obtain significant stress reduction by varying pulse length, we must require that $\tau_0 > 1/2$. Physically, this says that information from the interlayer boundaries must have sufficient time to reach the origin if stress reduction due to increased pulse length is to occur.

CHAPTER 8

ANALYSIS FOR A SINGLE FINITE SLAB

In this chapter we continue our investigation of single-pulse high-energy electron beam joining. Here, we apply the model equations presented in Chapter 7 to a problem in a finite domain. Further, we derive both short and long time solutions, applying the methods developed in Chapter 6. We further investigate the mechanical and thermal stress relaxation effects uncovered in previous chapters. In addition, we uncover the presence of a boundary effect and discuss thermoelastic decay. Finally, we investigate this problem numerically, and provide numerical solutions to illustrate the various effects.

8.1 Formulation of the Model

Here, we restate our governing equations in dimensionless form, with boundary conditions applicable to a single finite slab:

$$\frac{\partial \theta}{\partial t} = D\frac{\partial^2 \theta}{\partial x^2} - \epsilon(\frac{\partial \sigma}{\partial t} + \frac{\partial \theta}{\partial t}) + p\phi(x)G(t/\tau_0) \quad 0 < x < 1 \tag{8.1}$$

$$\frac{\partial^2 \sigma}{\partial t^2} = \frac{\partial^2 \sigma}{\partial x^2} - \frac{\partial^2 \theta}{\partial t^2} \quad 0 < x < 1 \tag{8.2}$$

$$\sigma = \frac{\partial v}{\partial x} - \theta \tag{8.3}$$

$$\frac{\partial \theta}{\partial x} = 0 \quad \text{at} \quad x = 0, 1 \tag{8.4}$$

$$\sigma = 0 \quad \text{at} \quad x = 0, 1 \tag{8.5}$$

$$\theta(x, 0) = 0 \tag{8.6}$$

$$\sigma(x, 0) = 0 \tag{8.7}$$

$$\frac{\partial \sigma}{\partial t}(x, 0) = -\frac{\partial \theta}{\partial t}(x, 0) \tag{8.8}$$

and note that the length scale L with which displacements and spatial variables have been scaled is the length of the entire slab. We further note that this changes the

meaning of the deposition profile, ϕ, which now contains a ratio of two length scales. In other words, ϕ is a function of Lx/l, where l is a characteristic length scale of the deposition profile. In addition, we have introduced boundary conditions on θ and σ. In particular, we have assumed that the slab is perfectly insulated, hence θ_x vanishes at each end. Recall that joining experiments are performed in a vacuum chamber, [6], hence this is a reasonable first approximation. Finally, we have assumed stress free boundary conditions at either end of the slab. This is again suggested by typical experimental configurations, [6].

8.2 Short Time Solution

Recall, in Chapter 6, we introduced an approximate method based on the observation that our source turns off after a finite time. We divided the problem into two pieces, that of finding an approximate solution on $(0, \tau_0)$ and that of finding an approximate solution on (τ_0, ∞). In this section we develop an approximate solution for the single slab problem on $(0, \tau_0)$. We assume that both ϵ and D are small parameters, and we study:

$$\frac{\partial \theta}{\partial t} = p\phi(x)G(t/\tau_0) \quad 0 < x < 1 \tag{8.9}$$

$$\frac{\partial^2 \sigma}{\partial t^2} = \frac{\partial^2 \sigma}{\partial x^2} - \frac{\partial^2 \theta}{\partial t^2} \quad 0 < x < 1 \tag{8.10}$$

$$\sigma = \frac{\partial v}{\partial x} - \theta \tag{8.11}$$

$$\frac{\partial \theta}{\partial x} = 0 \quad \text{at} \quad x = 0, 1 \tag{8.12}$$

$$\sigma = 0 \quad \text{at} \quad x = 0, 1 \tag{8.13}$$

$$\theta(x, 0) = 0 \tag{8.14}$$

$$\sigma(x, 0) = 0 \tag{8.15}$$

$$\frac{\partial \sigma}{\partial t}(x, 0) = -\frac{\partial \theta}{\partial t}(x, 0). \tag{8.16}$$

We further assume that the deposition profile ϕ is continuous and differentiable, and that $\phi'(x)$ vanishes at both endpoints. This prevents the appearance of any boundary layers in our solution for θ. That is, it removes the spatially singular nature of the perturbation expansion as discussed in the previous chapter. With these assumptions, we may solve for θ immediately:

$$\theta(x,t) = -p\phi(x)\int_0^t G(\zeta/\tau_0)d\zeta. \tag{8.17}$$

Then, using this solution for θ the problem for the stress field reduces to:

$$\frac{\partial^2\sigma}{\partial t^2} = \frac{\partial^2\sigma}{\partial x^2} - p\phi(x)(\delta(t) - \delta(t-\tau_0)) \tag{8.18}$$

$$\sigma(0,t) = \sigma(1,t) = 0 \tag{8.19}$$

$$\sigma(x,0) = \sigma_t(x,0) = 0. \tag{8.20}$$

Now, the solution to this problem may be found by eigenfunction expansion. The procedure is straightforward and we find:

$$\sigma(x,t) = -\frac{p}{2}\int_0^1 \phi(\zeta)\sum_{n=1}^{\infty}\frac{\sin(n\pi t)\sin(n\pi x)\sin(n\pi\zeta)}{n\pi}d\zeta + \tag{8.21}$$

$$\frac{pH(t-\tau_0)}{2}\int_0^1 \phi(\zeta)\sum_{n=1}^{\infty}\frac{\sin(n\pi(t-\tau_0))\sin(n\pi x)\sin(n\pi\zeta)}{n\pi}d\zeta. \tag{8.22}$$

Or, if we wish the solution valid on $(0,\tau_0)$:

$$\sigma(x,t) = -\frac{p}{2}\int_0^1 \phi(\zeta)\sum_{n=1}^{\infty}\frac{\sin(n\pi t)\sin(n\pi x)\sin(n\pi\zeta)}{n\pi}d\zeta. \tag{8.23}$$

8.3 Long Time Solution

In this section we obtain a solution which is valid on the interval (τ_0,∞). In Chapter 6, we introduced the method of multiple scales, and exploited the method to find a long time solution for a model problem. Our reason for using a multiple scale method was that a regular perturbation expansion failed, i.e. such an expansion becomes non-uniform in time. For the equations we study here, the same holds true.

Here, to remove secular terms, we again exploit a multiple scale method, although rather than the usual 'two-timing' procedure we introduce a 'three-timing' procedure. That is, we recognize and exploit the presence of three time scales in our problem. First, on the t time scale, wave propagation occurs. Next, on the Dt time scale, heat diffuses. Finally, on the ϵDt time scale, thermoelastic decay takes place. Since both D and ϵ are small parameters, these three timescales are distinct.

We begin by ordering our parameters with respect to ϵ, in particular, we let $D = \beta\epsilon$, where β is $O(1)$. Introducing this rescaling into our governing equations, noting that our source has turned off, and recalling that initial conditions are given by the short time solution we then have:

$$\frac{\partial\theta}{\partial t} = \beta\epsilon\frac{\partial^2\theta}{\partial x^2} - \epsilon(\frac{\partial\sigma}{\partial t} + \frac{\partial\theta}{\partial t}) \quad 0 < x < 1 \tag{8.24}$$

$$\frac{\partial^2\sigma}{\partial t^2} = \frac{\partial^2\sigma}{\partial x^2} - \frac{\partial^2\theta}{\partial t^2} \quad 0 < x < 1 \tag{8.25}$$

$$\sigma = \frac{\partial v}{\partial x} - \theta \tag{8.26}$$

$$\theta_x = 0 \quad \text{at} \quad x = 0, 1 \tag{8.27}$$

$$\sigma = 0 \quad \text{at} \quad x = 0, 1 \tag{8.28}$$

$$\theta(x, \tau_0) = \psi_0 \tag{8.29}$$

$$\sigma(x, \tau_0) = \psi_1 \tag{8.30}$$

$$\frac{\partial\sigma}{\partial t}(x, \tau_0) = \psi_2 \tag{8.31}$$

where the functions ψ_i are obtained from the short term solution. Next, we define two new time variables:

$$\tau = \epsilon t \qquad \eta = \epsilon^2 t$$

and seek solutions as functions of the three time variables in the form of a power series in ϵ:

$$\theta \sim \theta_0(x, t, \tau, \eta) + \epsilon\theta_1(x, t, \tau, \eta) + \cdots$$

$$\sigma \sim \sigma_0(x,t,\tau,\eta) + \epsilon\sigma_1(x,t,\tau,\eta) + \cdots.$$

We also replace our time derivatives by:

$$\frac{\partial}{\partial t} \longrightarrow \frac{\partial}{\partial t} + \epsilon\frac{\partial}{\partial \tau} + \epsilon^2\frac{\partial}{\partial \eta}$$

$$\frac{\partial^2}{\partial t^2} \longrightarrow \frac{\partial^2}{\partial t^2} + 2\epsilon\frac{\partial^2}{\partial t\partial \tau} + 2\epsilon^2\frac{\partial^2}{\partial t\partial \tau} + \epsilon^2\frac{\partial^2}{\partial \tau^2} + O(\epsilon^3).$$

Introducing our power series expansions into our governing equations, (8.24-8.31), and equating to zero coefficients of powers of epsilon we obtain an infinite set of equations for the θ_n and σ_n. We list the first three, which are sufficient to determine the leading order behavior:

$$\frac{\partial \theta_0}{\partial t} = 0 \tag{8.32}$$

$$\frac{\partial^2 \sigma_0}{\partial t^2} = \frac{\partial^2 \sigma_0}{\partial x^2} - \frac{\partial^2 \theta_0}{\partial t^2} \tag{8.33}$$

$$\frac{\partial \theta_0}{\partial x} = 0 \quad \text{at} \quad x = 0, 1 \tag{8.34}$$

$$\sigma_0 = 0 \quad \text{at} \quad x = 0, 1 \tag{8.35}$$

$$\theta_0(x, \tau_0) = \psi_0 \tag{8.36}$$

$$\sigma_0(x, \tau_0) = \psi_1 \tag{8.37}$$

$$\frac{\partial \sigma_0}{\partial t}(x, \tau_0) = \psi_2 \tag{8.38}$$

and

$$\frac{\partial \theta_1}{\partial t} = \beta\frac{\partial^2 \theta_0}{\partial x^2} - \frac{\partial \theta_0}{\partial \tau} - \frac{\partial \sigma_0}{\partial t} - \frac{\partial \theta_0}{\partial t} \tag{8.39}$$

$$\frac{\partial^2 \sigma_1}{\partial t^2} + 2\frac{\partial^2 \sigma_0}{\partial t\partial \tau} = \frac{\partial^2 \sigma_1}{\partial x^2} - \frac{\partial^2 \theta_1}{\partial t^2} - 2\frac{\partial^2 \theta_0}{\partial t\partial \tau} \tag{8.40}$$

$$\frac{\partial \theta_1}{\partial x} = 0 \quad \text{at} \quad x = 0, 1 \tag{8.41}$$

$$\sigma_1 = 0 \quad \text{at} \quad x = 0, 1 \tag{8.42}$$

$$\theta_1(x, \tau_0) = O(\epsilon) \tag{8.43}$$

$$\sigma_1(x, \tau_0) = O(\epsilon) \tag{8.44}$$

$$\frac{\partial \sigma_1}{\partial t}(x,\tau_0) + \frac{\partial \sigma_0}{\partial \tau}(x,\tau_0) = O(\epsilon) \tag{8.45}$$

and

$$\frac{\partial \theta_2}{\partial t} + \frac{\partial \theta_1}{\partial \tau} + \frac{\partial \theta_0}{\partial \eta} = \beta \frac{\partial^2 \theta_1}{\partial x^2} - \frac{\partial \theta_0}{\partial \tau} - \frac{\partial \sigma_1}{\partial t} - \frac{\partial \theta_1}{\partial t} - \frac{\partial \sigma_0}{\partial \tau} \tag{8.46}$$

$$\frac{\partial^2 \sigma_2}{\partial t^2} + 2\frac{\partial^2 \sigma_1}{\partial t \partial \tau} + 2\frac{\partial \sigma_0}{\partial t \partial \eta} = \frac{\partial^2 \sigma_2}{\partial x^2} - \frac{\partial^2 \theta_2}{\partial t^2} - 2\frac{\partial^2 \theta_1}{\partial t \partial \tau} - 2\frac{\partial^2 \theta_0}{\partial t \partial \eta} - \frac{\partial^2 \sigma_0}{\partial \tau^2} - \frac{\partial^2 \theta_0}{\partial \tau^2} \tag{8.47}$$

$$\frac{\partial \theta_2}{\partial x} = 0 \quad \text{at} \quad x = 0, 1 \tag{8.48}$$

$$\sigma_2 = 0 \quad \text{at} \quad x = 0, 1 \tag{8.49}$$

$$\theta_2(x,\tau_0) = O(\epsilon^2) \tag{8.50}$$

$$\sigma_2(x,\tau_0) = O(\epsilon^2) \tag{8.51}$$

$$\frac{\partial \sigma_2}{\partial t}(x,\tau_0) + \frac{\partial \sigma_1}{\partial \tau}(x,\tau_0) + \frac{\partial \sigma_2}{\partial \eta}(x,\tau_0) = O(\epsilon^2). \tag{8.52}$$

Now, we begin with the leading order equations. Equation (8.32) immediately implies that θ_0 is independent of t, that is $\theta_0 = \theta_0(x, \tau, \eta)$. Consequently, the leading order equations for σ_0 reduce to a simple initial-boundary value problem:

$$\frac{\partial^2 \sigma_0}{\partial t^2} = \frac{\partial^2 \sigma_0}{\partial x^2} \tag{8.53}$$

$$\sigma_0 = 0 \quad \text{at} \quad x = 0, 1 \tag{8.54}$$

$$\sigma_0(x,\tau_0) = \psi_1 \tag{8.55}$$

$$\frac{\partial \sigma_0}{\partial t}(x,\tau_0) = \psi_2 \tag{8.56}$$

which may be easily solved by eigenfunction expansion to yield:

$$\sigma_0 = \sum_{n=1}^{\infty} (a_n(\tau,\eta)\sin(n\pi t) + b_n(\tau,\eta)\cos(n\pi t))\sin(n\pi x) \tag{8.57}$$

where we have taken care to note that the coefficients in the Fourier series are functions of τ and η. Next, we turn to the $O(\epsilon)$ equations. Recall that the equation for θ_1 is:

$$\frac{\partial \theta_1}{\partial t} = \beta \frac{\partial^2 \theta_0}{\partial x^2} - \frac{\partial \theta_0}{\partial \tau} - \frac{\partial \sigma_0}{\partial t} - \frac{\partial \theta_0}{\partial t}. \tag{8.58}$$

From our leading order solution, we find that the last term on the right vanishes, while the third term on the right yields no secular terms when integrated. The first two terms on the right however are independent of t and hence we must require that:

$$\frac{\partial \theta_0}{\partial \tau} = \beta \frac{\partial^2 \theta_0}{\partial x^2} \tag{8.59}$$

which implies that:

$$\frac{\partial \theta_1}{\partial t} = -\frac{\partial \sigma_0}{\partial t}. \tag{8.60}$$

Similarly, we examine the equation for σ_1:

$$\frac{\partial^2 \sigma_1}{\partial t^2} + 2\frac{\partial^2 \sigma_0}{\partial t \partial \tau} = \frac{\partial^2 \sigma_1}{\partial x^2} - \frac{\partial^2 \theta_1}{\partial t^2} - 2\frac{\partial^2 \theta_0}{\partial t \partial \tau}. \tag{8.61}$$

Now, using (8.60), and again recalling that θ_0 is independent of t, we may rewrite as:

$$\frac{\partial^2 \sigma_1}{\partial t^2} - \frac{\partial^2 \sigma_1}{\partial x^2} = \frac{\partial^2 \sigma_0}{\partial t^2} - 2\frac{\partial^2 \sigma_0}{\partial t \partial \tau}. \tag{8.62}$$

Here, both terms on the right lead to secular terms, hence we must require that they vanish:

$$\frac{\partial^2 \sigma_0}{\partial t^2} - 2\frac{\partial^2 \sigma_0}{\partial t \partial \tau} = 0. \tag{8.63}$$

Inserting our solution for σ_0, (8.57), into (8.63) and using orthogonality yields two coupled equations for the a_n's and b_n's:

$$\frac{\partial b_n}{\partial \tau} - \frac{n\pi a_n}{2} = 0 \tag{8.64}$$

$$\frac{\partial a_n}{\partial \tau} + \frac{n\pi b_n}{2} = 0. \tag{8.65}$$

These are easily integrated to yield:

$$a_n = c_n(\eta)\cos(\frac{n\pi\tau}{2}) - d_n(\eta)\sin(\frac{n\pi\tau}{2}) \tag{8.66}$$

$$b_n = c_n(\eta)\sin(\frac{n\pi\tau}{2}) + d_n(\eta)\cos(\frac{n\pi\tau}{2}). \tag{8.67}$$

Finally, we must turn our attention to the $O(\epsilon^2)$ equations. Recall that the equation for θ_2 is:

$$\frac{\partial\theta_2}{\partial t} = -\frac{\partial\theta_1}{\partial\tau} - \frac{\partial\theta_0}{\partial\eta} + \beta\frac{\partial^2\theta_1}{\partial x^2} - \frac{\partial\theta_0}{\partial\tau} - \frac{\partial\sigma_1}{\partial t} - \frac{\partial\theta_1}{\partial t} - \frac{\partial\sigma_0}{\partial\tau}. \tag{8.68}$$

Now, the term involving σ_0 and the term involving σ_1 do not lead to secular terms and may be temporarily ignored. The terms involving θ_1 may be related to σ_0 through (8.60), and used to determine the θ_1 solution. Since we are only interested in the leading order solution, we do not carry this out. Finally, the remaining terms lead directly to secular terms and must be suppressed:

$$\frac{\partial\theta_0}{\partial\tau} + \frac{\partial\theta_0}{\partial\eta} = 0 \tag{8.69}$$

which implies:

$$\frac{\partial\theta_2}{\partial t} = -\frac{\partial\sigma_1}{\partial t} - \frac{\partial\theta_1}{\partial t} - \beta\frac{\partial^2\sigma_0}{\partial x^2}. \tag{8.70}$$

Next, we turn our attention to the equation for σ_2:

$$\frac{\partial^2\sigma_2}{\partial t^2} - \frac{\partial^2\sigma_2}{\partial x^2} = -2\frac{\partial^2\sigma_1}{\partial t\partial\tau} - 2\frac{\partial\sigma_0}{\partial t\partial\eta} - \frac{\partial^2\theta_2}{\partial t^2} - 2\frac{\partial^2\theta_1}{\partial t\partial\tau} - 2\frac{\partial^2\theta_0}{\partial t\partial\eta} - \frac{\partial^2\sigma_0}{\partial\tau^2} - \frac{\partial^2\theta_0}{\partial\tau^2}. \tag{8.71}$$

Using the fact that θ_0 is independent of t, equation (8.60), equation (8.70), and suppressing secular terms as before leads to the requirement that:

$$-\frac{\partial^2\sigma_0}{\partial\tau^2} + \beta\frac{\partial^3\sigma_0}{\partial t\partial x^2} - 2\frac{\partial^2\sigma_0}{\partial t\partial\eta} = 0. \tag{8.72}$$

Finally, using the solution for σ_0 and orthogonality, we find that the c_n's and d_n's must satisfy:

$$\frac{\partial c_n}{\partial\eta} + \frac{n^2\pi^2\beta c_n}{2} = \frac{n\pi d_n}{8} \tag{8.73}$$

$$\frac{\partial d_n}{\partial\eta} + \frac{n^2\pi^2\beta d_n}{2} = -\frac{n\pi c_n}{8}. \tag{8.74}$$

Again, these are easily solved:

$$c_n = \exp(\frac{-n^2\pi^2\beta\eta}{2})(c_{n0}\cos(\frac{n\pi\eta}{8}) + d_{n0}\sin(\frac{n\pi\eta}{8})) \tag{8.75}$$

$$d_n = \exp(\frac{-n^2\pi^2\beta\eta}{2})(-c_{n0}\sin(\frac{n\pi\eta}{8}) + d_{n0}\cos(\frac{n\pi\eta}{8})) \tag{8.76}$$

where c_{n0} and d_{n0} are to be determined through initial conditions. Finally, we collect our results. Eliminating τ and η in favor of t, we find the stress field is given by:

$$\begin{aligned}\sigma_0(x,t) &= \sum_{n=1}^{\infty} c_{n0}\exp(\frac{-n^2\pi^2\epsilon Dt}{2})\sin(n\pi t(1+\epsilon/2-\epsilon^2/8))\sin(n\pi x) \\ &+ \sum_{n=1}^{\infty} d_{n0}\exp(\frac{-n^2\pi^2\epsilon Dt}{2})\cos(n\pi t(1+\epsilon/2-\epsilon^2/8))\sin(n\pi x)\end{aligned} \tag{8.77}$$

$$\sigma_0(x,\tau_0) = \psi_1 \tag{8.78}$$

$$\frac{\partial\sigma_0}{\partial t}(x,\tau_0) = \psi_2. \tag{8.79}$$

In addition, the temperature field is given by the solution to:

$$\frac{\partial\theta_0}{\partial\tau} = \beta\frac{\partial^2\theta_0}{\partial x^2} \tag{8.80}$$

$$\frac{\partial\theta_0}{\partial\tau} + \frac{\partial\theta_0}{\partial\eta} = 0 \tag{8.81}$$

$$\frac{\partial\theta_0}{\partial x} = 0 \quad \text{at} \quad x = 0,1 \tag{8.82}$$

$$\theta_0(x,\tau_0) = \psi_0. \tag{8.83}$$

We note that the determining equations for θ_0 may be simplified by defining $\zeta = \tau - \eta$ and seeking a solution of the form $\theta_0 = \theta_0(x,\zeta)$. Then equation (8.81) is automatically satisfied and we are left with:

$$\frac{\partial\theta_0}{\partial\zeta} = \beta\frac{\partial^2\theta_0}{\partial x^2} \tag{8.84}$$

$$\frac{\partial\theta_0}{\partial x} = 0 \quad \text{at} \quad x = 0,1 \tag{8.85}$$

$$\theta_0(x,\tau_0) = \psi_0. \tag{8.86}$$

8.4 Numerical Solutions

In this section we report the results of a numerical investigation of the single slab problem. Equations (8.1-8.8) were discretized and an explicit finite difference scheme derived. Although stability is difficult to prove for this scheme, a Von-Neumann stability analysis suggests appropriate criteria. In particular, seeking solutions of the form:

$$\lambda^n e^{ikj\Delta x}, \tag{8.87}$$

to the discrete equations, where here spacetime is discretized as $(n\Delta t, j\Delta x)$ and k is an arbitrary wavenumber, leads to the following cubic polynomial for λ:

$$(\lambda-1)^3 + 4r(\lambda-1)^2\sin^2(\theta) + (1+\epsilon)4\alpha\lambda(\lambda-1)\sin^2(\theta) + 16\alpha r\lambda\sin^4(\theta) = 0. \tag{8.88}$$

Here, $\theta = (k\Delta x)/2$, $r = (D\Delta t)/(\Delta x^2)$, and $\alpha = (\Delta t/\Delta x)^2$. Stability is assured if the magnitude of the roots of this equation are less than or equal to one. Unfortunately, solutions of this cubic are too complicated to allow us to derive simple stability criteria. Nevertheless, we recognize that ϵ is a small parameter and derive approximate criteria by expanding the roots in powers of ϵ. To leading order we find:

$$\lambda \sim 1 - 4r\sin^2(\theta)$$

$$\lambda \sim (1 - 2\alpha\sin^2(\theta)) \pm 2\sin(\theta)\sqrt{\alpha^2\sin^2(\theta) - \alpha}.$$

Requiring that the magnitude of each root be less than or equal to one leads directly to:

$$\Delta t < \frac{\Delta x^2}{2D}$$

and

$$\Delta t < \Delta x.$$

The first of these conditions is typical of explicit heat solvers, while the second is simply the CFL condition. Again, we note that this does not constitute a proof of

stability, however good agreement with known exact solutions was found when these criteria were satisfied.

Various numerical experiments were carried out to illustrate and explore the various phenomena discussed thus far. First, in Figure 8.1 we illustrate the effect of diffusion on the developing temperature field. Using a deposition profile with compact support in the interior of the slab, we plot the temperature profile at the end of the pulse for $D = 0$ and $D = 0.01$. As expected the effect of diffusion is to smooth the developing thermal field. In Figure 8.2, we plot the magnitude of the stress at the end of the pulse for $D = 0$ and $D = 0.01$ in a region near the center of the deposition profile. We note that when diffusion is present, stress formation is decreased. However, this effect is minimal, even for the comparatively large value of D we have selected. More realistic values of D, i.e. on order of 10^{-6}, lead to a stress profile nearly identical to the $D = 0$ case. Further, we note that since we have chosen a deposition profile with compact support on the interior of the slab, our asymptotic results for the stress developed in Chapter 7 apply. For $D = 0$, the numerical and asymptotic results are virtually identical. For nonzero D the difference between the asymptotic result and the numerical result is essentially captured in Figure 8.2. Next, in Figure 8.3, we illustrate the effect of boundary conditions. In particular, we again turn off the effects of diffusion, i.e. we set $D = 0$ and take $\phi(x) = 1$. In an infinite media, the stress would increase monotonically at each point. Here, the stress free boundary conditions cause the creation of inward propagating rarefaction waves. The existence of these waves was discussed by Bailey, [34]. In Figure 8.3, we have plotted the developing stress amplitude at times $t = 0.1\tau_0$ till $t = \tau_0$. We note that the effect of the rarefaction waves is to reduce the stress in the interior of the slab. In Figure 8.4, we observe a new effect, namely the constructive interference of stress waves. In time, we follow the history of the stress at the midpoint of the slab. We have again chosen a deposition profile with compact support in the interior of the

slab, further we have chosen a deposition profile which is symmetric about $x = 1/2$. This implies that during the pulse the maximum stress will be felt at the midpoint. In Figure 8.4, we observe that the stress after the pulse reaches a value equal to twice its value at the end of the pulse. Here, the stress generated during the pulse breaks into a left and right travelling wave, they later recombine to create a temporary region of high stress. We further note that through repeated reflections, the stresses will change from tensile to compressive and back again. Finally, in Figure 8.5, we illustrate thermoelastic decay. We choose the deposition profile to be the lowest order spatial eigenfunction, i.e. $\phi(x) = \sin(\pi x)$. Then, choosing $P = 10$ and $\tau_0 = 0.1$, the initial amplitude of vibration at the midpoint of the slab will be one. In Figure 8.5 we plot a partial time history of the stress at the midpoint, namely we plot a time snapshot near $t = 1000$. As can be seen in the figure the amplitude of vibration has decayed to approximately 0.8. We note that our asymptotic result predicts that at $t = 1000$ the amplitude of vibration will have decayed to approximately 0.78134, in close agreement with the numerical solution.

8.5 Discussion

In this chapter, we have modeled our electron beam joining process as taking place in a single finite slab. First, as in previous chapters we developed a short time solution. This solution was predicated on the facts that D and ϵ are small parameters, and that the source term acts for a short time. As in earlier chapters, we may use this short time solution to study the formation of stresses during the pulse. If we choose a deposition profile with compact support in the interior of the slab, then the analysis of variations in stress formation during the pulse follows that of the previous chapter. We do not repeat such an analysis here, rather we focus on a new effect, unique to finite geometries. If the deposition profile does not have compact support in the interior of the slab, but rather attains a finite value at each endpoint, then the stress

free boundary conditions cause the creation of inward propagating rarefaction waves. In a worst case scenario, i.e. one where the maximum of ϕ occurs at $x = 1/2$, these rarefaction waves will reach the location of maximum stress at time $t = 1/2$. Hence if the pulse length, τ_0, is greater than or equal to $1/2$, the presence of these rarefaction waves will result in an overall stress reduction. We must note, that the definition of τ_0 here varies from that of the previous chapter. In this chapter, recall, the length scale chosen was that of the entire slab. So here, while we note the presence of these rarefaction waves, we do not try to quantify their effect further. In Chapter 9, we will return to this question.

Next, we turned to the long time solution. Here we introduced a 'three-timing' method which exploited the presence of three distinct timescales in the problem. We note, that while at least one author, [28], has attempted to develop such a method, our method differs from previous results in several fundamental ways. First, our parameter regime is new. That is, we are considering small D as well as small ϵ. This allows us to completely uncouple the thermal and stress aspects of the problem, while at the same time correctly capturing the effects of thermoelastic decay. In particular, an analytical solution for the stress may be found. Further, the temperature field may be found by solving a simple heat equation, with a wavelike time variable. We note, in contrast to previous schemes, our method can be applied to problems with non-linear thermal boundary conditions. Now, we can ask, what parameters govern thermoelastic decay? If we focus on the lowest order or slowest decaying mode, we see that this mode decays exponentially according to:

$$\exp(-\frac{\pi^2 \epsilon D t}{2}). \tag{8.89}$$

We can define a decay rate, the time it takes for the solution to decay by a factor of e^{-1}, as:

$$t_D = \frac{2}{\pi^2 \epsilon D}. \tag{8.90}$$

Or, in dimensional variables:

$$t'_D = \frac{2}{\pi^2}\frac{\rho c_E L^2}{\kappa}\frac{1}{\Gamma\delta}. \tag{8.91}$$

We note most particularly, the dependence of decay time on the reciprocal of the diffusivity of the material. As was observed in Chapter 4, decay time decreases with an increasing rate of thermal transport. Further, decay time varies with the elastic properties of the media as well. For example, a material with a large coefficient of thermal expansion, will remove stresses faster than one with a small coefficient of thermal expansion.

Finally, we comment on an effect seen in numerical solutions; the constructive interference of stress waves. As shown in the figures, the propagating stresses formed during the pulse reflect from each boundary and can later recombine. If these stresses have not decayed by a least a factor of 1/2, as can be calculated from the above analysis, their interference may result in stresses larger than those initially formed during the pulse. This suggests that stress estimated derived in the previous chapter, as well as those derived by Bailey, are in reality not maximum stresses. Rather, they should be viewed as estimates of the magnitude of developing stresses formed during the pulse.

At the end of Chapter 6, we discussed two effects of which we must be aware in electron beam joining experiments. In this chapter, as well as in Chapter 7, we again observe each of these effects. First, the propagation of stress waves while the pulse acts constitutes mechanical stress relaxation. Next, thermal diffusion in regions of rapid change tends to limit the formation of stresses and constitutes thermal stress relaxation. In addition, in this chapter we have observed three other important effects. As was best illustrated in our numerical simulations, the constructive interference of stress waves, after reflection by a boundary, can lead to large thermal stresses. A second boundary effect was also best illustrated by our numerical simulations, namely the possible existence of inward propagating

rarefaction waves. We note that these rarefaction waves tend to decrease stresses in the interior of the slab. Finally, in this chapter, we examined the effects of thermoelastic decay. We note that this decay takes place on a long time scale, and we investigated the parameters which govern the rate of decay. Because this effect acts on such a long time scale, we suggest that it is the least important of the five effects thus far uncovered.

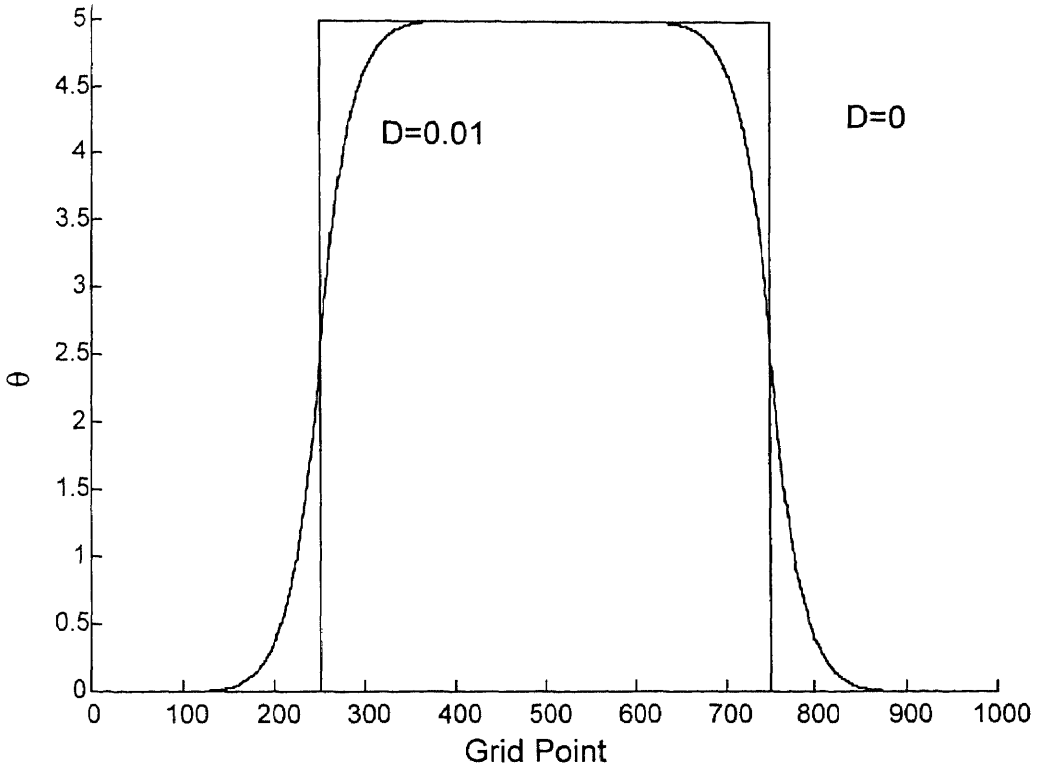

Figure 8.1 Developing temperature field for D=0 and D=0.01.

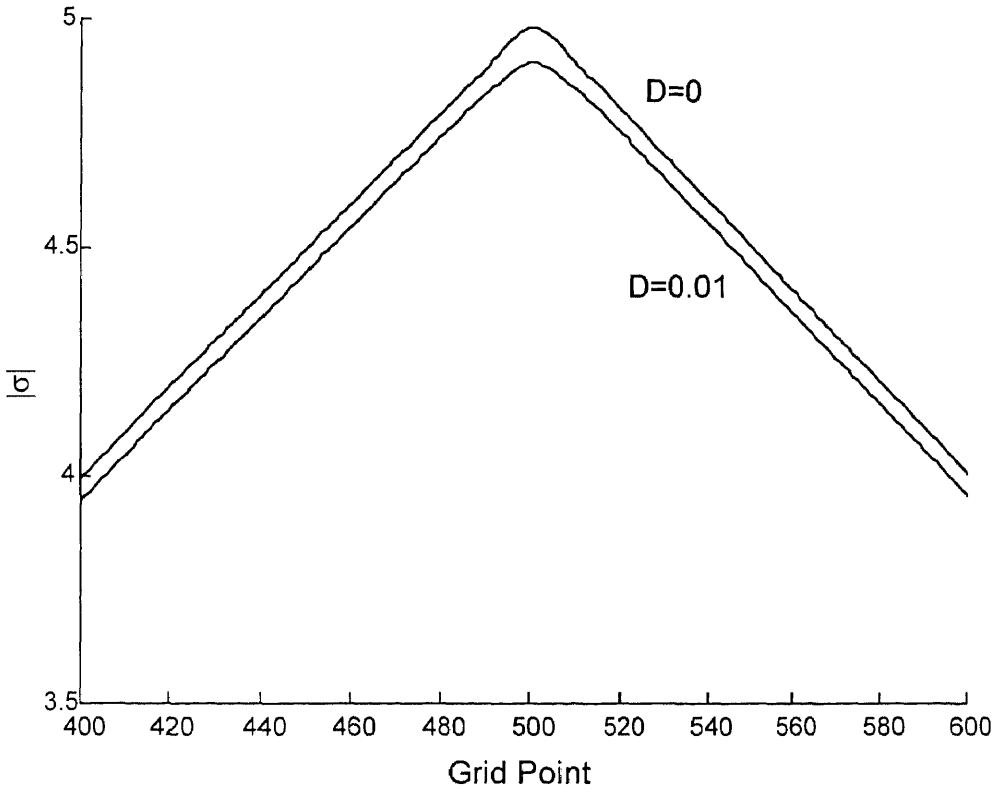

Figure 8.2 Developing stress field for D=0 and D=0.01.

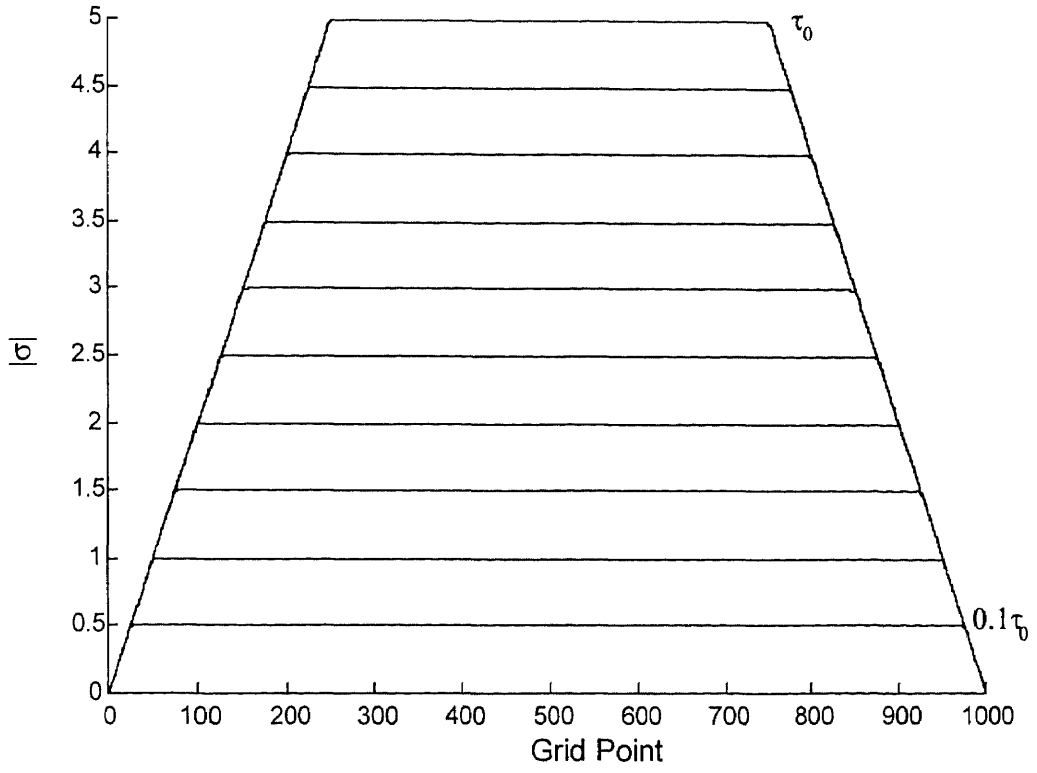

Figure 8.3 Developing stress field illustrating boundary effect.

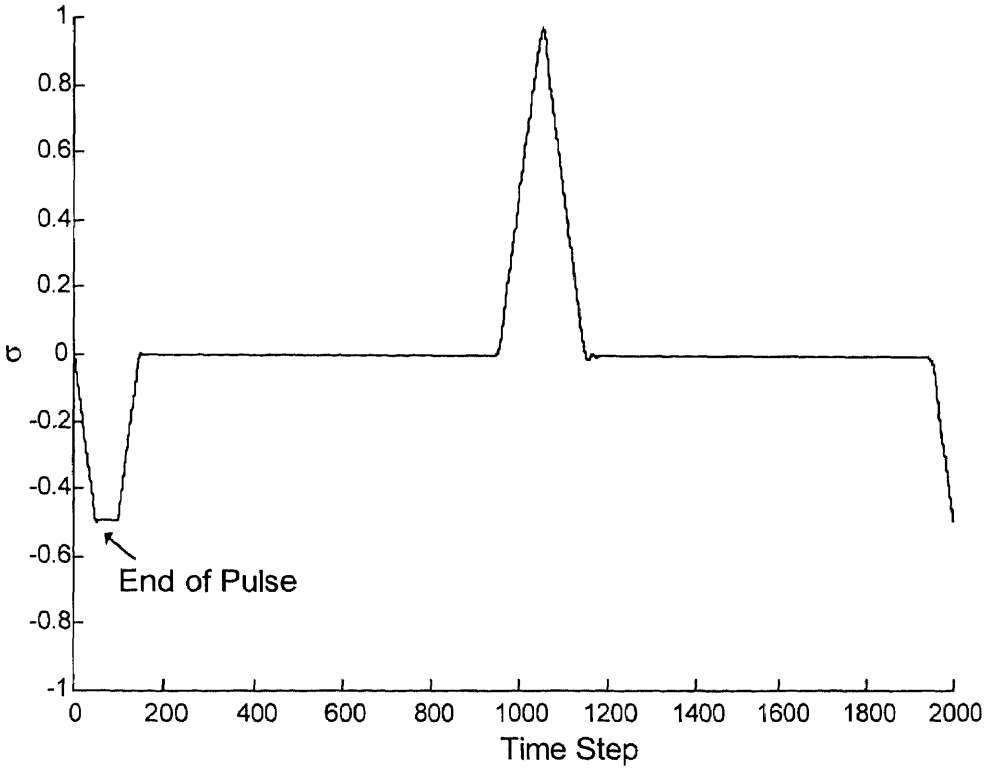

Figure 8.4 Time history of stress at midpoint of the slab.

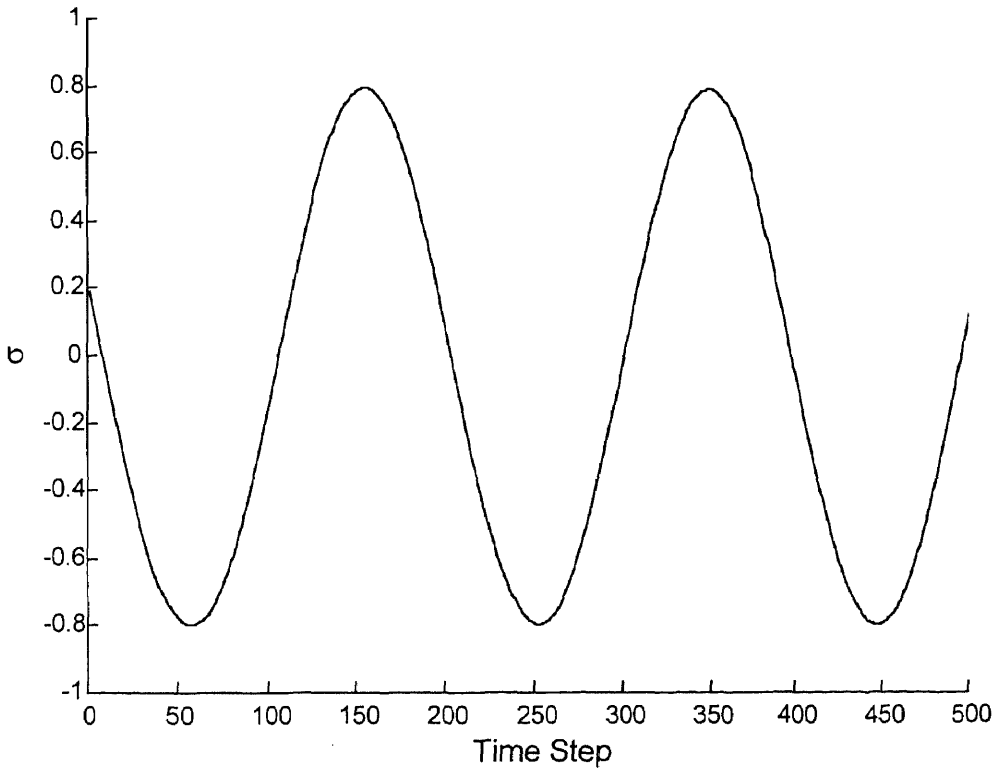

Figure 8.5 Partial time history of stress at midpoint of slab.

CHAPTER 9
MULTIPLE SLAB PHENOMENA

Thus far, we have considered our electron beam joining process as taking place in a single medium. In reality, as was discussed in Chapter 5, the electron beam joining process is intended to allow the joining of a wide variety of similar and dissimilar engineering materials. As such, we must consider how our results change in the presence of multiple layers with disparate elastic and thermal properties. Unfortunately, exact analytical solutions are hard to come by. In this chapter, we further develop the approximate methods illustrated in our single slab analyses, in the context of a three slab problem.

First, in Section 9.1, we formulate the general model for three slabs. In particular, we consider a thin region, i.e. the interlayer, surrounded by two thick slabs. The model is scaled as before, where here the scalings are with respect to interlayer properties. Next, in Section 9.2, we begin to develop short time solutions. We make the uncoupled approximation and consider the thermal aspect of the problem. As before, the non-dimensional diffusivity in each region is assumed to be a small parameter. Here, however, we do not simply disregard the singular nature of the perturbation. Rather, we employ a boundary layer analysis to develop a spatially uniform approximation to the short time thermal solution. Next, in Section 9.3 we turn to the elastic aspect of the problem. Here, thermal solution in hand, we recast the problem in terms of displacements. Again noting that the non-dimensional diffusivity in each region is small, we remove the source terms from the wave equation and capture the thermal effect entirely in the boundary conditions. We make use of the geometry of the problem. That is, noting that the interlayer is thin compared to the outer two slabs allows us to find the short time elastic solution through a geometric perturbation. In the inner solution, the outer two slabs become semi-infinite. In the outer solution, we capture the effect of rarefaction waves generated

at the boundaries. A spatially uniform short time solution is constructed, and its representation is given in 'travelling-wave' form. This form is particularly suited to short time computations, as for finite time, the solution consists of a finite number of terms. Finally, in Section 9.4, we present numerical solutions to the three slab problem. Examples illustrating the various effects uncovered are shown.

9.1 Formulation of the Model

In this section we formulate the general three slab model. We assume that three elastically and thermally distinct materials occupy the regions $-l_1 < x' < -L/2$, $-L/2 < x' < L/2$, and $L/2 < x' < l_2$. The three regions will be labeled one, two and three respectively. The middle region, i.e. region two, will often be referred to as the interlayer. We begin by formulating our governing equations in each region. First, in the ith region, we have:

$$\rho_i C_i \frac{\partial T_i}{\partial t'} = \kappa_i \frac{\partial^2 T_i}{\partial x'^2} - \alpha_i T_A (3\lambda_i + 2\mu_i) \frac{\partial^2 u_i'}{\partial x' \partial t'} + \frac{I\rho_i}{\pi r_b^2} \frac{1}{\rho_i} \frac{d\varepsilon}{dx'} G(t'/t_p) \tag{9.1}$$

$$(\lambda_i + 2\mu_i) \frac{\partial^2 \sigma_i'}{\partial x'^2} - (3\lambda_i + 2\mu_i) \frac{\partial^2 T_i}{\partial t'^2} = \rho_i \frac{\partial^2 \sigma_i'}{\partial t'^2} \tag{9.2}$$

$$\sigma_i' = (\lambda_i + 2\mu_i) \frac{\partial u_i'}{\partial x'} - (3\lambda_i + 2\mu_i) \alpha_i (T_i - T_A). \tag{9.3}$$

Note that here, in the source term in the heat equation, we do not include a spatially varying deposition profile $\phi(x)$ as was done previously. Rather, here the spatial variation arises naturally due to the differing specific heat's of each slab. Next, we impose boundary conditions on the elastic part of the problem. We assume stress free end conditions and impose:

$$\sigma_1'(-l_1, t') = 0 \tag{9.4}$$

$$\sigma_3'(l_2, t') = 0. \tag{9.5}$$

Then, at either interlayer boundary we require continuity of stress and displacement:

$$u_1'(-L/2, t') = u_2'(-L/2, t') \tag{9.6}$$

$$\sigma_1'(-L/2,t') = \sigma_2'(-L/2,t') \tag{9.7}$$

$$u_2'(L/2,t') = u_3'(L/2,t') \tag{9.8}$$

$$\sigma_2'(L/2,t') = \sigma_3'(L/2,t'). \tag{9.9}$$

Now, we impose boundary conditions on thermal aspect of the problem. We assume insulated end conditions and require:

$$\frac{\partial T_1}{\partial x'} = 0 \quad \text{at} \quad x' = -l_1 \tag{9.10}$$

$$\frac{\partial T_3}{\partial x'} = 0 \quad \text{at} \quad x' = l_2. \tag{9.11}$$

At the interlayer boundaries we assume perfect thermal contact and impose:

$$T_1(-L/2,t') = T_2(-L/2,t') \tag{9.12}$$

$$\kappa_1 \frac{\partial T_1}{\partial x'} = \kappa_2 \frac{\partial T_2}{\partial x'} \quad \text{at} \quad x' = -L/2 \tag{9.13}$$

$$T_2(L/2,t') = T_3(L/2,t') \tag{9.14}$$

$$\kappa_2 \frac{\partial T_2}{\partial x'} = \kappa_3 \frac{\partial T_3}{\partial x'} \quad \text{at} \quad x' = L/2. \tag{9.15}$$

Finally, we impose quiescent initial conditions:

$$T_i(x',0) = T_A \tag{9.16}$$

$$u_i'(x',0) = 0 \tag{9.17}$$

$$\frac{\partial u_i'}{\partial t'}(x',0) = 0. \tag{9.18}$$

Next, we scale our governing equations as was done in previous chapters. Here, we scale with respect to interlayer properties, that is we introduce:

$$\theta_i = \frac{T_i - T_A}{T_A}, \quad \Sigma_i = \frac{\sigma_i'}{\lambda_2 + 2\mu_2}, \quad u_i = \frac{u_i'}{L},$$

and scale x' with respect to interlayer length, and time with respect to interlayer wave speed:

$$x = \frac{x'}{L}, \quad t = \frac{c_2 t'}{L},$$

where:

$$c_i^2 = \frac{\lambda_i + 2\mu_i}{\rho_i}.$$

As in previous chapters, we encounter five dimensionless parameters:

$$\tau_0 = \frac{c_2 t_p}{L}, \quad D_i = \frac{\kappa_i}{\rho_i C_i L c_2}, \quad \Gamma_i = \frac{\alpha_i}{\rho_i C_i}(3\lambda_i + 2\mu_i),$$

$$\delta_i = \frac{3\lambda_i + 2\mu_i}{\lambda_i + 2\mu_i}\alpha_i T_A, \quad p_i = \frac{I}{\pi r_b^2 \rho_i C_i c_2}\frac{d\varepsilon}{dx},$$

and note that their physical interpretation is the same as in Chapter 7. Next, we rescale our dependent variables as follows:

$$\sigma_i = \frac{\Sigma_i}{\delta_2}, \quad v_i = \frac{u_i}{\delta_2},$$

and define:

$$\epsilon_i = \Gamma_i \delta_2.$$

Introducing the above scalings into our governing equations, we arrive at a dimensionless system. First, in region two we have:

$$\frac{\partial \theta_2}{\partial t} = D_2 \frac{\partial \theta_2}{\partial x^2} - \epsilon_2 \frac{\partial^2 v_2}{\partial x \partial t} + p_2 G(t/\tau_0) \tag{9.19}$$

$$\frac{\partial^2 \sigma_2}{\partial t^2} = \frac{\partial^2 \sigma_2}{\partial x^2} - \frac{\partial^2 \theta_2}{\partial t^2} \tag{9.20}$$

$$\sigma_2 = \frac{\partial v_2}{\partial x} - \theta_2. \tag{9.21}$$

Next, in region i, where here $i \neq 2$, we find:

$$\frac{\partial \theta_i}{\partial t} = D_i \frac{\partial \theta_i}{\partial x^2} - \epsilon_i \frac{\partial^2 v_i}{\partial x \partial t} + p_i G(t/\tau_0) \tag{9.22}$$

$$\frac{c_2^2}{c_i^2}\frac{\partial^2 \sigma_i}{\partial t^2} = \frac{\partial^2 \sigma_i}{\partial x^2} - \frac{\delta_i \rho_i}{\delta_2 \rho_2}\frac{\partial^2 \theta_i}{\partial t^2} \tag{9.23}$$

$$\sigma_i = \frac{\lambda_i + 2\mu_i}{\lambda_2 + 2\mu_2}\frac{\partial v_i}{\partial x} - \frac{\lambda_i + 2\mu_i}{\lambda_2 + 2\mu_2}\frac{\delta_i}{\delta_2}\theta_i. \tag{9.24}$$

Our elastic boundary conditions in regions one and three become:

$$\sigma_1(-l_1/L, t) = 0 \tag{9.25}$$

$$\sigma_3(l_2/L, t) = 0. \tag{9.26}$$

The elastic boundary conditions at the interlayer boundaries are now:

$$v_1(-1/2, t) = v_2(-1/2, t) \tag{9.27}$$

$$\sigma_1(-1/2, t) = \sigma_2(-1/2, t) \tag{9.28}$$

$$v_2(1/2, t) = v_3(1/2, t) \tag{9.29}$$

$$\sigma_2(1/2, t) = \sigma_3(1/2, t). \tag{9.30}$$

Next, the thermal boundary conditions for regions one and three become:

$$\frac{\partial \theta_1}{\partial x} = 0 \quad \text{at} \quad x = -l_1/L \tag{9.31}$$

$$\frac{\partial \theta_3}{\partial x} = 0 \quad \text{at} \quad x = l_2/L. \tag{9.32}$$

Then, the thermal boundary conditions at interlayer boundaries become:

$$\theta_1(-1/2, t) = \theta_2(-1/2, t) \tag{9.33}$$

$$\frac{\kappa_1}{\kappa_2}\frac{\partial \theta_1}{\partial x} = \frac{\partial \theta_2}{\partial x} \quad \text{at} \quad x = -1/2 \tag{9.34}$$

$$\theta_2(1/2, t) = \theta_3(1/2, t) \tag{9.35}$$

$$\frac{\partial \theta_2}{\partial x} = \frac{\kappa_3}{\kappa_2}\frac{\partial \theta_3}{\partial x} \quad \text{at} \quad x = 1/2. \tag{9.36}$$

Finally, our initial conditions are:

$$\theta_i(x, 0) = 0 \tag{9.37}$$

$$v_i(x, 0) = 0 \tag{9.38}$$

$$\frac{\partial v_i}{\partial t}(x, 0) = 0. \tag{9.39}$$

9.2 Short Time Thermal Solution

In this section we develop an approximate solution, valid for short times, to the thermal aspect of the problem. We begin by assuming that the coupling term in each heat equation may be disregarded for short times. This, of course, uncouples the thermal part of the problem. Then, we simply must solve:

$$\frac{\partial \theta_i}{\partial t} = D_i \frac{\partial^2 \theta_i}{\partial x^2} + p_i G(t/\tau_0) \tag{9.40}$$

$$\frac{\partial \theta_1}{\partial x} = 0 \quad \text{at} \quad x = -a \tag{9.41}$$

$$\frac{\partial \theta_3}{\partial x} = 0 \quad \text{at} \quad x = b \tag{9.42}$$

$$\theta_1(-1/2, t) = \theta_2(-1/2, t) \tag{9.43}$$

$$\frac{\kappa_1}{\kappa_2}\frac{\partial \theta_1}{\partial x} = \frac{\partial \theta_2}{\partial x} \quad \text{at} \quad x = -1/2 \tag{9.44}$$

$$\theta_2(1/2, t) = \theta_3(1/2, t) \tag{9.45}$$

$$\frac{\partial \theta_2}{\partial x} = \frac{\kappa_3}{\kappa_2}\frac{\partial \theta_3}{\partial x} \quad \text{at} \quad x = 1/2 \tag{9.46}$$

$$\theta_i(x, 0) = 0 \tag{9.47}$$

where here, we have denoted l_1/L by a and l_2/L by b. Next, we assume that the diffusivity, D_i, in each region is a small parameter. Consequently, we set $D_i = \epsilon\beta_i$, where ϵ is small and the β_i are $O(1)$. Then, a regular perturbation expansion immediately yields the leading order solutions:

$$\theta_i = p_i \int_0^t G(\zeta/\tau_0) d\zeta. \tag{9.48}$$

In our earlier analyses, we made sufficient assumptions upon the deposition profile, so that such a solution would be a uniform approximation to the actual solution, or simply ignored the difficulty. Here, we consider the possibility that boundary layers may develop. The obvious candidates for the location of boundary layers are at $x = -a, \pm 1/2, b$. We immediately note, that due to the assumption of insulated

boundaries at the outer two faces, the boundary layers at $x = -a$ and $x = b$ are empty and may be disregarded. Hence, we may restrict our attention to $x = \pm 1/2$. First, we explore the boundary layer at $x = -1/2$.

We begin by defining a stretched variable, η:

$$\eta = \frac{x + 1/2}{\sqrt{\epsilon}}.$$

Introducing η into our governing equations, (9.40-9.47), leads to the following boundary layer equations:

$$\frac{\partial \theta_1}{\partial t} = \beta_1 \frac{\partial^2 \theta_1}{\partial \eta^2} + p_1 G(t/\tau_0), \quad -\infty < \eta < 0 \tag{9.49}$$

$$\frac{\partial \theta_2}{\partial t} = \beta_2 \frac{\partial^2 \theta_2}{\partial \eta^2} + p_2 G(t/\tau_0), \quad 0 < \eta < \infty \tag{9.50}$$

$$\theta_1(0,t) = \theta_2(0,t) \tag{9.51}$$

$$\frac{\kappa_1}{\kappa_2}\frac{\partial \theta_1}{\partial x} = \frac{\partial \theta_2}{\partial x} \quad \text{at} \quad \eta = 0 \tag{9.52}$$

$$\theta_i(\eta, 0) = 0. \tag{9.53}$$

Now, strictly speaking, we should relabel our dependent variables, as they are now functions of η rather that x. To avoid proliferation of symbols, we do not do this, rather we simply keep this distinction in mind. The solution of our boundary layer equations is straightforward, and may be accomplished with the aid of the Laplace transform. We find:

$$\theta_1 = p_1 \int_0^t G(\zeta/\tau_0)d\zeta + \frac{p_2 - p_1}{1 + \frac{\kappa_1}{\kappa_2}\sqrt{\frac{\beta_2}{\beta_1}}} \int_0^t G(\zeta/\tau_0)\text{erfc}\left(\frac{-\eta}{2\sqrt{\beta_1(t-\zeta)}}\right)d\zeta \tag{9.54}$$

$$\theta_2 = p_2 \int_0^t G(\zeta/\tau_0)d\zeta + \frac{p_1 - p_2}{1 + \frac{\kappa_2}{\kappa_1}\sqrt{\frac{\beta_1}{\beta_2}}} \int_0^t G(\zeta/\tau_0)\text{erfc}\left(\frac{\eta}{2\sqrt{\beta_2(t-\zeta)}}\right)d\zeta \tag{9.55}$$

where here, erfc denotes the complementary error function.

Next, we examine the boundary layer at $x = 1/2$. We define the stretched variable η as:

$$\eta = \frac{x - 1/2}{\sqrt{\epsilon}}.$$

Again, introducing η into our governing equations, (9.40-9.47), we now arrive at:

$$\frac{\partial \theta_2}{\partial t} = \beta_2 \frac{\partial^2 \theta_2}{\partial \eta^2} + p_2 G(t/\tau_0) \qquad -\infty < \eta < 0 \tag{9.56}$$

$$\frac{\partial \theta_3}{\partial t} = \beta_3 \frac{\partial^2 \theta_3}{\partial \eta^2} + p_3 G(t/\tau_0) \qquad 0 < \eta < \infty \tag{9.57}$$

$$\theta_2(0,t) = \theta_3(0,t) \tag{9.58}$$

$$\frac{\kappa_3}{\kappa_2}\frac{\partial \theta_3}{\partial x} = \frac{\partial \theta_2}{\partial x} \quad \text{at} \quad \eta = 0 \tag{9.59}$$

$$\theta_i(\eta, 0) = 0. \tag{9.60}$$

Again, the solution of our boundary layer equations is straightforward, and we find:

$$\theta_3 = p_3 \int_0^t G(\zeta/\tau_0)d\zeta + \frac{p_2 - p_3}{1 + \frac{\kappa_3}{\kappa_2}\sqrt{\frac{\beta_2}{\beta_3}}} \int_0^t G(\zeta/\tau_0)\text{erfc}(\frac{\eta}{2\sqrt{\beta_3(t-\zeta)}})d\zeta \tag{9.61}$$

$$\theta_2 = p_2 \int_0^t G(\zeta/\tau_0)d\zeta + \frac{p_3 - p_2}{1 + \frac{\kappa_2}{\kappa_3}\sqrt{\frac{\beta_3}{\beta_2}}} \int_0^t G(\zeta/\tau_0)\text{erfc}(\frac{-\eta}{2\sqrt{\beta_2(t-\zeta)}})d\zeta. \tag{9.62}$$

Now, we have both an inner and outer solution for each region. A uniform approximation is obtained by adding the inner and outer solutions and subtracting away the matching term. The uniform solution for region one is given by:

$$\theta_1 = p_1 \int_0^t G(\zeta/\tau_0)d\zeta + \frac{p_2 - p_1}{1 + \frac{\kappa_1}{\kappa_2}\sqrt{\frac{D_2}{D_1}}} \int_0^t G(\zeta/\tau_0)\text{erfc}(\frac{-(x+1/2)}{2\sqrt{D_1(t-\zeta)}})d\zeta. \tag{9.63}$$

The uniform solution for region three is given by:

$$\theta_3 = p_3 \int_0^t G(\zeta/\tau_0)d\zeta + \frac{p_2 - p_3}{1 + \frac{\kappa_3}{\kappa_2}\sqrt{\frac{D_2}{D_3}}} \int_0^t G(\zeta/\tau_0)\text{erfc}(\frac{(x-1/2)}{2\sqrt{D_3(t-\zeta)}})d\zeta \tag{9.64}$$

and the uniform solution in region two is given by:

$$\begin{aligned} \theta_2 \;=\; & \frac{p_1 - p_2}{1 + \frac{\kappa_2}{\kappa_1}\sqrt{\frac{D_1}{D_2}}} \int_0^t G(\zeta/\tau_0)\text{erfc}(\frac{(x+1/2)}{2\sqrt{D_2(t-\zeta)}})d\zeta + \\ & \frac{p_3 - p_2}{1 + \frac{\kappa_2}{\kappa_3}\sqrt{\frac{D_3}{D_2}}} \int_0^t G(\zeta/\tau_0)\text{erfc}(\frac{-(x-1/2)}{2\sqrt{D_2(t-\zeta)}})d\zeta + p_2 \int_0^t G(\zeta/\tau_0)d\zeta. \end{aligned} \tag{9.65}$$

Finally, in the elastic part of the problem, we will need the thermal solution at $x = -a, b$. From the solutions given above, we compute them here. Again, we assume that the D_i are small. Then:

$$\theta_1(-a,t) \approx p_1 \int_0^t G(\zeta/\tau_0)d\zeta \tag{9.66}$$

$$\theta_3(b,t) \approx p_3 \int_0^t G(\zeta/\tau_0)d\zeta. \tag{9.67}$$

In addition, we need thermal gradients. It is easy to see, for example, that for small D_1:

$$\frac{\partial\theta_1}{\partial x} \approx \frac{p_2 - p_1}{1 + \frac{\kappa_1}{\kappa_2}\sqrt{\frac{D_2}{D_1}}}\delta(x + 1/2) \int_0^t G(\zeta/\tau_0)d\zeta. \tag{9.68}$$

That is, the derivative of θ_1 with respect to x may be approximated by a delta function acting at $x = -1/2$. Similar results hold for θ_2 and θ_3. However, each of these delta functions is found to act only at $x = \pm 1/2$. We note that this implies that thermal gradients vanish on the interior of each region.

9.3 Short Time Solution, Elastic Problem

In this section we develop an approximate solution, valid for short times, to the elastic aspect of the problem. We utilize the thermal solutions developed in the previous section, as well as the disparity of length scales between the interlayer and regions one and two, to simplify the analysis. Solutions are given in 'travelling-wave' form, which is particularly well-suited to short time computation.

We begin by restating the governing equations for the elastic problem, where here, in the wave equation, the stress has been eliminated in favor of the displacement. We have:

$$\frac{\partial^2 v_2}{\partial t^2} = \frac{\partial^2 v_2}{\partial x^2} - \frac{\partial\theta_2}{\partial x}, \quad -1/2 < x < 1/2 \tag{9.69}$$

$$\frac{1}{c^2}\frac{\partial^2 v_1}{\partial t^2} = \frac{\partial^2 v_1}{\partial x^2} - \delta\frac{\partial\theta_1}{\partial x}, \quad -a < x < -1/2 \tag{9.70}$$

$$\frac{1}{\mu^2}\frac{\partial^2 v_3}{\partial t^2} = \frac{\partial^2 v_3}{\partial x^2} - \alpha\frac{\partial\theta_3}{\partial x}, \quad 1/2 < x < b \tag{9.71}$$

$$\sigma_2 = \frac{\partial v_2}{\partial x} - \theta_2 \tag{9.72}$$

$$\sigma_1 = \lambda \frac{\partial v_1}{\partial x} - \lambda\delta\theta_1 \tag{9.73}$$

$$\sigma_3 = \gamma \frac{\partial v_3}{\partial x} - \gamma\alpha\theta_3 \tag{9.74}$$

where here, to simplify the notation, we have introduced:

$$\frac{1}{c^2} = \frac{c_2^2}{c_1^2}, \qquad \frac{1}{\mu^2} = \frac{c_2^2}{c_3^2},$$

$$\lambda = \frac{\lambda_1 + 2\mu_1}{\lambda_2 + 2\mu_2}, \qquad \gamma = \frac{\lambda_3 + 2\mu_3}{\lambda_2 + 2\mu_2},$$

$$\delta = \frac{\delta_1}{\delta_2}, \qquad \alpha = \frac{\delta_3}{\delta_2}.$$

Next, we write the boundary conditions solely in terms of displacements:

$$\frac{\partial v_1}{\partial x} = \delta\theta_1 \quad \text{at} \quad x = -a \tag{9.75}$$

$$v_1(-1/2, t) = v_2(-1/2, t) \tag{9.76}$$

$$v_2(1/2, t) = v_3(1/2, t) \tag{9.77}$$

$$\frac{\partial v_3}{\partial x} = \alpha\theta_3 \quad \text{at} \quad x = b. \tag{9.78}$$

The initial conditions in terms of displacements become:

$$v_i(x, 0) = 0 \tag{9.79}$$

$$\frac{\partial v_i}{\partial t}(x, 0) = 0. \tag{9.80}$$

Now, we are short two boundary conditions. In particular, we need one additional condition at each boundary of the interlayer. In conjunction with deriving the appropriate conditions, we wish to introduce an approximation. We note, that in equations (9.69-9.71) the source terms are proportional to the gradient of the temperature in the interior of each region. However, in the previous section,

we saw that for small diffusion, the gradient of the temperature vanished on the interior of each region. That is, the gradient of the temperature in any region could be approximated by delta functions acting at $x = \pm 1/2$. Consequently, in equations (9.69-9.71), we neglect the source terms. Now, we must find a way to retain the effect of these large thermal gradients at each boundary. Naturally, these gradients must enter into the remaining boundary conditions. We require continuity of stress at each interface and hence obtain:

$$\frac{\partial v_2}{\partial x} = \lambda \frac{\partial v_1}{\partial x} + Q_1(t) \quad \text{at} \quad x = -1/2 \tag{9.81}$$

$$\frac{\partial v_2}{\partial x} = \gamma \frac{\partial v_3}{\partial x} + Q_2(t) \quad \text{at} \quad x = 1/2 \tag{9.82}$$

where

$$Q_1(t) = \theta_2(-1/2, t) - \lambda \delta \theta_1(-1/2, t) \tag{9.83}$$

$$Q_2(t) = \theta_2(1/2, t) - \gamma \alpha \theta_3(1/2, t). \tag{9.84}$$

Here, in order to remain consistent with our assumption that thermal gradients may be ignored in the interior of each region, we must use the outer solution to evaluate the temperature field in these boundary conditions. In this manner, we retain the effect of the large thermal gradient at interlayer boundaries. We note that the effect of thermal diffusion at interlayer boundaries enters into the stress solution through the Duhamel-Neumann relations. Next, we further simplify the problem by making use of the disparity between the interlayer width and the outer slab's widths. In particular, we send a and b to infinity, i.e. we let the outer two slabs become semi-infinite. This may be viewed as an inner solution in a geometric perturbation. Later, we shall obtain corrections to account for the presence of these outer boundaries. With these simplifications, our problem reduces to:

$$\frac{\partial^2 v_2}{\partial t^2} = \frac{\partial^2 v_2}{\partial x^2}, \quad -1/2 < x < 1/2 \tag{9.85}$$

$$\frac{1}{c^2} \frac{\partial^2 v_1}{\partial t^2} = \frac{\partial^2 v_1}{\partial x^2}, \quad -\infty < x < -1/2 \tag{9.86}$$

$$\frac{1}{\mu^2}\frac{\partial^2 v_3}{\partial t^2} = \frac{\partial^2 v_3}{\partial x^2}, \quad 1/2 < x < \infty \tag{9.87}$$

$$\sigma_2 = \frac{\partial v_2}{\partial x} - \theta_2 \tag{9.88}$$

$$\sigma_1 = \lambda\frac{\partial v_1}{\partial x} - \lambda\delta\theta_1 \tag{9.89}$$

$$\sigma_3 = \gamma\frac{\partial v_3}{\partial x} - \gamma\alpha\theta_3 \tag{9.90}$$

$$v_1(-1/2, t) = v_2(-1/2, t) \tag{9.91}$$

$$\frac{\partial v_2}{\partial x} = \lambda\frac{\partial v_1}{\partial x} + Q_1(t) \quad \text{at} \quad x = -1/2 \tag{9.92}$$

$$v_2(1/2, t) = v_3(1/2, t) \tag{9.93}$$

$$\frac{\partial v_2}{\partial x} = \gamma\frac{\partial v_3}{\partial x} + Q_2(t) \quad \text{at} \quad x = -1/2. \tag{9.94}$$

In addition, at $\pm\infty$, we need boundary conditions. We require that displacements remain bounded:

$$|v_1| < \infty \quad \text{as} \quad x \to -\infty \tag{9.95}$$

$$|v_3| < \infty \quad \text{as} \quad x \to \infty. \tag{9.96}$$

Next, we apply the Laplace transform to equations (9.85-9.96). This yields a boundary value problem for the transformed variables, denoted by hat's, which is easily solved and results in:

$$\begin{aligned}\hat{v_1} = {} & \frac{2\hat{Q}_2 e^{-s} e^{s/2c} e^{sx/c}}{s(1+Z_1)(1+Z_2)(1-\beta e^{-2s})} - \frac{\hat{Q}_1 e^{s/2c} e^{sx/c}}{s(1+Z_1)(1-\beta e^{-2s})} \\ & - \frac{(1-Z_2)\hat{Q}_1 e^{-2s} e^{s/2c} e^{sx/c}}{s(1+Z_1)(1+Z_2)(1-\beta e^{-2s})}\end{aligned} \tag{9.97}$$

$$\begin{aligned}\hat{v_2} = {} & \frac{\hat{Q}_2 e^{-s/2} e^{sx}}{s(1+Z_2)(1+\beta e^{-2s})} - \frac{(1-Z_2)\hat{Q}_1 e^{-3s/2} e^{sx}}{s(1+Z_1)(1+Z_2)(1+\beta e^{-2s})} \\ & - \frac{\hat{Q}_1 e^{-s/2} e^{-sx}}{s(1+Z_1)(1-\beta e^{-2s})} + \frac{(1-Z_1)\hat{Q}_2 e^{-3s/2} e^{-sx}}{s(1+Z_1)(1+Z_2)(1-\beta e^{-2s})}.\end{aligned} \tag{9.98}$$

$$\begin{aligned}\hat{v_3} = {} & \frac{-2\hat{Q}_1 e^{-s} e^{s/2\mu} e^{-sx/\mu}}{s(1+Z_1)(1+Z_2)(1-\beta e^{-2s})} + \frac{\hat{Q}_2 e^{s/2\mu} e^{-sx/\mu}}{s(1+Z_2)(1-\beta e^{-2s})} \\ & + \frac{(1-Z_1)\hat{Q}_2 e^{-2s} e^{s/2\mu} e^{-sx/\mu}}{s(1+Z_1)(1+Z_2)(1-\beta e^{-2s})}\end{aligned} \tag{9.99}$$

where here $Z_1 = \lambda/c$, $Z_2 = \gamma/\mu$ and:

$$\beta = \frac{(1-Z_1)(1-Z_2)}{(1+Z_1)(1+Z_2)}.$$

We note that:

$$Z_1 = \frac{\rho_1 c_1}{\rho_2 c_2}, \qquad Z_2 = \frac{\rho_3 c_3}{\rho_2 c_2}.$$

That is, Z_1 and Z_2 are ratio's of impedances. To carry out the inversion, we note that:

$$\frac{1}{1-\beta e^{-2s}} = \sum_{n=0}^{\infty} \beta^n e^{-2ns} \tag{9.100}$$

and recall that the inverse Laplace transform of e^{-cs} is given by $H(t-c)$, where H denotes the Heaviside function. Then, we may invert with the aid of the convolution theorem and use the Duhamel-Neumann relations to obtain the stress in each region:

$$\begin{aligned}
\sigma_1 &= -\lambda\delta\theta_1 - \frac{Z_1}{1+Z_1}\int_0^t Q_1(\zeta)\sum_{n=0}^{\infty}\beta^n\delta(t-\zeta+x/c+1/2c-2n)d\zeta \qquad (9.101)\\
&\quad -\frac{Z_1(1-Z_2)}{(1+Z_1)(1+Z_2)}\int_0^t Q_1(\zeta)\sum_{n=0}^{\infty}\beta^n\delta(t-\zeta+x/c+1/2c-2-2n)d\zeta\\
&\quad +\frac{2Z_1}{(1+Z_1)(1+Z_2)}\int_0^t Q_2(\zeta)\sum_{n=0}^{\infty}\beta^n\delta(t-\zeta+x/c+1/2c-1-2n)d\zeta
\end{aligned}$$

$$\begin{aligned}
\sigma_2 &= -\theta_2 + \frac{1}{1+Z_2}\int_0^t Q_2(\zeta)\sum_{n=0}^{\infty}(-1)^n\beta^n\delta(t-\zeta+x-1/2-2n)d\zeta \qquad (9.102)\\
&\quad +\frac{1}{1+Z_1}\int_0^t Q_1(\zeta)\sum_{n=0}^{\infty}\beta^n\delta(t-\zeta-x-1/2-2n)d\zeta\\
&\quad -\frac{(1-Z_2)}{(1+Z_1)(1+Z_2)}\int_0^t Q_1(\zeta)\sum_{n=0}^{\infty}(-1)^n\beta^n\delta(t-\zeta+x-3/2-2n)d\zeta\\
&\quad -\frac{(1-Z_1)}{(1+Z_1)(1+Z_2)}\int_0^t Q_2(\zeta)\sum_{n=0}^{\infty}\beta^n\delta(t-\zeta-x-3/2-2n)d\zeta
\end{aligned}$$

$$\begin{aligned}
\sigma_3 &= -\gamma\alpha\theta_3 - \frac{Z_2}{1+Z_2}\int_0^t Q_2(\zeta)\sum_{n=0}^{\infty}\beta^n\delta(t-\zeta-x/\mu+1/2\mu-2n)d\zeta \qquad (9.103)\\
&\quad -\frac{Z_2(1-Z_1)}{(1+Z_1)(1+Z_2)}\int_0^t Q_2(\zeta)\sum_{n=0}^{\infty}\beta^n\delta(t-\zeta-x/\mu+1/2\mu-2-2n)d\zeta\\
&\quad +\frac{2Z_2}{(1+Z_1)(1+Z_2)}\int_0^t Q_1(\zeta)\sum_{n=0}^{\infty}\beta^n\delta(t-\zeta-x/\mu+1/2\mu-1-2n)d\zeta.
\end{aligned}$$

As promised, we have obtained a 'travelling-wave' form of the solution. The advantage of this form is now clear, for finite time, only a finite number of the delta functions appearing in the sums act. Hence when we wish to compute short time solutions, we need only consider a finite number of terms. Further, we note that typically β is a small parameter. In addition, each term in the above series is essentially a temperature solution evaluated at successively earlier times. Consequently, even for relatively long times, a good approximation to the stress solution may be obtained by only retaining the first few terms in each sum.

Now, we need to correct for the influence of the boundaries at $x = -a, b$. First, we deal with the boundary at $x = -a$. We begin, by defining a new variable, $\eta = x + a$, and again letting a tend to infinity. This has the effect of sending regions two and three off to infinity and reducing the problem to that in region one. That is, we are left with:

$$\frac{1}{c^2}\frac{\partial^2 v_1}{\partial t^2} = \frac{\partial^2 v_1}{\partial \eta^2} \qquad 0 < \eta < \infty \tag{9.104}$$

$$\frac{\partial v_1}{\partial \eta} = \delta\theta_1 \quad \text{at} \quad \eta = 0 \tag{9.105}$$

$$|v_1| < \infty \quad \text{as} \quad \eta \to \infty \tag{9.106}$$

$$v_1(0,\eta) = 0 \tag{9.107}$$

$$\frac{\partial v_1}{\partial t}(\eta, 0) = 0. \tag{9.108}$$

This system is easily solved with the aid of the Laplace transform. We find:

$$v_1 = -\delta c \int_0^t \theta_1(0,\zeta) H(t - \zeta - \eta/c) d\zeta \tag{9.109}$$

or, in terms of the stress:

$$\sigma_1 = -\lambda\delta\theta_1 + \lambda\delta \int_0^t \theta_1(0,\zeta)\delta(t - \zeta - \eta/c) d\zeta. \tag{9.110}$$

Note, this represents a right travelling wave originating at the left boundary. That is, this is the rarefaction wave generated at the boundary, which was observed in the

previous chapter. Next, by adding this solution to (9.101) and subtracting off the matching term, we obtain:

$$\begin{aligned}\sigma_1 &= -\lambda\delta\theta_1 - \frac{Z_1}{1+Z_1}\int_0^t Q_1(\zeta)\sum_{n=0}^{\infty}\beta^n\delta(t-\zeta+x/c+1/2c-2n)d\zeta \qquad (9.111)\\ &-\frac{Z_1(1-Z_2)}{(1+Z_1)(1+Z_2)}\int_0^t Q_1(\zeta)\sum_{n=0}^{\infty}\beta^n\delta(t-\zeta+x/c+1/2c-2-2n)d\zeta\\ &+\frac{2Z_1}{(1+Z_1)(1+Z_2)}\int_0^t Q_2(\zeta)\sum_{n=0}^{\infty}\beta^n\delta(t-\zeta+x/c+1/2c-1-2n)d\zeta\\ &+\lambda\delta\int_0^t\theta_1(-a,\zeta)\delta(t-\zeta-(x+a)/c)d\zeta.\end{aligned}$$

We note, this solution is valid provided that waves generated at $x=-1/2$ do not reach the boundary at $x=-a$. This restricts the time of validity of the solution. In particular, we must require that $t<a/c$, however since we are interested in short time solutions, this is no real restriction at all. Finally, repeating the above analysis near $x=b$, we obtain the boundary corrected solution for σ_3:

$$\begin{aligned}\sigma_3 &= -\gamma\alpha\theta_3 - \frac{Z_2}{1+Z_2}\int_0^t Q_2(\zeta)\sum_{n=0}^{\infty}\beta^n\delta(t-\zeta-x/\mu+1/2\mu-2n)d\zeta \qquad (9.112)\\ &-\frac{Z_2(1-Z_1)}{(1+Z_1)(1+Z_2)}\int_0^t Q_2(\zeta)\sum_{n=0}^{\infty}\beta^n\delta(t-\zeta-x/\mu+1/2\mu-2-2n)d\zeta\\ &+\frac{2Z_2}{(1+Z_1)(1+Z_2)}\int_0^t Q_1(\zeta)\sum_{n=0}^{\infty}\beta^n\delta(t-\zeta-x/\mu+1/2\mu-1-2n)d\zeta\\ &+\gamma\alpha\int_0^t\theta_3(b,\zeta)\delta(t-\zeta+(x-b)/\mu)d\zeta. \qquad (9.113)\end{aligned}$$

Again, we note that in constructing this solution we have ignored possible reflections from the right hand boundary. Hence we must require that $t<b/\mu$. Since b is large, this is of little concern.

9.4 Numerical Solutions

In this section, we present the results of numerical simulations of our governing equations. As was done for the single finite slab, the governing equations were discretized and an explicit finite difference scheme derived. Again stability is difficult

to prove for this scheme, however we conjecture that both a CFL condition and a heat solver condition must be satisfied. For a full discussion, see Chapter 8.

Various numerical experiments were carried out to illustrate multiple slab phenomena. First, in Figure 9.1 we show a sample developing thermal field during the pulse. In order to clearly show the thin thermal boundary layers which appear at each interlayer boundary, we set $D_2 = 0.01$, $a = b = 1$, and take all three slabs to be identical except for specific heats. That is, we take $p_1 = p_3 = 0.25p_2$. In this manner, we focus on the interlayer. We note that away from the interlayer boundaries the temperature is piecewise constant, as predicted by our asymptotic theory. We further note that the width of the boundary layer is exaggerated by our choice of D_2 which is many times larger than realistic values. Next, in Figure 9.2, we plot the developing stress field during the pulse, for the situation considered in Figure 9.1. By limiting our domain, we see the effect of rarefaction waves generated at the outer boundaries. These rarefaction waves are seen to interfere with and reduce developing stresses in the interior regions. We note that this stress field is virtually identical with that predicted by our asymptotic theory, even though we have included an exaggerated value of the diffusivity in the numerical solution. In Figure 9.3, we illustrate the effects of impedance mismatch on the developing stress field. To clearly illustrate, we assume that $p_1 = p_3 = 0$, so that stress is only generated in the interlayer. The material properties of all three regions are identical, with the exception of the density. In particular, we assume that region one is five times as dense as regions two and three. As can be seen in the plot, the stresses generated at the interlayer boundary between region one and two are considerably higher than those generated between regions one and three.

Next, we compare our asymptotic and numerical results in the context of a simple case study. That is, we apply our code and our asymptotic solutions to the study of a suggested experimental configuration. In particular, we assume that

region one is silicon carbide, region three is inconel, and region two is brazing metal. Material properties for SiC and inconel may be found in [38]. In order to compute material properties for the interlayer, we averaged by component metal in the common braze, Cusin-1-ABA. This brazing metal is composed of 63 percent silver, 1.75 percent titanium, 34.25 percent copper, and 1 percent tin. Again, material properties for these components may be found in [38]. Then, we choose the dimensionless power in the interlayer, i.e. p_2, such that at the end of the pulse, the interlayer temperature would have increased by one thousand degrees Kelvin. That is, we choose p_2 so that $p_2\tau_0 = 3$. Next, holding $p_2\tau_0$ fixed as we varied τ_0, we computed temperature and stress fields numerically for various values of τ_0. In Figure 9.4, we show a sample computed temperature field. We note that the heat capacities of regions two and three are close, hence temperature variation between these two regions is not large. Further, we note that the thermal conductivity of region three is higher than that of region one. Hence we observe more diffusive smoothing of temperature gradients at the right hand interlayer boundary. In Figure 9.5, we plot the evolving stress field for the case where $\tau_0 = 1$. The outer sample widths were chosen large enough so that rarefactions would not reach interlayer boundaries during the pulse. Note that the maximum stress does not occur at the midpoint of the interlayer, but due to an asymmetry in material properties is shifted into region three. Finally, in Figure 9.6, we plot the stress amplitude at the midpoint of the sample as a function of τ_0 for $t = \tau_0$. Again, in this plot the quantity $p_2\tau_0$ is held fixed. The solid curve was obtained from our asymptotic solutions, while the points denoted by stars represent numerical solutions. We note the excellent agreement between numerical and analytical results. As can be observed in the plot, numerical solutions lie slightly below the analytical ones. This is due to the presence of diffusion in our numerical simulations.

9.5 Discussion

In this chapter, we analyzed a multiple slab model of our electron beam joining process. We again sought to develop approximate short time solutions, i.e. we wished to determine how stresses formed during the pulse. In order to do so, we made several approximations. First, as in previous chapters, for short times we recognized that we may rely on the uncoupled theory. This allowed us to separate the thermal and elastic aspects of the problem. Recognizing that the key to obtaining useful stress estimates relies upon first obtaining a simplified thermal solution, we used singular perturbation techniques to obtain a simplified, but uniformly valid thermal solution. We noted that for small values of the diffusivity, thermal gradients vanished in the interior of each slab. Next, we utilized this observation in the solution of the elastic part of the problem. By rewriting our governing equations in terms of displacements, we realized that thermal effects could be captured entirely in the boundary conditions. In addition, since we were after a short time solution, we utilized the disparity in length scales between the interlayer and the outer slabs. This allowed us to treat the outer slabs as semi-infinite, and obtain a solution to the problem. Then, we corrected for the outer boundaries presence, and obtained inward propagating solutions due to stress relaxation at the outer boundaries.

Next, we illustrate how our multiple slab solution yields new information about the joining process by comparison with our previous theories. As in Chapter 7, we focus our attention on the stress at a single point. In particular, we examine the stress at the interlayer midpoint, $x = 0$. First, for $\tau_0 < 1/2$ we find:

$$\sigma_2(0, \tau_0) = -\theta_2(0, \tau_0). \tag{9.114}$$

Using our uniform approximation to the temperature field, this becomes:

$$\sigma_2(0, \tau_0) = -p_2\tau_0 + \frac{p_2 - p_1}{1 + \frac{\kappa_2}{\kappa_1}\sqrt{\frac{D_1}{D_2}}} \int_0^{\tau_0} \operatorname{erfc}\left(\frac{1}{4\sqrt{D_2(t-\zeta)}}\right) d\zeta + \tag{9.115}$$

$$\frac{p_2 - p_3}{1 + \frac{\kappa_2}{\kappa_3}\sqrt{\frac{D_3}{D_2}}} \int_0^{\tau_0} \text{erfc}(\frac{1}{4\sqrt{D_2(t-\zeta)}})d\zeta.$$

Note that this expression is equal to our infinite slab result plus two positive correction terms. These terms are due to thermal diffusion at the interlayer boundaries. Hence, once again, we see that the effect of diffusion is to smooth thermal stresses. We again note however, that this diffusive smoothing is a small effect. Next, we ignore this diffusive correction, and examine the solution for $1/2 < \tau_0 < 3/2$. We find:

$$\sigma_2 = -p_2\tau_0 + \frac{(p_2 - \lambda\gamma p_1)}{1 + Z_1}(\tau_0 - 1/2) + \frac{(p_2 - \gamma\alpha p_3)}{1 + Z_2}(\tau_0 - 1/2). \tag{9.116}$$

Note that in this time interval, information from the interlayer boundaries has had sufficient time to reach the point $x = 0$. Consequently, we see terms due to regions one and three arising in this solution. To illustrate how such a solution may be useful from a design point of view, we make further simplifications and assume that $p_1 = p_3$, $Z_1 = Z_2 = 1$, $\lambda = \gamma = 1$, and $\alpha = \delta$. That is, we assume that regions one and three are identical, and that only there thermal expansion coefficients differ from that of region two. Then our solution becomes:

$$\sigma_2(0, \tau_0) = -\frac{p_2}{2} - \delta p_1(\tau_0 - 1/2). \tag{9.117}$$

Note that if $p_1 = 0$, this reduces to Bailey's result, and that if $\delta = 1$ this reduces to the single infinite slab solution derived in Chapter 7. The appearance of δ in the solution allows us to study how thermal expansion mismatch effects the formation of stresses at the point under consideration. We see that the stress at $x = 1/2$ varies linearly from Bailey's result, when $\delta = 0$, to our infinite slab result, when $\delta = 1$, and beyond. Now, if we again fix the energy deposited into the interlayer, that is we fix $E = p_2\tau_0$, we may rewrite our expression for the stress as:

$$\sigma_2(0, \tau_0) = -\frac{E}{2\tau_0} - \frac{\delta C_2 E(\tau_0 - 1/2)}{C_1\tau_0}. \tag{9.118}$$

In Figure 9.7 we plot the stress amplitude as a function of τ_0, with E held fixed, for various values of δ. We see that thermal expansion mismatch affects the variation of stress amplitude with pulse length. We note that Bailey's theory tends to underestimate the stresses.

Now, having analyzed a multiple slab scenario, we reconsider the various phenomena of importance in electron beam joining experiments. These phenomena may be divided into two parts, those that occur while the beam acts, and those that occur after the beam has been turned off. While the beam acts, that is on the time interval $(0, \tau_0)$, the development of stresses is of primary importance. For, after the pulse has passed, in some sense stresses merely propagate. We began our analysis on this time interval in Chapter 6, where we considered the mass-spring piston-cylinder oscillator as a model of the electron beam process. There, we observed that two types of stress relaxation occur while the beam acts. First, we have mechanical stress relaxation. As we have seen in Chapters 7 through 9, this occurs because stress waves begin to propagate while the beam is on. In Chapter 7, by considering a 'virtual interlayer', embedded in a single infinite slab, we derived expressions for the magnitude of stresses formed during the pulse. These expressions were shown to reduce to Bailey's results in the appropriate limits. In addition, by considering a more realistic case than that considered by Bailey, we began to capture the effect of multiple layers. Most importantly, we observed that in order to achieve stress reduction at $x = 0$ by varying the dimensionless pulse length, τ_0, it was necessary that $\tau_0 > 1/2$. We note that in the symmetric case, $x = 0$ will be the point with greatest stress during the pulse, and in realistic asymmetric cases should be very close to it. In this chapter, we improved upon our results for variation of stress amplitude with pulse length. Again, we see that in order to achieve stress reduction by varying τ_0, it is necessary that $\tau_0 > 1/2$. In addition, by examining one simple case, we saw how differing material properties can affect the variation

of stress with pulse length. In particular, we examined the case of simple thermal expansion mismatch, and found that Bailey's results tend to underestimate stresses, and that our infinite slab theory may overestimate them. Next, during the pulse, we also noted that we have thermal stress relaxation. That is, in regions of rapid change of temperature, thermal diffusion acts during the pulse. In this chapter, we developed a boundary layer theory to account for such regions. This modified our expressions for developing stresses, including for example, differences due to disparate thermal conductivities between regions. We again note, this effect always tends to smooth thermal gradients and reduce stress formation. Unfortunately, this effect is small, and in realistic situations, varying thermal conduction properties is an inefficient way to achieve stress reduction. Now, after the beam turns off, we encountered several additional phenomena of interest. First, as was observed in Chapter 8 numerically, and Chapter 9 both analytically and numerically, rarefaction waves are generated at the outer slab boundaries. These waves propagate inwards, and tend to reduce stresses in the interior regions. As we have observed in this chapter, for thin interlayers they cannot reach the interlayer on the time scale during which the pulse acts. Hence, they cannot limit the development of stresses, but may reduce propagating stresses and in this manner limit damage. For thicker interlayers these rarefaction waves can influence developing stresses. This effect was observed numerically. More importantly, we observed numerically in Chapter's 8 and 9, that propagating stress waves may constructively interfere after reflecting off of the outer boundaries. This must be taken into account when designing an electron beam joining experiment. Due to the complexity of the possible interactions, we suggest that numerical investigations of such interactions would be of the most use. Finally, in Chapter 8, we investigated the phenomena of thermoelastic decay. We found that decay acted on a long time scale, that for a single slab was characterized by the reciprocal of the coupling constant times the diffusion constant. Unfortunately, due

to the length of time necessary to achieve significant decay, this phenomenon does not appear to be useful in dissipating stresses.

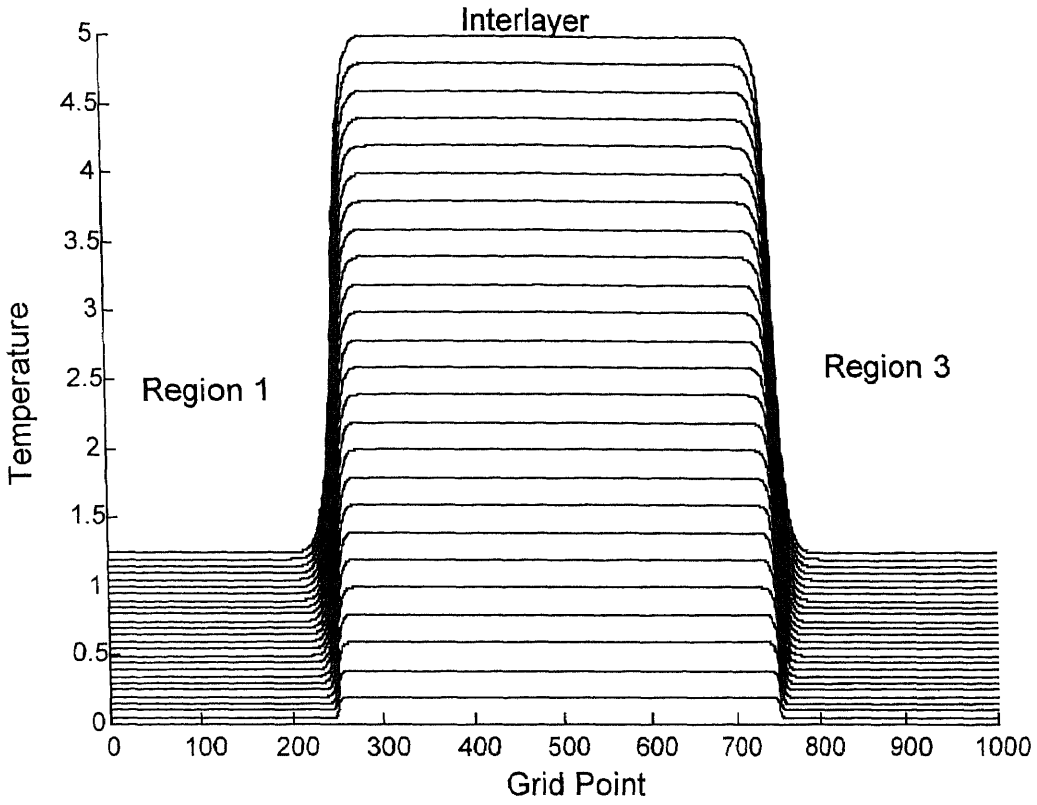

Figure 9.1 Developing thermal field for 3-slab problem.

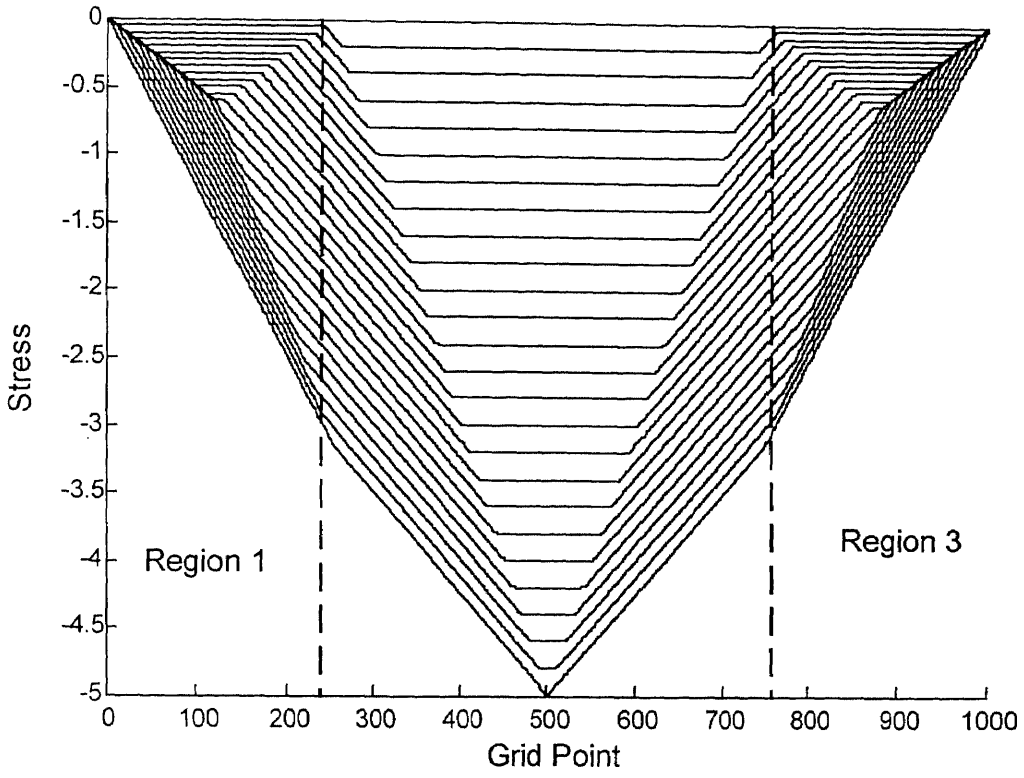

Figure 9.2 Developing stress field for 3-slab problem.

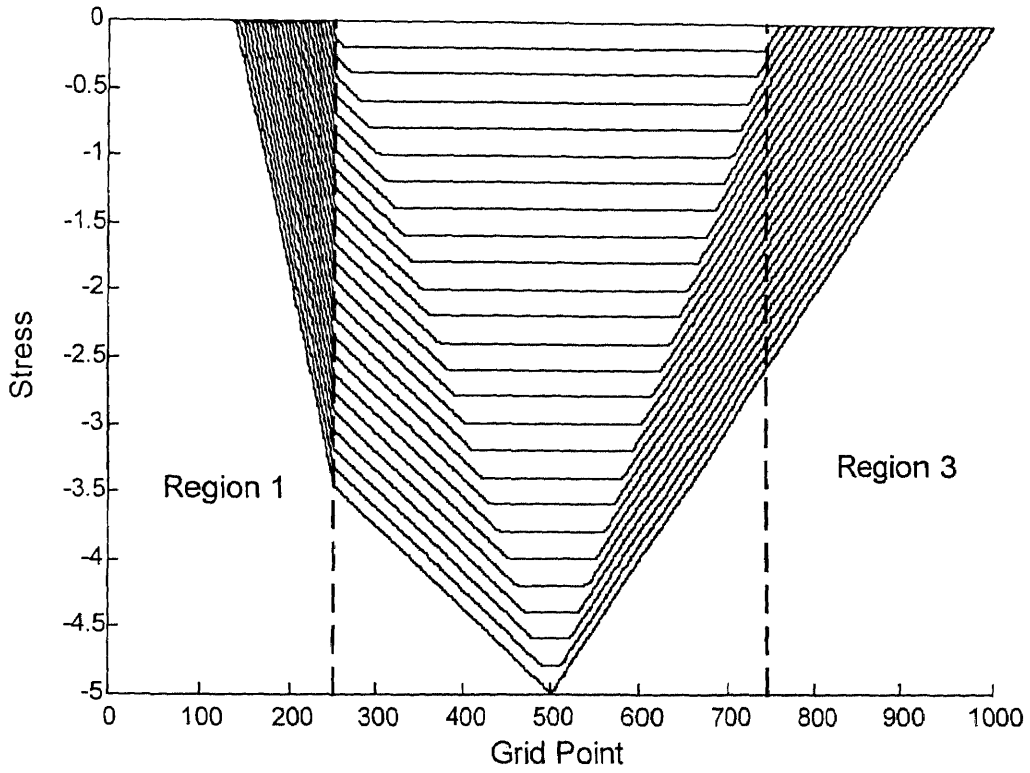

Figure 9.3 Illustration of impedence mismatch.

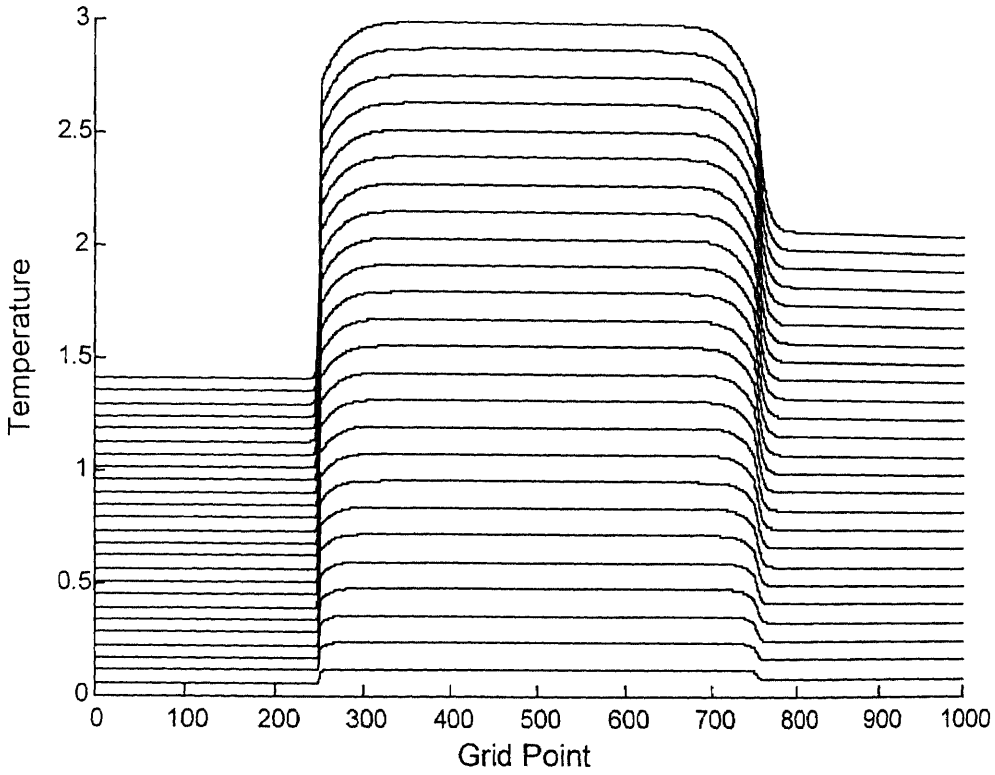

Figure 9.4 Evolving temperature field for case study.

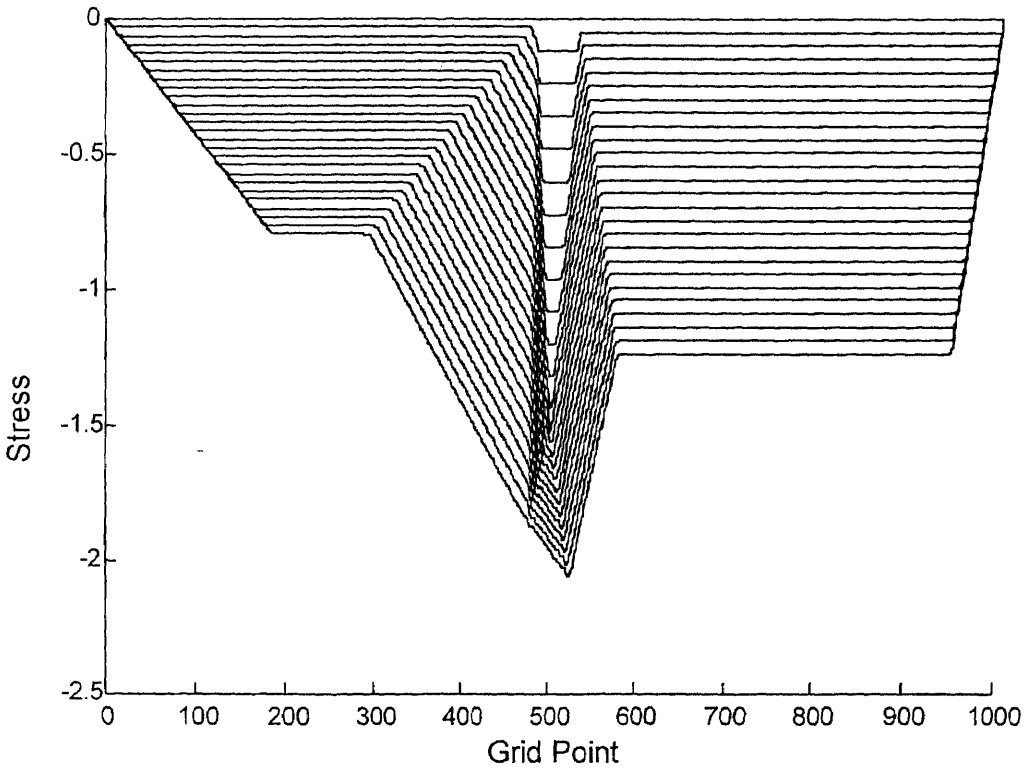

Figure 9.5 Evolving stress field for case study.

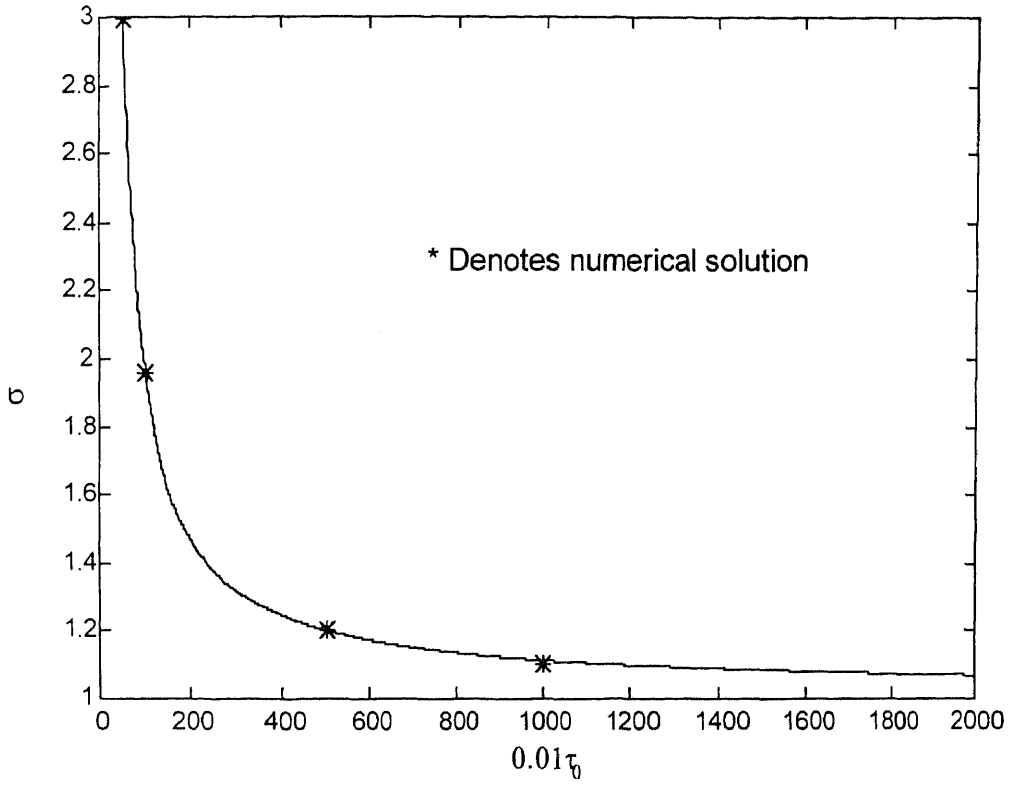

Figure 9.6 Variation of stress at midpoint of sample with pulse length.

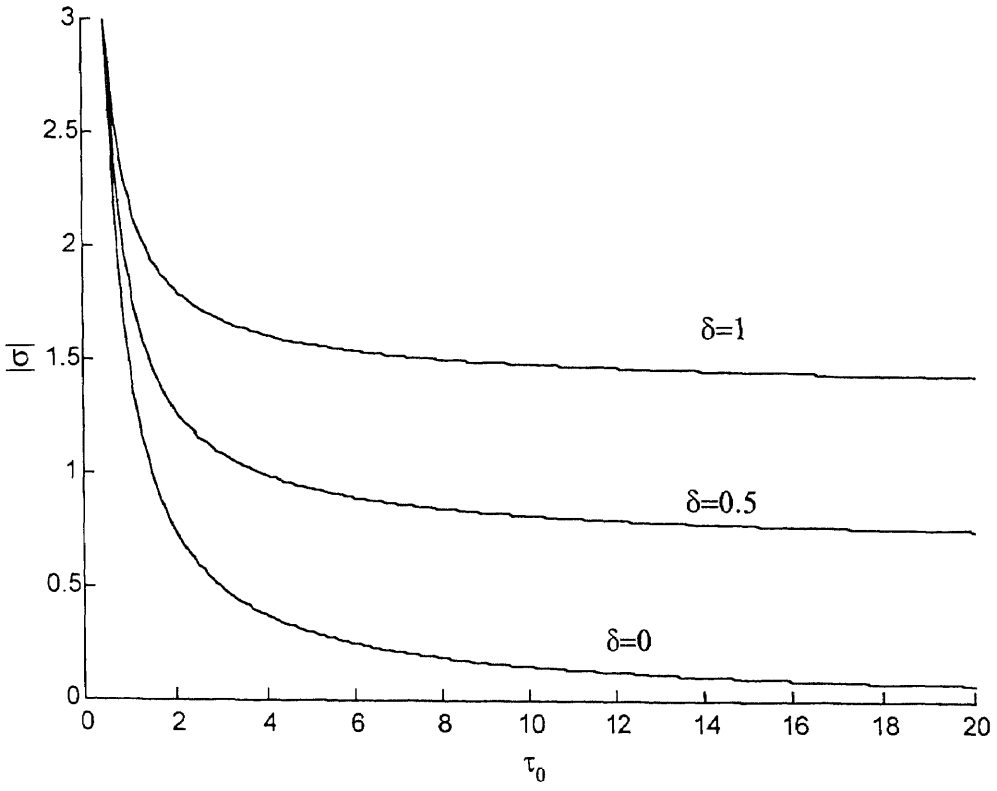

Figure 9.7 Illustration of thermal expansion mismatch effect.

APPENDIX A

ELECTRIC FIELD FOR SUSCEPTOR CONFIGURATION

In this appendix we present the exact solution to the reduced electric field equations for the susceptor-ceramic-susceptor configuration. We find

$$V_0(x) = a(v_0)\exp(ik_1h(v_0)x) + b(v_0)\exp(-ik_1h(v_0)x) \tag{A.1}$$

$$U_0(x) = c(v_0)\exp(ik_2x) + d(v_0)\exp(-ik_2x) \tag{A.2}$$

where

$$h(v_0) = \sqrt{1 + i\nu g(v_0)} \tag{A.3}$$

$$a(v_0) = A(v_0)d(v_0) \tag{A.4}$$

$$b(v_0) = B(v_0)d(v_0) \tag{A.5}$$

$$c(v_0) = \exp(-2ik_2)d(v_0) \tag{A.6}$$

$$d(v_0) = \frac{2k\exp(-ikd)}{C(v_0)} \tag{A.7}$$

$$A(v_0) = \frac{1}{2}((\frac{k_2}{k_1h(v_0)} + 1)\exp(-2ik_2) + (1 - \frac{k_2}{k_1h(v_0)})) \tag{A.8}$$

$$B(v_0) = \frac{1}{2}((1 - \frac{k_2}{k_1h(v_0)})\exp(-2ik_2) + (1 + \frac{k_2}{k_1h(v_0)})) \tag{A.9}$$

$$\begin{aligned} C(v_0) \;=\; & A(v_0)(k + k_1h(v_0))\exp(-ik_1h(v_0)d) + \\ & B(v_0)(k - k_1h(v_0))\exp(ik_1h(v_0)d). \end{aligned} \tag{A.10}$$

APPENDIX B

ELECTRIC FIELD FOR INSULATED TARGET

In this appendix we present the exact solution to the reduced electric field equations for the insulated target configuration. We find

$$U_0(x) = a(v_0)\exp(ik_1x) + b(v_0)\exp(-ik_1x) \tag{B.1}$$

$$V_0(x) = c(v_0)\exp(ik_2h(v_0)x) + d(v_0)\exp(-ik_2h(v_0)x) \tag{B.2}$$

where

$$h(v_0) = \sqrt{1 + i\nu g(v_0)} \tag{B.3}$$

$$a(v_0) = A(v_0)d(v_0) \tag{B.4}$$

$$b(v_0) = B(v_0)d(v_0) \tag{B.5}$$

$$c(v_0) = \exp(-2ik_2h(v_0)d)d(v_0) \tag{B.6}$$

$$d(v_0) = 2k\exp(-ik)/((k_1+k)A(v_0)\exp(-ik_1) + (k-k_1)B(v_0)\exp(ik_1)) \tag{B.7}$$

and

$$A(v_0) = (1/2)((k_2/k_1)h(v_0)(\exp(-2ik_2h(v_0)d) - 1) + (\exp(-2ik_2h(v_0)d) + 1)) \tag{B.8}$$

$$B(v_0) = (-1/2)((k_2/k_1)h(v_0)(\exp(-2ik_2h(v_0)d) - 1) - (\exp(-2ik_2h(v_0)d) + 1)). \tag{B.9}$$

REFERENCES

1. W. Sutton, "Key issues in microwave process technology," in *Proceedings of the symposium 'Microwave Processing of Materials III'*, (Pittsburg, PA), pp. 3–20, Materials Research Society, April 1992.

2. G. Vogt and W. Unruh, "Microwave hybrid heating of alumina filaments," in *Proceedings of the symposium 'Microwaves: theory and applications in materials processing II'*, (Westerville, Ohio), pp. 297–306, The American Ceramic Society, April 1993.

3. M. Janney, H. Kimrey, and J. Kiggans, "Microwave proceesing of ceramics: Guidelines used at the oak ridge national laboratory," in *Proceedings of the symposium 'Microwave Processing of Materials II'*, (Pittsburg, PA), pp. 173–185, Materials Research Society, 1992.

4. Y. Fang, D. Agrawal, D. Roy, and R. Roy, "Microwave sintering of calcium strontium zirconium phosphate ceramics," in *Proceedings of the symposium 'Microwave Processing of Materials III'*, (Pittsburg, PA), pp. 109–114, Materials Research Society, April 1992.

5. K. Leiser, R. DiFiore, A. Cozzi, and D. Clark, "Microwave heating rates of silicon carbide/alumina cement susceptors," in *Proceedings of the Cocoa Beach Engineering Ceramics Division Composites Meeting*, January 1997. In press.

6. F. Mako, R. Silberglitt, and L. Len, "Pulsed electron beam joining of materials," *U.S. Patent 5,599,468*, 1997.

7. G. Kriegsmann, "Microwave heating of dispersive media," *SIAM Journal of Applied Mathematics*, vol. 53, pp. 655–669, 1993.

8. W. Westphal, "Dielectric constant and loss measurements on high-temperature materials," tech. rep., Laboratory for Insulation Research Technical Report, MIT, October 1963.

9. G. Kriegsmann, "Thermal runaway in microwave heated ceramics: A one-dimensional model," *Journal of Applied Physics*, vol. 71, pp. 1960–1966, 1992.

10. S. Londen, "On a nonlinear volterra integral equation," *Journal of Differential Equations*, vol. 14, pp. 106–120, 1973.

11. J. Roberts and W. Mann, "On a certain nonlinear integral equation of the volterra type," *Pacific J. Math.*, vol. 1, pp. 431–445, 1951.

12. W. Mann and F. Wolf, "Heat transfer between solids and gasses under nonlinear boundary conditions," *Quart. Appl. Math.*, vol. 11, pp. 163–184, 1951.

13. P. Chambre, "Nonlinear heat transfer problem," *Journal of Applied Physics*, vol. 30, pp. 1683–1688, 1959.

14. P. Linz, *Analytical and Numerical Methods of Volterra Equations*. Philadelphia, PA: SIAM, 1985.

15. D. Lagoudas and Z. Ding, "Modeling of thermoelectric heat transfer in shape memory alloy actuators: Transient and multiple cycle solutions," *International Journal of Engineering Sciences*, 1996. (In press).

16. L. Perko, *Differential Equations and Dynamical Systems*. New York, NY: Springer-Verlag, 1991.

17. C. Lin and L. Segel, *Mathematics Applied to Deterministic Problems in the Natural Sciences*. Philadelphia PA: SIAM, 1988.

18. B. Boley and J. Weiner, *Theory of Thermal Stresses*. Mineola, NY: Dover Publications, 1960.

19. W. B. III and F. Froes, "Joining similar and dissimilar advanced engineered materials," *JOM*, pp. 13–15, March 1995.

20. A. Carim, D. Schwartz, and R. Silberglitt, "Joining and adhesion of advanced inorganic materials," in *MRS Symposium Proceedings*, vol. 314, (Pittsburg, PA), Materials Research Society, 1993.

21. R. Graves, *The Greek Myths*. New York, NY: Penguin Books, 1960.

22. J. Duhamel, "Second memoire sur les phenomenes thermo-mecaniques," *Journal de l'Ecole Polytechnique*, vol. 15, pp. 1–57, 1837.

23. V. Danilowskaya, "Thermal stresses in an elastic halfspace due to a sudden heating of its boundary," *Prikl. Mat. Mekh.*, vol. 14, pp. 316–318, 1950.

24. V. Danilowskaya, "Temperature field and thermal stresses produced in elastic semi-space by a flux of radiation energy incident on the boundary of semispace," *Izv. Akad. Nauk SSSR*, vol. 9, pp. 129–132, 1959.

25. L. Germanovich, I. Kill, and N. Tsodokova, "On thermal stresses in halfspace heated by concentrated flux of energy," *P.M.M.*, vol. 52, pp. 674–684, 1988.

26. Y. Lee and H. Julien, "Calculated temperature and stress distribution in the edge cladding of a pulsed-laser slab," *Trans. ASME J. Heat Transfer*, vol. 111, pp. 243–248, 1989.

27. B. Boley and I. Tolins, "Transient coupled thermoelastic problems in the half-space," *Journal of Applied Mechanics*, pp. 637–646, 1962.

28. A. Soler and M. Brull, "On the solution to transient coupled thermoelastic problems by perturbation techniques," *Journal of Applied Mechanics*, pp. 389–399, 1965.

29. J. Achenbach, "The propagation of stress discontinuities according to the coupled equations of thermoelasticity," *Acta Mechanica*, vol. 3, pp. 342–351, 1967.

30. D. Stickler and R. Nickell, "Thermoelastic damping of stress waves induced by volumetric energy depostion," *The Journal of the Acoustical Society of America*, vol. 50, pp. 224–229, 1971.

31. A. Bardenshtein, S. Bgaev, and D. Vaisburd, "Temperature dependence of the threshold of the brittle fracture of a solid by a dense pulsed electron beam," *Sov. Phys. Dokl.*, vol. 36, pp. 720–722, October 1991.

32. Y. F. I. et.al., "Dissipation of stress-wave energy and structural changes in steels under pulsed electron beam irradiation," *Sov. Phys. Dokl.*, vol. 36, pp. 874–876, December 1991.

33. B. Turman, S. Glass, J. Halbleib, D. Helmich, and R. Loehman, "Electron beam joining of structural ceramics," tech. rep., Sandia National Laboratory Report SAND95-0595, April 1995.

34. V. Bailey, "High energy electron beam interaction with materials," in *Proceedings of the High-Energy Electron-Beam Welding and Materials Processing Conference*, (Cambridge, MA), American Welding Society, 1992.

35. J. Halbleib and R. Kensek, "Its:the integrated tiger series of electron/photon transport codes - version 3.0," *IEEE Transactions of Nuclear Science*, vol. 39, pp. 1025–1029, 1992.

36. T. Sanford, J. Halbleib, D. Beutler, and D. Knott, "Experimental verification of dosimetry predictions of bremsstrahlung attenuation as a function of material and electron energy," *IEEE Transactions of Nuclear Science*, vol. 40, pp. 1409–1417, 1993.

37. J. Halbleib and G. Scrivner, "Efficent beta/gamma monte carlo transport in repetitive structures," *IEEE Transactions of Nuclear Science*, vol. 40, pp. 1402–1408, 1993.

38. J. Shackelford, W. Alexander, and J. P. editors, *CRC Material Science and Engineering Handbook*. Boca Raton, Florida: CRC Press, Inc., 1994.